COORDINATED ASSEMBLY OF THE MITOCHONDRIAL ELECTRON TRANSPORT CHAIN

by

Jonathan Garrett Van Vranken

A dissertation submitted to the faculty of
The University of Utah
in partial fulfillment of the requirements for the degree of

Doctor of Philosophy

Department of Biochemistry

The University of Utah

December 2017

The University of Utah Graduate School

STATEMENT OF DISSERTATION APPROVAL

The dissertation of **Jonathan Garrett Van Vranken**

has been approved by the following supervisory committee members:

Jared P. Rutter	, Chair	**10/24/2017** Date Approved
Dennis R. Winge	, Member	**10/26/2017** Date Approved
Janet M. Shaw	, Member	**10/24/2017** Date Approved
Timothy G. Formosa	, Member	**10/26/2017** Date Approved
Adam L. Hughes	, Member	**10/24/2017** Date Approved

and by **Christopher Peter Hill** , Chair/Dean of

the Department/College/School of **Biochemistry**

and by David B. Kieda, Dean of The Graduate School.

ABSTRACT

Mitochondrial oxidative phosphorylation is an efficient source of cellular energy. This pathway couples the oxidation of NADH and $FADH_2$ to the establishment of an electrochemical gradient across the inner mitochondrial membrane to facilitate ATP generation. The respiratory chain is comprised of five complexes; however, these are not simple enzymes. Rather, they are highly intricate membrane-bound complexes. As such, the biogenesis of these complexes presents the cell with numerous problems. Thus, the cell expresses dozens of assembly factors that are required to support the biogenesis of individual complexes. In the end, this promotes cellular energy production and protects the cell from potentially damaging insults.

Succinate dehydrogenase (SDH) or complex II is a member of the electron transport chain (ETC) and TCA cycle. It plays a central role in cellular energy generation and mutations in the genes encoding SDH subunits and assembly factors are associated with human disease, including cancer and neurodegeneration. This highly conserved family supports the maturation of SDHA/Sdh1, the catalytic subunit of SDH. As such, Sdh8 functions as an Sdh1-specific chaperone and prevents the spurious generation of reactive oxygen species during the assembly process. In Drosophila, Sdhaf4 is required to prevent neurodegeneration and maintain normal motility. In the end, this work has expanded our understanding of the SDH assembly pathway and provided novel insights into the development of SDH-deficient pathologies.

In addition to the canonical cytosolic pathway, eukaryotic cells have maintained a mitochondrial fatty acid synthesis pathway (FASII). This pathway is homologous to prokaryotic fatty acid synthesis and utilizes a number of enzymes that interact transiently with the acyl carrier protein (ACP) to support elongation of nascent acyl chains. Herein, we describe a novel and unexpected role for ACP and FASII in the assembly and activation of the ETC. As such, FASII-dependent synthesis of ACP-bound acyl chains activates a network of complex-specific assembly factors to support the assembly of the ETC complexes and synthesis of their essential cofactors. In the end, FASII and ACP couple mitochondrial acetyl-CoA to ETC biogenesis.

This dissertation is dedicated to my parents, who have always supported my education.

TABLE OF CONTENTS

LIST OF TABLES

Tables

LIST OF FIGURES

Figures

ACKNOWLEDGEMENTS

Throughout my time in the University of Utah Department of Biochemistry I feel fortunate to have been involved in a community of learning. I am grateful for the advice, guidance, and training that I received from my faculty members and colleagues, alike.

I would like to thank Dr. Jared Rutter for training me to be an independent scientist and teaching me how to think. The years I have spent training with him have been an honor and a privilege that I will never forget. Jared has always fostered an environment built on respect and trust. As such, I have been encouraged to identify and pursue my own lines of inquiry. Despite this independence, Jared has always been available to support my research and facilitate my training. I will be forever gracious for his generosity, support, and encouragement. I hope that I will be able to live up to his standards both in the lab and in life.

I want to thank other faculty who played important roles in my training. I will always be grateful to my graduate committee—Dr. Dennis Winge, Dr. Janet Shaw, Dr. Tim Formosa, and Dr. Adam Hughes—for their unique insights and collective guidance. In particular, I would like to thank Dr. Winge, whose passion and enthusiasm for science has been an inspiration. Additionally, I would like to thank Dr. Carl Thummel from the University of Utah for his help in the characterization of the SDHAF4 protein family. Finally, I need to thank Dr. Steve Gygi and his lab from Harvard Medical School for help with proteomic experiments.

I need to show my appreciation for my colleagues and fellow trainees in the Rutter Lab. I could not imagine working in a more supportive and enjoyable environment. In particular, I need to thank Yu-Chan Chen for teaching me all the techniques and procedures I needed to be a successful graduate student. She has taught me everything I know.

Finally, I need to thank my family for all their support throughout graduate school. They always encouraged me to pursue my passions and without their help I would not have been able to follow my dreams.

CHAPTER 1

INTRODUCTION

Uncharacterized mitochondrial proteins

Mitochondria are dynamic organelles that play important roles in a number of cellular processes including metabolism, signal transduction, and apoptosis. Owing in part to its diverse roles within the cell, it has become increasingly clear that mitochondrial dysfunction is involved in the pathogenesis of a diverse array of human disease including diabetes, neurodegeneration, and cancer. Thus, mitochondrial function is essential for maintaining cellular homeostasis, while defects in these essential functions often manifest as disease. Because the influence of this organelle impacts both normal physiology and disease pathogenesis, considerable effort has been allocated to the complete characterization of the mitochondrial proteome (*1, 2*). Despite this effort, however, nearly a quarter of the mitochondrial proteins remain uncharacterized, including many genes that have maintained a high degree of conservation throughout eukaryotic evolution, implying involvement in an essential cellular process. Furthermore a high percentage of genes encoding mitochondrial proteins are predicted to be associated with inherited human disease. Thus, we predict that the interrogation of uncharacterized mitochondrial proteins will reveal important insights into normal cellular physiology as well as human disease.

In total, we identified 29 proteins or protein families to focus our initial investigation. This has lead to the characterization of numerous proteins and has expanded our understanding of mitochondrial biology considerably (*3-9*). This list initially focused strictly on proteins that remained completely uncharacterized. However, there remain numerous targets that have been studied but not in sufficient depth to provide a complete understanding of their function. Thus, it is likely that the mitochondrial proteome encodes a number of other genes that remain under-characterized and warrant further investigation. Using a combination of biochemical and genetic methods and taking advantage of the model system *Saccharomyces cerrevisiae* (budding yeast) we will seek to define the cellular role of these un- or under-characterized mitochondrial proteins.

The electron transport chain

While it is now abundantly clear that mitochondria are intimately involved in a vast array of cellular processes, this organelle is classically regarded as the compartmentalized site of oxidative phosphorylation (Figure 1-1). As such, the catabolism of glucose, fatty acids, and amino acids converge in the mitochondria as acetyl-CoA. This principal metabolite, which exclusively fuels cellular respiration, is oxidized by the tricarboxylic acid (TCA) cycle, providing the reducing equivalents (NADH and $FADH_2$) that fuel the electron transport chain (ETC) This series of complexes then passes electrons through a number of redox active cofactors thereby generating a membrane potential across the inner mitochondrial membrane, which ATP synthase can exploit to generate adenosine triphosphate.

In mammals, the ETC is comprised of five membrane-bound protein complexes and two mobile electron carriers, which altogether consists of nearly 100 individual protein subunits, expressed from two distinct genomes. This machine of unrivaled complexity and elegance is capable of generating ~34 molecules of ATP from the oxidation of one molecule of glucose. Indeed the ETC can serve as an efficient source of cellular energy; however, it can also generate potentially deleterious byproducts that are capable of damaging the cell. Therefore, the cell has evolved numerous mechanisms to promote and regulate the assembly the ETC.

ETC biogenesis does not happen spontaneously. Instead, the cell has evolved numerous mechanisms to support the assembly and activity of these complexes. In fact, the process of ETC biogenesis presents the cell with numerous problems the cell must overcome in order to maintain cellular energy homeostasis and redox balance. First, the cell must coordinate the synthesis and interaction of dozens of individual protein subunits in order to support the step-wise assembly of individual complexes. Furthermore, these individual subunits are translated from two distinct genomes in two distinct compartments that are separated by double membranes. This problem is exacerbated by the nature of the ETC complexes themselves. First, some subunits of these complexes are embedded in the IMM and, therefore, are hydrophobic and prone to aggregation prior to and during assembly. Furthermore, the complexes contain redox-active cofactors that can perform inappropriate reactions when they are not properly secluded within the native complex. As a result, the eukaryotic genome has maintained dozens of dedicated factors to assist the assembly of these complexes by facilitating cofactor insertion, preventing nonproductive interactions, and stabilizing assembly intermediates (*10, 11*).

Importantly, the threat imposed on the cell by the ETC does not end following biogenesis. In fact, the fully assembled ETC and its numerous redox-active cofactors are the primary source of reactive oxygen species (ROS) in the cell. Thus, it is not enough for the cell to simply assemble these complexes. Instead, it must work diligently to maintain the fidelity of these complexes such that energy generation can be maximized and ROS minimized. This is particularly problematic in times of nutrient imbalance when the reducing capacity of the ETC is high but electron flux is limited due to lack of substrate (*12*). Thus, the cell must be able to balance mitochondrial oxidative capacity with substrate availability in order to prevent the spurious leak of electrons and ROS. In the end, the ability to modulate the assembly and activity of the ETC in response to substrate availability will promote efficient energy production while minimizing the deleterious byproducts of oxidative phosphorylation.

References

1. A. Sickmann, J. Reinders, Y. Wagner, C. Joppich, R. Zahedi, H. E. Meyer, B. Schonfisch, I. Perschil, A. Chacinska, B. Guiard, P. Rehling, N. Pfanner, C. Meisinger, The proteome of Saccharomyces cerevisiae mitochondria. *Proceedings of the National Academy of Sciences of the United States of America* **100**, 13207-13212 (2003).

2. D. J. Pagliarini, S. E. Calvo, B. Chang, S. A. Sheth, S. B. Vafai, S. E. Ong, G. A. Walford, C. Sugiana, A. Boneh, W. K. Chen, D. E. Hill, M. Vidal, J. G. Evans, D. R. Thorburn, S. A. Carr, V. K. Mootha, A mitochondrial protein compendium elucidates complex I disease biology. *Cell* **134**, 112-123 (2008).

3. H. X. Hao, O. Khalimonchuk, M. Schraders, N. Dephoure, J. P. Bayley, H. Kunst, P. Devilee, C. W. Cremers, J. D. Schiffman, B. G. Bentz, S. P. Gygi, D. R. Winge, H. Kremer, J. Rutter, SDH5, a gene required for flavination of succinate dehydrogenase, is mutated in paraganglioma. *Science* **325**, 1139-1142 (2009).

4. J.-M. Heo, N. Livnat-Levanon, E. B. Taylor, K. T. Jones, N. Dephoure, J. Ring, J. Xie, J. L. Brodsky, F. Madeo, S. P. Gygi, K. Ashrafi, M. H. Glickman, J. Rutter,

A stress-responsive system for mitochondrial protein degradation. *Molecular Cell* **40**, 465-480 (2010).

5. D. K. Bricker, E. B. Taylor, J. C. Schell, T. Orsak, A. Boutron, Y.-C. Chen, J. E. Cox, C. M. Cardon, J. G. Van Vranken, N. Dephoure, C. Redin, S. Boudina, S. P. Gygi, M. Brivet, C. S. Thummel, J. Rutter, A mitochondrial pyruvate carrier required for pyruvate uptake in yeast, Drosophila, and humans. *Science* **337**, 96 (2012).

6. Y.-C. Chen, Eric B. Taylor, N. Dephoure, J.-M. Heo, A. Tonhato, I. Papandreou, N. Nath, Nicolas C. Denko, Steven P. Gygi, J. Rutter, Identification of a protein mediating respiratory supercomplex stability. *Cell Metabolism* **15**, 348-360 (2012).

7. J. G. Van Vranken, D. K. Bricker, N. Dephoure, S. P. Gygi, J. E. Cox, C. S. Thummel, J. Rutter, SDHAF4 pomotes mitochondrial succinate dehydrogenase activity and prevents neurodegeneration. *Cell Metabolism* **20**, 241-252 (2014).

8. Y. C. Chen, G. K. E. Umanah, N. Dephoure, S. A. Andrabi, S. P. Gygi, T. M. Dawson, V. L. Dawson, J. Rutter, Msp1/ATAD1 maintains mitochondrial function by facilitating the degradation of mislocalized tail‐anchored proteins. *The EMBO Journal* **33**, 1548-1564 (2014).

9. J. G. Van Vranken, M.-Y. Jeong, P. Wei, Y.-C. Chen, S. P. Gygi, D. R. Winge, J. Rutter, The mitochondrial acyl carrier protein (ACP) coordinates mitochondrial fatty acid synthesis with iron sulfur cluster biogenesis. *eLife* **5**, e17828 (2016).

10. E. Fernandez-Vizarra, V. Tiranti, M. Zeviani, Assembly of the oxidative phosphorylation system in humans: What we have learned by studying its defects. *Biochimica et biophysica acta* **1793**, 200-211 (2009).

11. F. Diaz, H. Kotarsky, V. Fellman, C. T. Moraes, Mitochondrial disorders caused by mutations in respiratory chain assembly factors. *Seminars in Fetal & Neonatal Medicine* **16**, 197-204 (2011).

12. K. E. Wellen, C. B. Thompson, Cellular metabolic stress: considering how cells respond to nutrient excess. *Molecular Cell* **40**, 323-332 (2010).

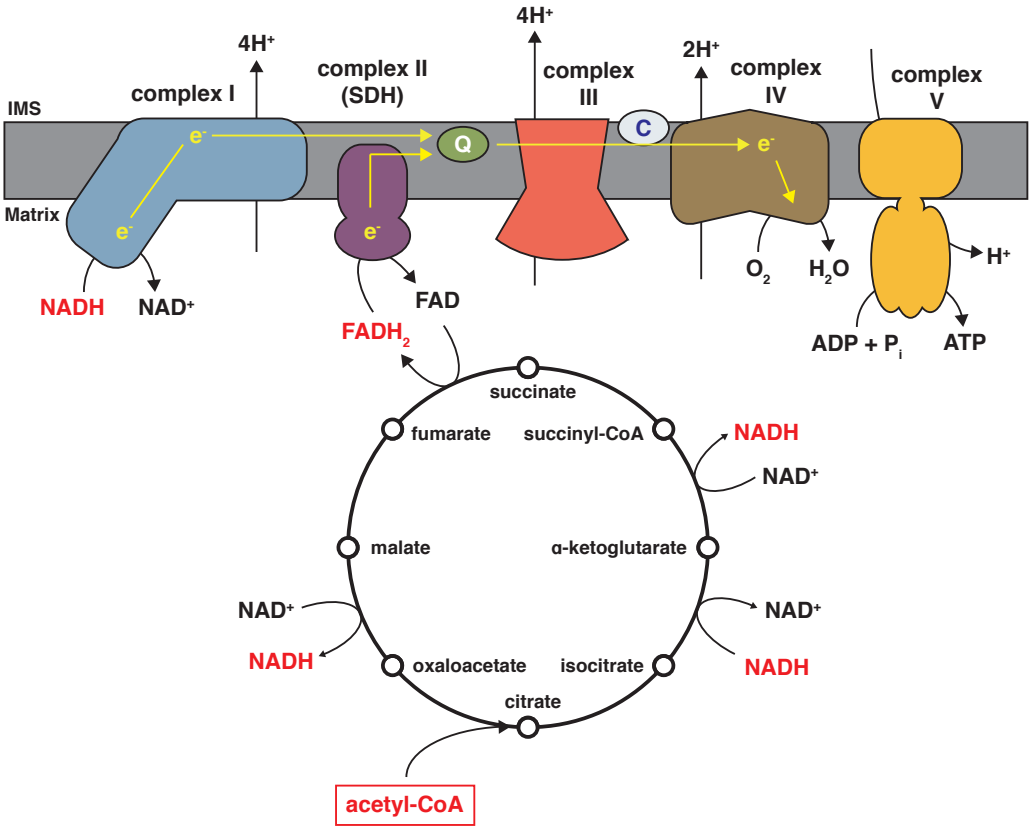

Figure 1-1. The electron transport chain.
Electrons derived from NADH and FADH2 are passed from complex I and complex II, respectively to coenzyme Q. Complex III takes the electrons from coenzyme Q and passes them to cytochrome c. Finally, complex IV uses the electrons to reduce oxygen to water. This movement of electrons is coupled to the pumping of electrons across the inner mitochondrial membrane. This establishes an electrochemical gradient that complex V can exploit to generate ATP.

CHAPTER 2

PROTEIN-MEDIATED ASSEMBLY OF SUCCINATE DEHYDROGENASE AND ITS COFACTORS

Jonathan G. Van Vranken, Un Na, Dennis R. Winge, and Jared Rutter

Reprinted with permission from Critical Reviews in Biochemistry and Molecular Biology, vol. 50(2), pp. 168-68

Critical Reviews in Biochemistry and Molecular Biology

http://informahealthcare.com/bmg
ISSN: 1040-9238 (print), 1549-7798 (electronic)
Editor: Michael M. Cox
Crit Rev Biochem Mol Biol, 2015; 50(2): 168–180
 DOI: 10.3109/10409238.2014.990556

informa
healthcare

REVIEW ARTICLE

Protein-mediated assembly of succinate dehydrogenase and its cofactors

Jonathan G. Van Vranken[1], Un Na[1,2], Dennis R. Winge[1,2], and Jared Rutter[1]

[1]Department of Biochemistry and [2]Department of Internal Medicine, University of Utah School of Medicine, Salt Lake City, UT, USA

Abstract

Succinate dehydrogenase (or complex II; SDH) is a heterotetrameric protein complex that links the tribarboxylic acid cycle with the electron transport chain. SDH is composed of four nuclear-encoded subunits that must translocate independently to the mitochondria and assemble into a mature protein complex embedded in the inner mitochondrial membrane. Recently, it has become clear that failure to assemble functional SDH complexes can result in cancer and neurodegenerative syndromes. The effort to thoroughly elucidate the SDH assembly pathway has resulted in the discovery of four subunit-specific assembly factors that aid in the maturation of individual subunits and support the assembly of the intact complex. This review will focus on these assembly factors and assess the contribution of each factor to the assembly of SDH. Finally, we propose a model of the SDH assembly pathway that incorporates all extant data.

Keywords

Assembly factors, redox-active cofactors, respiratory chain, succinate dehydrogenase

History

Received 3 September 2014
Revised 14 November 2014
Accepted 18 November 2014
Published online 9 December 2014

Electron transport chain complex assembly

Mitochondrial ATP synthesis is dependent on the concerted efforts of the electron transport chain (ETC), which couples the generation of an electrochemical gradient to the oxidation of NADH and $FADH_2$ and the reduction of oxygen to water. The ETC is composed of four multimeric complexes and two mobile electron carriers (coenzyme Q and cytochrome *c*), all of which are embedded in or associated with the inner mitochondrial membrane (IMM). Electrons derived from the oxidation of NADH by complex I or succinate from the tricarboxylic acid (TCA) cycle by complex II (succinate dehydrogenase; SDH) are passed along the ETC, coupled with the pumping of protons and establishment of the proton gradient across the IMM. In the end, controlled flow of protons down this electrochemical gradient is utilized by complex V (ATP synthase) to catalyze ATP synthesis.

The assembly of the ETC complexes presents the cell with the problem of coordinating the synthesis and stepwise interactions of individual subunits, transcribed and translated from two distinct genomes in two distinct compartments, into intricate membrane bound complexes. This problem is exacerbated by the nature of the ETC complexes themselves. First, some subunits are embedded in the IMM and, therefore, are hydrophobic and prone to aggregation prior to and during assembly. Furthermore, the complexes contain redox-active cofactors that can perform inappropriate and deleterious reactions when they are not properly secluded within the native complex. As a result, a number of dedicated factors assist the assembly of these complexes by facilitating cofactor insertion, preventing non-productive interactions and stabilizing assembly intermediates (Diaz *et al*., 2011; Fernandez-Vizarra *et al*., 2009). While mammalian ETC complexes I, III and IV contain 44, 11 and 14 subunits, respectively, and include proteins encoded by both mitochondrial and nuclear genomes, complex II or SDH, is the product of just four nuclear-encoded genes. Despite this somewhat simple quaternary structure, it has been made clear recently that SDH, like all ETC complexes, requires assembly factors for its biogenesis.

Succinate dehydrogenase and human disease

The critical role of SDH in mitochondrial metabolism has long been appreciated, however, it has more recently emerged that mutations affecting SDH cause a number of human diseases (Hoekstra & Bayley, 2013; Rutter *et al*., 2010; Table 1). Interestingly, loss of function mutations in SDH core subunits do not cause a single, common pathology, but rather lead to a variety of disease phenotypes that can be grouped into two categories – cancer and neurodegeneration. With respect to SDH-deficient cancers and other tumor syndromes, mutations in the core subunits are most commonly associated with paraganglioma, pheochromocytoma, renal cell carcinoma (RCC) and WT gastrointestinal stromal tumors (WT-GIST). Paragangliomas are neuro-endocrine tumors that occur in cells of the neural crest and tend to be co-localized with oxygen sensing tissues such as the carotid body, while pheochromocytomas represent a related class of tumors that affect the adrenal gland. These two tumors are most

Address for correspondence: Jared Rutter, Department of Biochemistry, University of Utah School of Medicine, Salt Lake City, UT, USA. E-mail: rutter@biochem.utah.edu

DOI: 10.3109/10409238.2014.990556

commonly associated with mutations in *SDHB*, *SDHC* and *SDHD*, however *SDHA* mutations have recently been implicated in rare cases (Astuti *et al*., 2001; Baysal, 2000; Burnichon *et al*., 2010; Peczkowska *et al*., 2008). Mutations in *SDHA*, *SDHB* and *SDHC* have also been associated with WT-GIST, a mesenchymal tumor of the digestive tract (Janeway *et al*., 2011; Pantaleo *et al*., 2011, 2014). Finally, the link between RCC and SDH dysfunction is supported by the discovery of two families with inherited renal cell tumor syndromes resulting from germline mutations in *SDHB* (Vanharanta *et al*., 2004). Taken together, it is clear that normal SDH activity serves to suppress tumors in humans. In addition to the cancers described above, defects in SDH activity also cause a variety of neurodegenerative disorders. In fact, the classical presentation of patients with mutations in *SDHA* is Leigh Syndrome, an early-onset, progressive neurodegenerative disorder (Bourgeron *et al*., 1995). *SDHA* mutations have also been associated with milder forms of atrophy and myopathy (Bourgeron *et al*., 1995; Horváth *et al*., 2006). Although mutations in *SDHC* are rarely, if ever, associated with neurologic disorders, *SDHB* mutations have been shown to cause infantile leukodystrophy (Alston *et al*., 2012) and SDHD mutations have recently been identified in patients with progressive encephalomyopathy (Jackson *et al*., 2014). Therefore, SDH activity not only suppresses tumors but also supports normal neurologic development and function. While it is fascinating that mutations in all four subunits of SDH have been found to cause one of the diseases described above, it is perhaps even more interesting that numerous patients present with disease accompanied by a loss of SDH activity, but have no mutations of any of the core subunits (Jain-Ghai *et al*., 2013). These genetic observations clearly implicate additional auxiliary factors in the maintenance of cellular SDH activity. Furthermore, this supports the notion that a thorough characterization of the SDH assembly pathway will ultimately lead to the discovery of new human disease alleles in the genes that encode SDH assembly factors.

Table 1. SDH associated genes and clinical phenotypes.

Yeast gene	Human ortholog	Disease
SDH1	*SDHA*	Leigh Syndrome Paraganglioma/Pheochromocytoma WT-GIST
SDH2	*SDHB*	Paraganglioma/Pheochromocytoma Renal Cell Carcinoma WT-GIST Infantile Leukodystrophy
SDH3	*SDHC*	Paraganglioma/Pheochromocytoma Renal Cell Carcinoma WT-GIST
SDH4	*SDHD*	Paraganglioma/Pheochromocytoma WT-GIST Progressive Encephalomyopathy
SDH5	*SDHAF2*	Paraganglioma/Pheochromocytoma
SDH6	*SDHAF1*	Infantile Leukodystrophy
SDH7	*SDHAF3*	N/A
SDH8	*SDHAF4*	N/A

Enzymology and structure of succinate dehydrogenase

Eukaryotic SDH is a heterotetrameric complex composed of four nuclear-encoded subunits (Sun *et al*., 2005; Figure 1). SDH is unique amongst eukaryotic ETC complexes in that it functions as part of both the TCA cycle and the ETC and thus couples two of the primary energy-harvesting pathways within the cell. In addition to this distinction, SDH is the only ETC complex that does not pump protons across the IMM nor does it contain any proteins encoded by the mitochondrial genome. In the context of the TCA cycle, SDH catalyzes the oxidation of succinate to fumarate and uses the electrons derived from this oxidation to catalyze the reduction of ubiquinione to ubiquinol. These electrons are passed to Complex III and then Complex IV, thereby contributing to the establishment of the electrochemical gradient across the IMM in support of ATP synthesis. The structure of SDH can be characterized as a hydrophilic head that protrudes into the

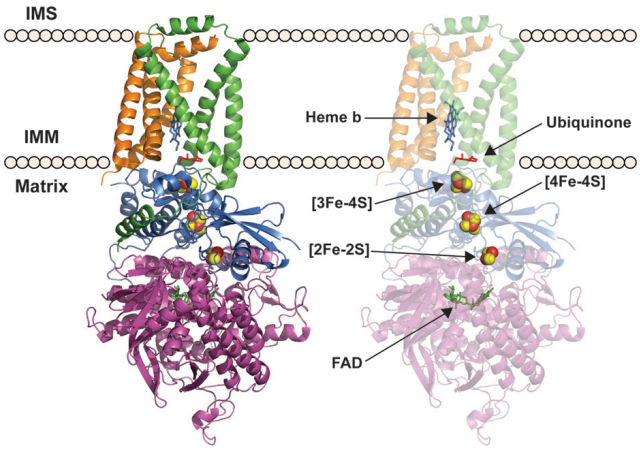

Figure 1. Porcine succinate dehydrogenase (PDB accession number: 1ZOY) embedded in the mitochondrial inner membrane. SdhA (purple ribbon); SdhB (blue ribbon); SdhC (green ribbon); SdhD (brown ribbon); FAD (green stick); FeS centers, [2Fe–2S], [4Fe–4S], [3Fe–4S] from the bottom (red and yellow sphere); Ubiquinone in the Q_P site (red stick); Heme b (blue stick). (see colour version of this figure at www.informahealthcare.com/bmg).

mitochondrial matrix attached to the IMM by a hydrophobic membrane anchor (Sun *et al*., 2005; Yankovskaya *et al*., 2003; Figure 1).

The membrane anchor domain of SDH consists of Sdh3 (SDHC in mammals) and Sdh4 (SDHD; Sun *et al*., 2005; Yankovskaya *et al*., 2003) and serves as the site of ubiquinone binding to connect this hydrophobic mobile electron carrier to the hydrophilic domain of SDH (Figure 1). The hydrophilic domain represents the catalytic core of SDH and is composed of Sdh1 (SDHA in mammals) and Sdh2 (SDHB), each of which contain the redox-active cofactors that facilitate the transfer of electrons from succinate to ubiquinone (Sun *et al*., 2005; Yankovskaya *et al*., 2003; Figure 1). Sdh1 contains a covalently bound FAD cofactor adjacent to the succinate-binding site (Figure 1). Sdh2 harbors the three Fe–S centers that mediate electron transfer from the flavin cofactor to the ubiquinone (Figure 1). The Fe–S clusters of Sdh2, which consist of a 2Fe–2S center adjacent to the FAD site of Sdh1, followed by a 4Fe–4S and finally a 3Fe–4S center proximal to the ubiquinone binding site, serve essentially as a wire used to transfer electrons through the complex (Figure 1). In addition to its important role in the process of electron transfer, Sdh2 also serves as the interface linking the catalytic Sdh1 subunit to the membrane bound Sdh3 and Sdh4 subunits (Sun *et al*., 2005; Yankovskaya *et al*., 2003). Interestingly, recent reports indicate that soluble Sdh1–Sdh2 dimers exist in the absence of one or both of the membrane anchors (Kim *et al*., 2012). This suggests that Sdh1 and Sdh2 are likely to dimerize prior to membrane association, rather than sequentially docking onto the membrane anchor.

The SDH enzymatic reaction begins with the binding of succinate to the open state of Sdh1, which undergoes a conformational change bringing succinate into close proximity with the covalently bound FAD cofactor. Oxidation of succinate is coupled to the two-electron reduction of FAD. Since the Fe–S centers of SDH are single electron carriers, two successive single electron transfer steps are required to re-oxidize $FADH_2$ back to FAD. In the end, the two electrons gained from the oxidation of succinate are used to reduce ubiquinone to ubiquinol, which passes the electrons on to Complex III.

Assembly of SDH

Until recent years, the process of SDH assembly remained highly enigmatic and was primarily focused on the core SDH subunits themselves (Cecchini *et al*., 2002; Lemire & Oyedotun, 2002). Our newfound understanding of this process has been facilitated by the discovery of proteins dedicated to the maturation of individual subunits and the assembly of the holo-complex. Importantly, the discovery of these factors has revealed that SDH assembly is a tightly coordinated process in which the concerted functions of core subunits, dedicated assembly factors and other ancillary factors must coordinate their various activities to achieve the step-wise assembly of this membrane bound complex. Based on the knowledge gained in recent years, it is possible to organize the process of SDH assembly into discrete, subunit-specific events. These events, which include cofactor insertion, stabilization of subcomplex assembly intermediates and prevention of deleterious solvent interactions, result in the maturation of individual subunits and support the complete assembly of SDH. In the subsequent sections, we will review the current understanding of the SDH assembly pathway focusing, in particular, on the factors that facilitate this process (Figure 3).

Sdh1 – the catalytic subunit

Architecture of Sdh1

Sdh1 catalyzes the oxidation of succinate to fumarate. The crystal structure of porcine SDH has revealed that mammalian SDHA assumes a Rossmann-type fold with four distinct domains – an FAD binding domain (residues 52–267 and 355–439; human sequence), a capping domain (residues 268–354), a helical domain (residues 440–537) and a C-terminal domain (residues 548–616). The structure indicates the presence of a covalent bond between FAD and His99 (His90 in yeast) with the FAD being further coordinated by a number of additional residues, which form a well-ordered hydrogen bonding network (Sun *et al*., 2005; Figure 1). In addition to the native SDH, a co-crystal structure of SDH bound to a competitive inhibitor, 3-nitropropionic acid (NPA) was also determined and facilitated the mapping of the putative succinate binding site, which, as expected, is directly adjacent to the FAD. While the precise mechanism for succinate oxidation by Sdh1 has not yet been elucidated, these studies have provided valuable information as to the residues involved in this reaction. The structure demonstrates that the nitryl group of NPA interacts with the FMN group of FAD as well as the main chain of Glu261 and the side chains of Thr260 and His248 while the NPA carboxyl group is anchored by the amide of Glu246, the guanidinium group of Arg403 and the imidazole of His359 (Sun *et al*., 2005).

Biosynthesis and delivery of FAD

FAD is an essential cofactor of Sdh1 and the flavinylation of Sdh1 is dependent on adequate FAD levels in the mitochondrial matrix. Therefore, the synthesis and maintenance of free FAD pools in this compartment plays a vital role in the maturation of Sdh1 (Kim & Winge, 2013). In yeast, the biosynthesis of FAD and its delivery to mitochondria is dependent on the activities of three proteins – riboflavin kinase (Fmn1), FAD synthetase (Fad1) and a putative mitochondrial FAD transporter (Flx1). FAD is derived from dietary riboflavin (vitamin B_2) and its conversion requires the activities of two ATP-dependent enzymes, Fmn1 and Fad1. Fmn1, the riboflavin kinase, phosphorylates the tricyclic isoalloxazine ring yielding flavin mononucleotide (FMN; Santos *et al*., 2000). Although a number of enzymes within the cell use FMN as a cofactor, the majority of FMN is subsequently adenylated and converted to FAD by the FAD synthetase, Fad1 (Wu *et al*., 1995).

Flx1 belongs to the eukaryotic superfamily of IMM carriers and has been described as a putative IMM FAD carrier, but the published literature disagrees as to the exact molecular function of Flx1 (Bafunno *et al*., 2004; Tzagoloff *et al*., 1996). At any rate, cells lacking Flx1 exhibit low matrix FAD concentrations and reduced activity of two matrix flavoproteins, SDH and lipoamide dehydrogenase, due to a defect in

DOI: 10.3109/10409238.2014.990556

flavinylation of these two enzymes (Kim *et al*., 2012; Tzagoloff *et al*., 1996). Therefore, while there is no known direct link between Flx1 and Sdh1, it is clear that Flx1 plays an important role in Sdh1 cofactor insertion as Sdh1 flavinylation is severely compromised in *flx1*Δ cells. This decrease in flavinylation also leads to the destabilization of Sdh1. Interestingly, the *flx1*Δ defect in Sdh1 flavinylation can be suppressed by the overexpression of Fad1 or Sdh5, a dedicated SDH assembly factor that will be discussed in significant detail in the subsequent section (Hao *et al*., 2009).

It is important to note that in mammalian cells, it is not clear whether an Flx1 ortholog is required for SDH maturation. The mammalian ortholog of the *FAD1* gene, *FLAD1*, yields two transcripts encoding two isoforms of FAD synthetase, one of which is cytosolic and the other has a mitochondrial targeting motif (Torchetti *et al*., 2010). Thus, mammalian cells might synthesize FAD within the mitochondrial matrix perhaps making any IMM carrier dispensable.

Sdh1 cofactor insertion

The first known step in the maturation of Sdh1, which is imported into the mitochondrial matrix as an apo-protein, is the insertion and covalent attachment of its FAD cofactor (Robinson *et al*., 1994). Interestingly, succinate appears to be an important allosteric effector of this process as it and several other TCA cycle intermediates stimulate flavinylation significantly *in vitro* (Brandsch & Bichler, 1989). Unlike some bacterial Sdh1 orthologs, eukaryotic Sdh1 is not competent to become flavinylated in the absence of other proteins, which is typically interpreted to mean that the flavinylation of Sdh1 is not autocatalytic (Kounosu, 2014; Robinson & Lemire, 1996). As a result, simply maintaining matrix FAD pools is not sufficient for Sdh1 flavinylation. Early studies focused on this process revealed that there likely exists a protein in the mitochondrial matrix required for flavinylation of Sdh1 as the degree to which Sdh1 can be flavinylated *in vitro* is proportional to the concentration of isolated matrix fraction used in the assay (Robinson & Lemire, 1996). This insight was subsequently validated by the discovery of Sdh5.

Yeast Sdh5 was discovered in the course of studying a collection of uncharacterized mitochondrial proteins with a high degree of conservation throughout eukaryotes (Hao *et al*., 2009). Deletion of *SDH5* in yeast prevented respiratory dependent growth and caused a dramatic reduction in oxygen consumption – two phenotypes indicative of a strong respiratory deficiency. In an attempt to better understand this phenotype, an unbiased tandem affinity purification was performed and it identified Sdh1 as the sole binding partner of Sdh5. This result, consistent with a clear respiratory deficiency, strongly implicated Sdh5 in the maintenance of SDH activity. This connection with SDH was further strengthened by the observation that yeast cells lacking Sdh5 exhibited a complete loss of SDH activity and, in this regard, essentially mirrored an *sdh1*Δ deletion strain. Despite these phenotypic similarities, however, Sdh1 protein was still clearly detectable, albeit at reduced levels, in an *sdh5*Δ mutant strain and, interestingly, the SDH complex remained intact (Hao *et al*., 2009; Kim *et al*., 2012).

Based on the above evidence, it is clear that Sdh5 is required for maintaining SDH activity and that this function is mediated through a direct physical interaction with Sdh1. These data raised the possibility that the primary defect in *sdh5*Δ cells might be failure to covalently flavinylate Sdh1, resulting in a catalytically dead subunit. Indeed, direct interrogation of Sdh1 flavinylation revealed a complete failure to form the covalent bond between Sdh1 His90 and the FAD cofactor. This finding is consistent with related studies that demonstrate flavinylation-deficient Sdh1 His90Ser mutants assemble into a catalytically inactive SDH complex as do *sdh5*Δ mutants (Hao *et al*., 2009; Robinson *et al*., 1994).

It is clear that Sdh5 is required for Sdh1 flavinylation but through what mechanism? The first important clues resulted from further interrogation of the nature of the Sdh1–Sdh5 interaction. BN-PAGE experiments demonstrated that Sdh5 is not a member of the SDH holo-complex but rather migrates to an approximate molecular weight of 90 kDa, consistent with an Sdh1–Sdh5 dimer. Further investigation of this interaction revealed that the formation of this complex is important in maintaining the stability of both proteins. The steady-state levels of Sdh1 are ∼50% reduced in an *sdh5*Δ mutant strain. Conversely, deletion of *SDH1* causes a near complete destabilization of Sdh5, a result that strongly implicates Sdh5 as a dedicated factor whose sole purpose is to act on Sdh1. While Sdh1 protein is required to maintain the stability of Sdh5, this relationship is not dependent on Sdh1 being competent for flavinylation as substitution of Sdh1 His90 with a Ser residue does not lead to destabilization of Sdh5. It is important to note that only a minor fraction of Sdh1 in the matrix is in association with Sdh5 at any given time. Furthermore, deletion of *SDH2* causes the steady-state level of Sdh5 to increase, most likely due to an increase in the fraction of Sdh1 that is bound to Sdh5. As this complex exists independent of all other SDH subunits and accumulates in strains that prevent SDH assembly, it is clear that the actions of Sdh5 and the process of flavinylation are early steps in the SDH assembly pathway (Hao *et al*., 2009; Kim *et al*., 2012).

Further insights into the role of Sdh5 in Sdh1 flavinylation came from structural characterization of yeast Sdh5 by NMR (Eletsky *et al*., 2012). No FAD was detected in purified samples of Sdh5, nor did the addition of FAD to purified Sdh5 cause any perturbation in Sdh5 chemical shifts, suggesting that Sdh5 does not act as a delivery vehicle that brings FAD to apo-Sdh1 (Eletsky *et al*., 2012). The NMR studies revealed that the Sdh5 core assumes a compact 5 α-helical bundle and revealed a concentrated patch of conserved residues on the surface of these α-helices, which is theorized to be the Sdh1 binding site (Eletsky *et al*., 2012)

While it is not yet possible to define the precise mechanism by which Sdh5 supports Sdh1 flavinylation, there is sufficient data to hypothesize as to the role of Sdh5 in this process. Biochemical studies have demonstrated that Sdh5 does not directly bind FAD, thus it seems unlikely that Sdh5 plays a role in physically delivering FAD to Sdh1. While the Sdh1 binding site on Sdh5 has been defined in the above NMR-based study, the region of Sdh1 that binds Sdh5 remains unknown. This information would provide insight into the role of Sdh5 in Sdh1 flavinylation, but for now we are

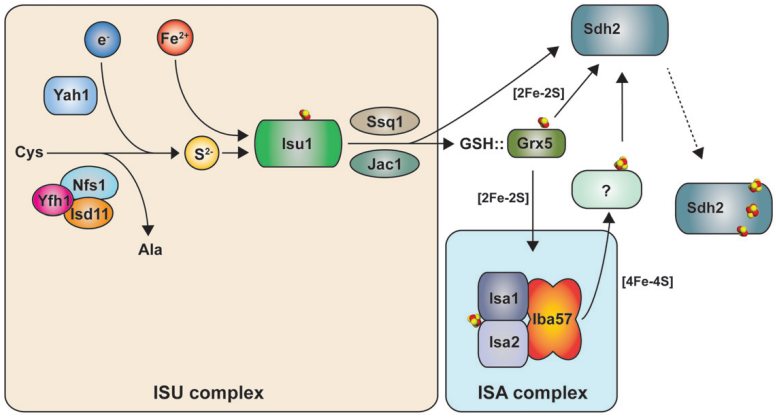

Figure 2. Iron-sulfur cluster synthesis and delivery to Sdh2. The tan box depicts the *de novo* synthesis of 2Fe–2S clusters within the ISU complex. Clusters are formed on the Isu1 scaffold protein with sulfide ions provided by the Nfs1 cysteine desulfurase and Yah1 ferredoxin. It is not clear how ferrous ions are delivered to the ISU complex. The preformed 2Fe–2S cluster is released from the scaffold complex through the actions of Hsp70 (Ssq1) and DnaJ (Jac1) to a transfer complex consisting of GSH-bound Grx5. The GSH–Grx5 delivers 2Fe–2S clusters to the ISA complex for the subsequent 4Fe–4S cluster synthesis depicted in the blue box. However, it is elusive whether the GSH-Grx5 is also required for 2Fe–2S cluster delivery to recipient proteins, in this case, Sdh2. It is also unknown whether the preformed 4Fe–4S clusters are directly delivered to Sdh2 or another factor is in need for this delivery step. All arrows with solid lines indicate transfer of components of Fe–S clusters or pre-formed Fe–S clusters.

forced to theorize as to such details. It seems likely that Sdh5 binds adjacent to the FAD binding site on apo-Sdh1, which could serve one or more of many possible roles. First, it could facilitate the non-covalent insertion of FAD into the pocket, which would enable subsequent autocatalytic covalent flavinylation. Second, Sdh5 could act as a chaperone for unflavinylated apo-Sdh1, thus supporting flavinylation by stabilizing apo-Sdh1 in a flavinylation-competent conformation. Finally, it is possible that Sdh5 might participate directly in the covalent flavinylation reaction by providing catalytic residues to this active site. Regardless of the precise mechanism, it is clear that Sdh5 specifically binds to apo-Sdh1 and is required for its covalent flavinylation (Figure 3).

Sdh8 is a chaperone for flavinylated Sdh1

Following Sdh5-dependent covalent flavinylation, Sdh1 is destined to form a soluble dimer with Sdh2; however, there remains a population of Sdh1 that exists in an unbound state free from any other core subunits in the mitochondrial matrix. It is likely that Sdh1 is present in excess to other core SDH subunits within the mitochondrial matrix as deletion of Sdh1 destabilizes the remaining core subunits, Sdh2, Sdh3 and Sdh4, while Sdh1 protein levels are maintained, albeit at a reduced level, upon deletion of any of the other core subunits. This free, flavinylated Sdh1 appears to be maintained in a soluble, assembly-competent state by a newly discovered, subunit-specific chaperone, Sdh8 (Figure 3).

SDH8 is conserved throughout eukaryotes and encodes a small protein that is localized to the mitochondrial matrix (Van Vranken *et al*., 2014). Yeast cells lacking Sdh8 exhibit slow growth on non-fermentable carbon sources but are still respiratory competent. The first observation that suggested a role for Sdh8 in SDH assembly or activity was its metabolomics phenotype. Yeast cells and *Drosophila* mutants lacking Sdh8 (or its ortholog) exhibit a significant but subtle block in the TCA cycle centered at SDH (i.e. an accumulation of succinate and a depletion of fumarate and malate, the two TCA cycle intermediates downstream of SDH). It is important to note that the magnitude of succinate accumulation is much less than a mutant lacking one of the four core subunits or Sdh5, which exhibits a complete loss of SDH activity. Consistent with this finding, *sdh8*Δ mutant yeast maintain approximately 40% of wild-type SDH activity and abundance of SDH holo-complexes. Interestingly, deletion of the *Drosophila* ortholog, *dSdhaf4*, causes a much more severe phenotype. These mutants accumulate significantly more succinate and have a ∼90% decrease in SDH activity, while assembled SDH complexes are nearly undetectable. Thus, while Sdh8 clearly supports SDH biogenesis, it does not appear to be absolutely required for assembling functional SDH complexes as some level of SDH activity is maintained in organisms lacking Sdh8 or its orthologs (Van Vranken *et al*., 2014).

While metabolomics clearly implicated Sdh8 in enabling SDH activity, the first evidence as to its particular function came when Sdh1 was discovered to be its primary binding partner. Further interrogation of the specificity of this interaction revealed that Sdh8 bound to Sdh1 independent of any other SDH core subunits and importantly, Sdh5. In addition, it was determined that the Sdh1–Sdh8 interaction depends on covalent flavinylation of Sdh1, as Sdh8 fails to interact with Sdh1 in an *sdh5*Δ background and also fails to interact with two covalent flavinylation-deficient Sdh1 mutants (H90S and H90A). BN-PAGE analysis further confirmed that Sdh8 is not associated with the SDH

DOI: 10.3109/10409238.2014.990556

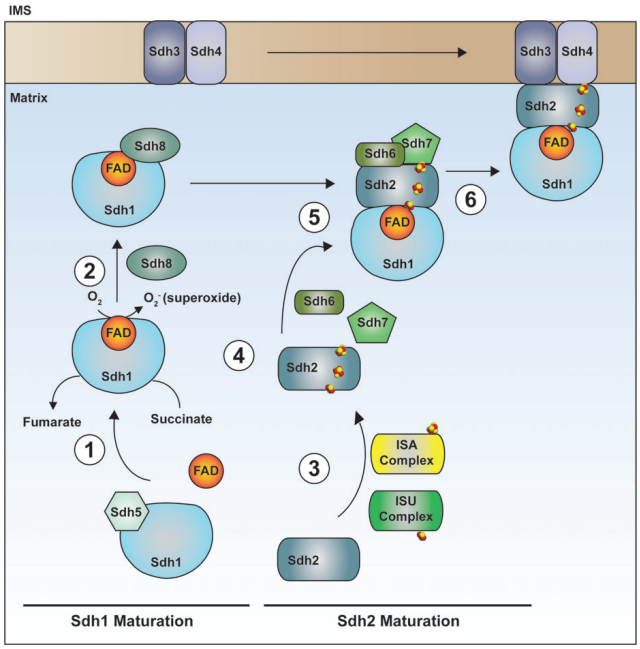

Figure 3. Model of the SDH assembly pathway. Each SDH core subunit is translated in the cytosol and must be subsequently translocated to the mitochondria. (1) Upon mitochondrial import, apo-Sdh1 is rapidly bound by the subunit-specific chaperone, Sdh5, forming a dimeric complex that supports covalent attachment of the FAD cofactor. (2) Following covalent flavinylation, the Sdh1–Sdh5 dimer disintegrates resulting in a pool of flavinylated Sdh1 that is unbound by any other core subunits. This leads to the formation of a complex comprised of Sdh1 and Sdh8, another subunit-specific chaperone. (3) The formation of this complex supports the formation of the subsequent Sdh1–Sdh2 soluble dimer and also prevents the spurious production of superoxide by flavinylated Sdh1. Meanwhile, apo-Sdh2 must also mature into a complex-competent subunit. This process involves the insertion of three Fe–S clusters generated by the ISU and ISA complexes. (4) Following maturation of Sdh2, it interacts with Sdh6 and Sdh7, which serve to protect exposed Fe–S clusters during the assembly process and (5) further associates with a mature Sdh1 subunit forming a heterotetrameric assembly intermediate. (6) Finally, the Sdh1–Sdh2 hydrophillic head docks to the IMM via interactions with the Sdh3–Sdh4 membrane anchor domain, which may or may not pre-assemble at the IMM. In the end, the concerted efforts of core subunits, dedicated assembly factors and other ancillary factors facilitate the stepwise assembly of SDH. (see colour version of this figure at www.informahealthcare.com/bmg).

holo-complex, but forms a stable subcomplex with Sdh1, which hyper-accumulates in *sdh2*Δ and *sdh4*Δ backgrounds. Consistent with this finding, Sdh8 steady-state protein levels also increase in these conditions, presumably to occupy the augmented pool of unbound and flavinylated Sdh1. Furthermore, deletion of Sdh1 causes significant destabilization of Sdh8, indicating that the stability of Sdh8 depends upon its ability to form a complex with Sdh1. Taken together, these data indicate that Sdh8 is a subunit-specific chaperone that occupies flavinylated Sdh1 prior to the formation of the Sdh1–Sdh2-soluble dimer (Van Vranken *et al*., 2014; Figure 3).

Why exactly does unbound Sdh1 require such a chaperone? The first evidence came from assessing the steady-state levels of SDH core subunits in the *sdh8*Δ mutant. While there was little or no destabilization of Sdh1, the primary binding partner of Sdh8, there was a marked decrease in the steady-state abundance of Sdh2. This was accompanied by, and probably a result of, a decrease in the Sdh1–Sdh2 soluble dimer as assessed by co-immunoprecipitation. Although this result is somewhat difficult to interpret, it suggests that the interaction between Sdh1 and Sdh8 facilitates the formation of the Sdh1–Sdh2 dimer by maintaining Sdh1 in a state that is competent for Sdh2 binding. Therefore, in the absence of Sdh8, Sdh1 does not interact as efficiently with Sdh2, which is unstable on its own. Interestingly, studies focused on *Drosophila dSdhaf4* demonstrate that this assembly factor is required for maintaining the stability of SdhA. Therefore, it is possible that in higher eukaryotes Sdh8 orthologs support the formation of the hydrophilic head by maintaining subunit stability. Overall, this data suggests that the chaperone activity of Sdh8 promotes SDH assembly by stabilizing Sdh1 and maintaining it in an assembly-competent state prior to interaction with Sdh2 (Van Vranken *et al*., 2014).

In addition to promoting formation of the Sdh1–Sdh2 dimer, Sdh8 might also function to prevent potentially deleterious interactions of free and flavinylated Sdh1 with the solvent. Indeed, studies focused on SDH have demonstrated that impaired electron transport at the level of the FAD can generate significant quantities of superoxide (Ishii *et al*., 2005; Messner & Imlay, 2002; Yankovskaya *et al*., 2003). Furthermore, previous studies in mammalian cells demonstrate that silencing of SDHB (Sdh2 ortholog), but not SDHA (Sdh1 ortholog) causes an increase in ROS levels (Guzy *et al*., 2008; Ishii *et al*., 2005). This increase in oxidative stress mediated by Sdh1 is thought to be dependent on the ability of the exposed FAD cofactor to interact with the surrounding solvent. In a phenomenon referred to as auto-oxidation, free Sdh1 oxidizes succinate to fumarate independent of the SDH holo-complex. This oxidation causes a reduction of the FAD cofactor, which then reduces molecular oxygen to form superoxide (Messner & Imlay, 2002). If Sdh8 functions to prevent Sdh1 auto-oxidation then overexpression of Sdh1 should be toxic to *sdh8*Δ mutant cells. In fact, Sdh1 overexpression proved toxic to both WT and *sdh8*Δ mutant cells; however, cells lacking Sdh8 were particularly sensitive

to this stress. Furthermore, overexpression of Sdh8 was capable of partially rescuing the toxicity associated with overexpressed Sdh1. Additional studies demonstrated that *sdh8*Δ mutant cells exhibited higher levels of oxidative stress and that the growth phenotype associated with *sdh8*Δ mutant cells was predominantly the result of oxidative stress rather than respiratory deficiency. Indeed, while overexpression of YAP1, a transcription factor involved in mediating oxidative stress, is capable of rescuing the *sdh8*Δ growth phenotype it fails to have any impact on the SDH deficiency of these cells (Van Vranken *et al*., 2014). Therefore, Sdh8 might have two important functions related to Sdh1. It appears to facilitate assembly with Sdh2 and may also function to seclude the FAD cofactor from the solvent, thus preventing spurious oxidation (Van Vranken *et al*., 2014).

Sdh2 – the electron wire

Architecture of Sdh2

Sdh2 (SDHB in mammals) is the Fe–S cluster-containing subunit of SDH. The crystal structure of porcine heart SDH demonstrates that SDHB contains two distinct domains (Sun *et al*., 2005; Figure 1). The N-terminal domain (residues 37–142; human sequence) consists of a single small α-helix and a five-strand β-sheet. This domain harbors the FAD-proximal 2Fe–2S center, which is ligated by Cys93, Cys98, Cys101 and Cys113. The C-terminal domain (residues 142–280) consists of six α-helices and harbors the 4Fe–4S and 3Fe–4S centers, which are coordinated by Cys186, Cys189, Cys192 and Cys253 and Cys196, Cys243 and Cys249, respectively. These three Fe–S centers essentially act as a wire that carries electrons from FAD to ubiquinone. SDHB also serves to connect the catalytic subunit, SDHA, with the hydrophobic anchor domain. Both the N-terminal domain and the C-terminal domain mediate the interaction with SDHA. Meanwhile, the C-terminal domain is mainly responsible for the interaction with the hydrophobic anchor domain. Importantly, SDHB contributes several residues to the ubiquinone-binding site, which otherwise is mediated by the hydrophobic anchor domain. In this way, the terminal 3Fe–4S center is poised adjacent to the ubiquinone to enable the final electron transfer (Sun *et al*., 2005).

Iron–sulfur cluster biogenesis

The aforementioned Fe–S clusters are key cofactors required for electron transfer from FAD to the Q_P site. Fe–S clusters are preformed in the mitochondrial matrix on a scaffold complex (ISU) consisting of four proteins, Nfs1, Isd11, Yfh1 and Isu1 (or Isu2; yeast nomenclature) (Lill *et al*., 2012; Schmucker *et al*., 2011; Tsai & Barondeau, 2010). The sulfide ions necessary for cluster biogenesis are provided by the Nfs1 cysteine desulfurase, along with its effector proteins Isd11 and Yfh1 (Pandey *et al*., 2012, 2013) and the Yah1 ferredoxin reductant (Sheftel *et al*., 2010). Fe(II) and sulfide ions form 2Fe–2S clusters on the Isu1 (or Isu2) scaffold proteins prior to transfer to client proteins. The preformed cluster is transferred to the monothiol Grx5, an Fe–S shuttle protein, through the binding of the DnaJ protein Jac1 to Isu1, which dissociates the ISU complex (Majewska *et al*., 2013) and the recruitment of the Hsp70 enzyme Ssq1. The cluster is released from Isu1 by the ATPase activity of Ssq1 (Ciesielski *et al*., 2012; Majewska *et al*., 2013; Uzarska *et al*., 2013). Grx5, which is pre-associated with Ssq1, transiently binds the 2Fe–2S cluster together with glutathione (GSH) for subsequent transfer steps (Banci *et al*., 2014; Johansson *et al*., 2011; Uzarska *et al*., 2013). The human ortholog of Jac1 was shown to also bind Fe–S client proteins, so Grx5-mediated cluster transfer may occur in pre-bound complexes with client proteins (Maio *et al*., 2014). Clusters consisting of 4Fe–4S and perhaps 3Fe–4S stoichiometries are matured on a downstream ISA scaffold complex consisting of Isa1, Isa2 and Iba57 (Gelling *et al*., 2008; Muhlenhoff *et al*., 2011; Sheftel *et al*., 2012) and perhaps Nfu1 (Cameron *et al*., 2011; Lill *et al*., 2012; Navarro-Sastre *et al*., 2011). Nfu1 is likely a targeting factor to Fe–S client proteins in bacteria (Py *et al*., 2012). Yeast depleted of ISU components or the Fe–S targeting factors Grx5, ISA components and Nfu1 are impaired in SDH activity (Jensen & Culotta, 2000; Muhlenhoff *et al*., 2011; Rodriguez-Manzaneque *et al*., 2002). Mutations in human orthologs of Isd11, Isu1, Iba57 or Nfu1 (Ajit Bolar *et al*., 2013; Cameron *et al*., 2011; Crooks *et al*., 2012; Ferrer-Cortes *et al*., 2013; Hall *et al*., 1993; Lim *et al*., 2013; Navarro-Sastre *et al*., 2011) or RNAi depletion of Isa1, or Isa2 lead to compromised SDH function (Sheftel *et al*., 2012; Figure 2).

Recently, mutations in a novel mitochondrial protein BolA3 were shown to result in defects in similar respiratory complexes and 2-oxoacid dehydrogenases as mutations in Nfu1 (Baker *et al*., 2014; Cameron *et al*., 2011), suggesting that BolA3 may likewise function in late stages of mitochondrial Fe–S biogenesis or transfer. BolA proteins typically function with glutaredoxins (Li & Outten, 2012), therefore, one prediction is that BolA3 has a role in conjunction with Grx5.

Sdh2 cofactor insertion

The architecture of Sdh2 raises several questions regarding cofactor insertion and maturation. Analogous to Sdh1, which receives its FAD cofactor within the mitochondrial matrix, Sdh2 receives its three Fe–S clusters in the matrix after import (Figure 3). Based on the Fe–S biogenesis pathway outlined above, one prediction is that the 2Fe–2S center in the N-terminal domain of Sdh2 is received from the Grx5:GSH complex, whereas the clusters in the C-terminal domain may be populated by the late-stage targeting factors ISA and Nfu1. Recently, Maio *et al*. (2014) reported that the mammalian Jac1 ortholog HSC20, the Ssq1 ortholog HSPA9 and the Isu1 scaffold, ISCU, form a complex with SDHB. This SDHB assembly intermediate was visualized on BN-PAGE after co-immunoprecipitation of SDHB. SDH activity appeared to be attenuated upon depletion of HSC20 or HSPA9 using siRNA knock down. Therefore, the study suggested that cluster transfer to SDHB occurs within this complex. *In vitro* synthesized SDHB is readily imported into isolated mitochondria. Co-immunoprecipitation of the imported SDHB at different time points revealed that the interaction of SDHA with SDHB comes later than the formation of the HSC20/HSPA9/ISCU/SDHB complex, indicating that cluster transfer

DOI: 10.3109/10409238.2014.990556

may precede binding of SDHB to SDHA. However, the ISA components and Nfu1 failed to be co-adsorbed with the HSC20 pulldown. These results may imply that only the 2Fe–2S center is transferred within the HSC20/HSPA9/ISCU/SDHB complex and a subsequent transfer step mediates insertion of the C-terminal SDHB clusters. This process could be either a zip-up from 2Fe–2S through 3Fe–4S or a zip-down from 3Fe–4S through 2Fe–2S. Alternatively, SDHB may remain associated with HSC20 during the insertion of the 4Fe–4S and 3Fe–4S centers, although the targeting factors may not stably associate with the HSC20/HSPA9/ISCU/SDHB complex (Maio *et al*., 2014).

It should be noted that reduced Cys thiolates are required for Fe–S clusters to be assembled into Sdh2 as oxidized Cys ligands cannot coordinate Fe–S clusters. However, it is unknown whether cells depend on the thioredoxin/thioredoxin reductase, glutathione/glutathione reductase or peroxiredoxin to ensure the presence of thiolates for Fe–S coordination. It is also intriguing how meta-stable Sdh2 intermediates are protected specially from ROS after Fe–S cluster insertion. It has been well known that Fe–S clusters are extremely susceptible for damage upon exposure to oxygen (Imlay, 2006). Since 2Fe–2S and 3Fe–4S clusters are exposed to solvent in Sdh2 prior to association with Sdh1 and the membrane anchor domain, it is possible that specialized chaperones are required to sequester these Fe–S clusters from oxidative stressors present in the solvent.

In the following section, we discuss two recently reported SDH assembly factors required for the maturation of Sdh2.

Sdh6 and Sdh7 are chaperone required for Sdh2 maturation

Sdh6 (SDHAF1 in human) is the first SDH assembly factor reported. Mutations in human SDHAF1 compromise the stable assembly of SDH, which leads to SDH deficiency associated with infantile leukoencephalophaty (Ghezzi *et al*., 2009, Ohlenbusch *et al*., 2012). Sdh6 is a small mitochondrial matrix protein that belongs to the LYR motif protein family, which is defined by the presence of a short LX(L/A)YRXX(L/I)(R/K) motif. Previous studies showed that the functions of several other LYR motif proteins are related to Fe–S cluster metabolism. Ghezzi *et al*. reported that yeast or human cells lacking wild-type Sdh6 (or its ortholog) exhibited significantly reduced SDH activity, accompanied by attenuation of SDH assembly (Ghezzi *et al*., 2009). They suggested the possibility that Sdh6 is an assembly factor required for the Fe–S containing subunit, Sdh2, based on the fact that Sdh6 is an LYR motif protein. While prescient, this hypothesis remained unproven as the biochemical data supporting it were not yet available. We recently reported that Sdh6 is indeed an assembly factor required for stable Sdh2 maturation during SDH assembly (Na *et al*., 2014). In yeast cells lacking Sdh6, Sdh2 steady-state levels were significantly diminished, but Sdh1 steady-state levels and covalent flavinylation remained unaffected. Moreover, Sdh6 appeared to accumulate in *sdh3*Δ or *sdh4*Δ cells lacking the SDH membrane anchor domain where an Sdh1/Sdh2 subcomplex accumulated. Furthermore, immunoprecipitation of Sdh6 in mitochondrial lysates from cells lacking Sdh4 resulted in co-precipitation of Sdh1 and Sdh2, but immunoprecipitation of Sdh6 in WT or *sdh2*Δ mutants failed to yield Sdh1 or Sdh2. Thus, these results suggested that Sdh6 interacts with an Sdh1/Sdh2 complex and the interface for the interaction resides within Sdh2 (Figure 3). Indeed, Sdh6 overexpression in *sdh1*Δ mutants, in which Sdh2 is extremely labile, increased Sdh2 accumulation, thus, corroborating the postulate that Sdh6 acts on Sdh2 during SDH assembly.

Why does Sdh2 require the function of Sdh6 during the process of SDH assembly? One possibility is that Sdh6 is a chaperone stabilizing Sdh2 prior to Sdh1 association. However, Sdh2 overexpression failed to restore SDH activity in *sdh6*Δ mutants. Thus, Sdh6 likely exerts its function on Sdh2 maturation rather simply maintaining an apo-Sdh2 pool. Unbiased high-copy genetic suppressor screening provided a hint regarding Sdh6 function (Na *et al*., 2014). Yap1, a transcription factor that increases expression of a repertoire of genes required for oxidative stress tolerance was recovered from this screen. Yap1 overexpression enhanced the respiratory growth of *sdh6*Δ mutants and restored SDH activity. Conversely, artificially increased superoxide generation in the presence of paraquat severely impaired the respiratory growth of *sdh6*Δ cells. Moreover, Sdh2 protein levels under this condition were dramatically decreased. Given that ROS levels were not increased in *sdh6*Δ mutants, this exacerbated phenotype with paraquat suggests that Sdh6 is important for protecting Sdh2 from ROS-induced damage.

In the meantime, a genetic interaction between Sdh6 and Acn9 (renamed Sdh7), another protein in the LYR motif protein family, was observed. Sdh7 is also a small mitochondrial matrix protein, required for normal respiratory growth. Overexpression of Sdh6 in *sdh7*Δ mutants slightly rescued the respiratory growth defect although overexpression of Sdh7 in *sdh6*Δ mutants failed to do so. Metabolite profiling suggested an SDH deficiency in *sdh7*Δ mutant cells as succinate accumulated in the mutants. BN-PAGE analysis and SDH activity assay confirmed SDH deficiency with reduced SDH complex levels in *sdh7*Δ mutants. Biochemical analysis of *sdh7*Δ mutants suggested that Sdh7 function is similar to that of Sdh6 (Na *et al*., 2014). Among the SDH structural subunits, the steady-state levels of Sdh2 were the most impaired in *sdh7*Δ mutants. Sdh7 exhibited increased abundance and interaction with the Sdh1/Sdh2 subcomplex in cells lacking the SDH membrane anchor. In addition, Yap1 overexpression restored SDH activity and paraquat supplement markedly attenuated Sdh2 steady-state levels in *sdh7*Δ cells. However, Sdh2 overexpression failed to restore SDH activity in *sdh7*Δ cells. Thus, these results suggested that Sdh7 is another assembly factor for protecting Sdh2 from ROS damage. Deletion of the *Drosophila melanogaster SDH7* ortholog, *dSdhaf3*, caused a dramatic SDH deficiency with muscular and neuronal defects that are reminiscent of neurodegeneration observed in humans with mutations in *SDHAF1* (Na *et al*., 2014).

It is clear that Sdh6 and Sdh7 support the assembly of SDH under normal physiological conditions, although their deficiencies do not result in total ablation of SDH biogenesis. This might be due to a theoretical bypass pathway that can substitute for Sdh6 and Sdh7 functions. Otherwise, the importance of these two assembly factors is limited with

passive roles for Sdh2 maturation under certain circumstances. Our study shows that iron salt supplementation enhances the respiratory growth of *sdh6*Δ cells and *sdh7*Δ cells. It has been shown that ROS-inactivated aconitase under aerobic conditions regains activity following iron salt supplementation (Kennedy *et al*., 1983). The active site of aconitase harbors a 4Fe–4S cluster, which loses one Fe atom upon exposure to superoxide, resulting in inactivation. Increased concentration of iron salts facilitates re-insertion of Fe(II) ion back into the damaged 3Fe–4S center, leading to reactivation of aconitase. Therefore, it is possible that Sdh6 and Sdh7 are involved in shielding the aforementioned solvent-exposed Fe–S centers from ROS until an Sdh1/Sdh2 complex is fully assembled with Sdh3 and Sdh4. A recent study on Fe–S cluster insertion to SDHB has revealed that SdhB (Sdh2) can be expressed as two separate domains *in vivo* and SDHAF1 (Sdh6) interacts with the C-terminal domain of SdhB, but not with the N-terminal domain (Maio *et al*., 2014). The C-terminal domain harbors 4Fe–4S and 3Fe–4S centers (Sun *et al*., 2005). Therefore, it is possible that Sdh6 is required for protecting the solvent-exposed 3Fe–4S center from ROS damage. However, there is no data suggesting how Sdh7 would exert its protection on Sdh2.

The origin of the damaging ROS is unclear, but a likely source is either the 2-oxoacid dehydrogenases including 2-oxoglutarate dehydrogenase and pyruvate dehydrogenase or the respiratory complexes (Quinlan *et al*., 2014). However, it is also possible that ROS generated intrinsically within an Sdh1/Sdh2 subcomplex might play a role. Like flavinylated monomeric Sdh1, an Sdh1/Sdh2 subcomplex is also competent to catalyze succinate oxidation (Lemire & Oyedotun, 2002; Nihei *et al*., 2001). It is expected that the electrons extracted from succinate oxidation can travel to Fe–S centers. Once the electrons reach the solvent-exposed surface via Fe–S centers, the electrons can react with oxygen to generate local ROS that can damage Fe–S centers in the vicinity. Therefore, one alternative role of Sdh6 and Sdh7 might be that they interact with an Sdh1/Sdh2 complex to inhibit the electron transfer to Fe–S centers within the subcomplex.

It has also been suggested that Sdh6 may be directly involved in the process for Fe–S insertion into Sdh2 based on the observation that the SDH assembly factor SDHAF1 (Sdh6) was recovered in the immunoadsorption of HSC20 (Maio *et al*., 2014). It remains unclear, however, whether SDHAF1 is a dedicated Fe–S targeting factor for SDHB since no additional evidence is available to show that Sdh6 has an active role in Fe–S cluster formation.

Sdh3 and Sdh4 – the hydrophobic anchor

Architecture of the hydrophobic anchor

The SDH membrane anchor consists of an Sdh3–Sdh4 heterodimer and an intercalated heme b moiety. The structure of mammalian SDH demonstrates that SDHC contains four total helices while SDHD contains five (Sun *et al*., 2005; Figure 1). The N-terminal helix of SDHD is localized to the mitochondrial matrix and interacts with SDHB to promote membrane localization of the hydrophilic dimer. Each subunit contributes two transmembrane helices to the formation of a four-helix bundle, which comprises the core of the membrane anchor, while the remaining transmembrane helix from each subunit flanks the core. The remaining helices from each subunit protrude from the membrane and arrange in antiparallel fashion in the IMS essentially capping the transmembrane core. In addition to the helical arrangement of this domain, the structure reveals that SDHC and SDHD coordinate a heme b cofactor at the interface of the core four-helix bundle, which interacts with the porphyrin ring. Each subunit contributes a conserved histidine residue that coordinates the heme iron while two arginine residues, one from SDHC and one from SDHD, as well as another histidine residue from SDHC interact with the heme propionate groups (Sun *et al*., 2005).

The membrane anchor domain contains the site of ubiquinone binding and reduction, which ultimately facilitates electron transfer from succinate to subsequent ETC complexes (Sun *et al*., 2005). In fact, this domain contains two ubiquinone binding sites that are distinguished by their disparate affinities for ubiquinone (Oyedotun & Lemire, 2001; Silkin *et al*., 2007). The high-affinity site (Q_P-proximal) lies on the matrix-proximal side of the IMM and is the dominant ubiquinone binding site (Figure 1). The Q_P site is composed of residues from SDHC, SDHD and SDHB including the terminal 3Fe–4S cluster of SDHB (Sun *et al*., 2005). The second binding site (Q_D-distal) lies closer to the IMS side of the IMM and is a lower affinity site. This site is composed entirely of residues from SDHD (Sun *et al*., 2005). Ubiquinone reduction occurs in two stepwise single electron transfers, in contrast to the two-electron reduction of FAD. Importantly, the Q_P site stabilizes the partially reduced semiquinone intermediate and facilitates full reduction of ubiquinone to ubiquinol, thereby preventing the generation of reactive oxygen species (ROS; Yankovskaya *et al*., 2003).

Assembly of the hydrophobic anchor

With respect to assembly of the hydrophobic anchor, there remain more questions than answers. Sdh3 and Sdh4 are translated in the cytosol and imported to mitochondria through the TOM complex. They may then be transferred to the TIM23 complex in the IMM and laterally released to the final destination like other α-helical transmembrane IMM proteins (Dudek *et al*., 2013). Unfortunately, membrane insertion represents the bulk of our knowledge regarding assembly of this dimer and thus many questions remain. Do Sdh3 and Sdh4 folding and subsequent dimer formation require a chaperone? How is the Sdh3–Sdh4 assembly intermediate stabilized prior to formation of the holocomplex? Although little is known about this process, it is intriguing that stable Sdh3/Sdh4 dimerization requires the hydrophilic domain as deletion of either Sdh1 or Sdh2 causes near complete loss of both Sdh3 and Sdh4 (Kim *et al*., 2012; Na *et al*., 2014). Thus, it appears that biogenesis of the hydrophobic anchor is in some manner connected to the rest of the assembly process.

Perhaps the most intriguing question regarding the hydrophobic anchor relates to the heme b cofactor. In fact, it is unclear whether heme b is actually required for the electron transfer from FAD to ubiquinone in the Q_P site. The heme b lies further away from the 3Fe–4S (13.3 Å) than the Q_P site

DOI: 10.3109/10409238.2014.990556

does (7.6 Å; Sun *et al*., 2005; Yankovskaya *et al*., 2003). Moreover, the redox potential of heme b (−185 mV) is much lower than the 3Fe–4S (+60 mV) in SDH (Hägerhäll, 1997). Therefore, these two barriers would make the electron transfer from 3Fe–4S to heme b thermodynamically unfavorable compared to the direct electron transfer to ubiquinone (+113 mV). In fact, SDH complexes lacking heme b (from yeast cells expressing Sdh3 H106A and Sdh4 C78A heme-ligand mutants) appeared to be able to catalyze succinate-dependent quinone reduction (Oyedotun *et al*., 2007). It should be noted, however, that the heme b is important for the structural integrity of the membrane anchor domain in mammalian cells. SDH and SDHD steady-state levels were decreased in cells expressing SDHC His-ligand mutants (H127A or H127Y) in the absence of wild-type SDHC (Lemarie *et al*., 2011).

Regardless of its precise function, the heme b cofactor is present in SDH across all species, suggesting its importance in either electron transfer or complex stability. However, it is not yet known how Sdh3 and Sdh4 are assembled with heme b in the IMM. Does an assembly factor deliver and/or insert the heme b into a pre-existing Sdh3/Sdh4 dimer? It has been shown that several assembly factors, including Coa1, Coa2 and Shy1, are required for proper heme insertion into the complex IV subunit Cox1 in the IMM (Atkinson *et al*., 2010; Mashkevich *et al*., 1997; Pierrel *et al*., 2007, 2008). Therefore, one might expect that an assembly factor is required for SDH hemylation. Overall, studies addressing the assembly of this domain represent an important next step in understanding SDH biogenesis.

Conclusion

Prior to the discovery of the assembly factors reviewed herein, it was difficult to fully appreciate the complexity of the SDH assembly pathway. This is perhaps best illustrated by the fact that at least four and quite possible more, dedicated assembly factors are required for the maturation of the two soluble subunits alone. This does not even consider the process of assembling the Sdh3–Sdh4 hydrophobic domain. In the end, the assembly of SDH does not happen spontaneously, but is rather the result of a highly intricate and stepwise process facilitated by the concerted efforts of a number of accessory assembly factors.

These discoveries have dramatically increased our understanding of the assembly process and allow us to propose a more complete model of the SDH assembly pathway (Ghezzi *et al*., 2009; Hao *et al*., 2009; Na *et al*., 2014; Van Vranken *et al*., 2014; Figure 3). Following cytosolic translation, Sdh1 and Sdh2 are imported into the mitochondrial matrix as apo-proteins. Each of these subunits must subsequently mature in a process that is facilitated by subunit-specific assembly factors. Upon import, Sdh1 must be flavinylated and is bound by Sdh5, which enables this process. Although the precise mechanism remains poorly defined, Sdh5 most likely maintains apo-Sdh1 in a confirmation that facilitates insertion and covalent binding of FAD. Once Sdh1 has been covalently flavinylated, Sdh5 is released and holo-Sdh1 binds another subunit-specific chaperone, Sdh8. Sdh8 appears to serve dual roles in the process of assembly. First, Sdh8 prevents the generation of superoxide by Sdh1 through limiting the spurious reduction of oxygen. In addition to this, Sdh8 also appears to facilitate the formation of the Sdh1–Sdh2 soluble dimer. Like Sdh1, apo-Sdh2 must also mature prior to complex formation. The initial step in the maturation of this subunit is the insertion of the three Fe–S clusters generated by the ISU and ISA complexes. At this point, both Sdh1 and Sdh2 have matured into holo-proteins and can proceed through the assembly process. Sdh2 comes into association with two additional chaperones, Sdh6 and Sdh7 as it forms a soluble complex with Sdh1, thereby displacing Sdh8 and generating a heterotetrameric assembly intermediate. This intermediate, which is facilitated by Sdh6 and Sdh7, serves to protect surface-exposed Fe–S clusters and possibly prevents the spurious generation of superoxide by the redox active Sdh1–Sdh2 dimer. Finally, the Sdh1–Sdh2 dimer is bound by the Sdh3–Sdh4 hydrophobic domain, which may or may not be pre-assembled in the IMM, bringing the hydrophilic head in close association with the IMM and forming the active holo-complex (Figure 3).

In general, the contribution of subunit-specific assembly factors to the process of SDH assembly can be organized into three distinct functions. First, they mediate the insertion of essential cofactors. All ETC complexes utilize cofactors to perform the redox chemistry necessary to oxidize and reduce substrates and transfer electrons. Therefore, the maturation of individual subunits and subsequent assembly of active complexes is dependent on the post-translational insertion of essential redox-active cofactors. This is highlighted by the fact that eukaryotic genomes have maintained a specific Sdh1/SDHA flavinylation factor, which is absolutely required for the covalent attachment of FAD to this subunit. It remains to be determined whether Sdh6 or Sdh7 also has an active role in the insertion of one or more of the Fe–S clusters in Sdh2.

Second, assembly factors act as subunit-specific chaperones that stabilize individual subunits and assembly intermediates. The process of SDH, and more generally, ETC assembly, relies on the step-wise assembly of potentially dozens of individual subunits translated from two different genomes to form a single intricately constructed complex. As the structures of individual subunits are optimized to exist and function in the context of fully assembled complexes, it is not surprising that individual subunits and sub-complexes require chaperones to maintain stability during assembly. In terms of SDH assembly, this has been validated by discovery of specific factors that mediate the stability of both individual subunits and multimeric assembly intermediates. Indeed, work in *Drosophila* has demonstrated that the fly ortholog of Sdh8 is required for stabilization of holo-SdhA. Furthermore, the requirement for stabilizing holo-assembly intermediates is more manifested in the case of assembly intermediates containing oxidatively labile cofactors such as Fe–S centers. Sdh6 and Sdh7 appear to specifically bind and stabilize the Sdh1–Sdh2 soluble dimer prior to membrane association via Sdh3/Sdh4.

Third, assembly factors serve to prevent spurious and potentially deleterious interactions between individual redox-active subunits and the surrounding solvent. As a result of the unique chemistry enabled by their cofactors, individual ETC complex subunits are potentially toxic when not secluded

within a fully assembled complex. Indeed, the cell contains numerous protein complexes that need to be assembled in an organized fashion; however, dedicated assembly factors are much more common for those complexes in which individual subunits contain redox-active cofactors. This is highlighted by the role of Sdh8 as a chaperone for covalently flavinylated Sdh1. In isolation, flavinylated Sdh1 is capable of oxidizing succinate, which results in the spurious generation of superoxide upon reduction of molecular oxygen. By occupying free Sdh1, Sdh8 serves to minimize these deleterious chemical reactions, thus protecting the matrix from ROS. Sdh6 and Sdh7, which specifically bind the potentially redox-active Sdh1–Sdh2 dimer, could potentially mediate similar protection as Sdh8.

In addition to providing valuable insights into the SDH assembly pathway the recent discovery of SDH assembly factors has also facilitated a greater understanding of SDH-deficient pathologies (Table 1). The literature has many reports of patients with SDH deficiencies; however, it is clear that only a subset of these cases can be explained by mutations in the genes encoding the four core subunits. With the discovery of a number of proteins intimately involved in the SDH assembly pathway, this disparity may now start to be resolved. Indeed, it is now clear that loss of function mutations in SDH assembly factors are capable of causing the same pathologies as the core subunits themselves. Analogous to mutations in *SDHA*, mutations in *SDHAF1*, the human ortholog of *SDH6*, were discovered as a cause of leukoencephalopathy, a neurodegenerative disorder similar to Leigh Syndrome (Ghezzi *et al*., 2009). Furthermore, mutations in *SDHAF2*, the human ortholog of *SDH5*, were shown to be the causative lesion in at least two families with familial paraganglioma syndrome, mirroring the physiological consequences of core subunit mutations (Hao *et al*., 2009). Currently, there are no published reports describing human mutations in *SDHAF3* (*SDH7*) or *SDHAF4* (*SDH8*); however, these genes have only recently been implicated in the SDH assembly pathway. We suspect that, in time, mutations in these genes will ultimately be discovered in patients with SDH-deficient pathologies, thus further clarifying the connection between succinate dehydrogenase and human disease.

Declaration of interest

The authors report no declaration of interest.

References

Ajit Bolar N, Vanlander AV, Wilbrecht C, *et al*. (2013). Mutation of the iron-sulfur cluster assembly gene IBA57 causes severe myopathy and encephalopathy. Hum Mol Genet 22:2590–602.

Alston CL, Davison JE, Meloni F, *et al*. (2012). Recessive germline SDHA and SDHB mutations causing leukodystrophy and isolated mitochondrial complex II deficiency. J Med Gen 49:569–77.

Astuti D, Latif F, Dallol A, *et al*. (2001). Gene mutations in the succinate dehydrogenase subunit SDHB cause susceptibility to familial pheochromocytoma and to familial paraganglioma. Am J Hum Genet 69:49–54.

Atkinson A, Khalimonchuk O, Smith P, *et al*. (2010). Mzm1 influences a labile pool of mitochondrial zinc important for respiratory function. J Biol Chem 285:19450–9.

Bafunno V, Giancaspero TA, Brizio C, *et al*. (2004). Riboflavin uptake and FAD synthesis in *Saccharomyces cerevisiae* mitochondria: involvement of the Flx1p carrier in FAD export. J Biol Chem 279: 95–102.

Baker II PR,, Friederich MW, Swanson MA, *et al*. (2014). Variant non ketotic hyperglycinemia is caused by mutations in LIAS, BOLA3 and the novel gene GLRX5. Brain 137:366–79.

Banci L, Brancaccio D, Ciofi-Baffoni S, *et al*. (2014). [2Fe-2S] cluster transfer in iron-sulfur protein biogenesis. Proc Natl Acad Sci USA 111:6203–8.

Baysal BE. (2000). Mutations in SDHD, a mitochondrial complex II gene, in hereditary paraganglioma. Science 287:848–51.

Bourgeron T, Rustin P, Chretien D, *et al*. (1995). Mutation of a nuclear succinate dehydrogenase gene results in mitochondrial respiratory chain deficiency. Nat Genet 11:144–9.

Brandsch R, Bichler V. (1989). Covalent cofactor binding to flavoenzymes requires specific effectors. Eur J Biochem 182:125–8.

Burnichon N, Briere JJ, Libe R, *et al*. (2010). SDHA is a tumor suppressor gene causing paraganglioma. Hum Mol Genet 19: 3011–20.

Cameron JM, Janer A, Levandovskiy V, *et al*. (2011). Mutations in iron-sulfur cluster scaffold genes NFU1 and BOLA3 cause a fatal deficiency of multiple respiratory chain and 2-oxoacid dehydrogenase enzymes. Am J Hum Genet 89:486–95.

Cecchini G, Schroder I, Gunsalus RP, Maklashina E. (2002). Succinate dehydrogenase and fumarate reductase from *Escherichia coli*. Biochim Biophys Acta 1553:140–57.

Ciesielski SJ, Schilke BA, Osipiuk J, *et al*. (2012). Interaction of J-protein co-chaperone Jac1 with Fe-S scaffold Isu is indispensable in vivo and conserved in evolution. J Mol Biol 417:1–12.

Crooks DR, Jeong SY, Tong WH, *et al*. (2012). Tissue specificity of a human mitochondrial disease: differentiation-enhanced mis-splicing of the Fe-S scaffold gene ISCU renders patient cells more sensitive to oxidative stress in ISCU myopathy. J Biol Chem 287:40119–30.

Diaz F, Kotarsky H, Fellman V, Moraes CT. (2011). Mitochondrial disorders caused by mutations in respiratory chain assembly factors. Semin Fetal Neonatal Med 16:197–204.

Dudek J, Rehling P, van der Laan M. (2013). Mitochondrial protein import: common principles and physiological networks. BBA-Mol Cell Res 1833:274–85.

Eletsky A, Jeong M-Y, Kim H, *et al*. (2012). Solution NMR structure of yeast succinate dehydrogenase flavinylation factor Sdh5 reveals a putative Sdh1 binding site. Biochemistry 51:8475–7.

Fernandez-Vizarra E, Tiranti V, Zeviani M. (2009). Assembly of the oxidative phosphorylation system in humans: what we have learned by studying its defects. Biochim Biophys Acta 1793:200–11.

Ferrer-Cortes X, Font A, Bujan N, *et al*. (2013). Protein expression profiles in patients carrying NFU1 mutations. Contribution to the pathophysiology of the disease. J Inherit Metab Dis 36:841–7.

Gelling C, Dawes IW, Richhardt N, *et al*. (2008). Mitochondrial Iba57p is required for Fe/S cluster formation on aconitase and activation of radical SAM enzymes. Mol Cell Biol 28:1851–61.

Ghezzi D, Goffrini P, Uziel G, *et al*. (2009). SDHAF1, encoding a LYR complex-II specific assembly factor, is mutated in SDH-defective infantile leukoencephalopathy. Nat Genet 41:654–6.

Guzy RD, Sharma B, Bell E, *et al*. (2008). Loss of the SdhB, but Not the SdhA, subunit of complex II triggers reactive oxygen species-dependent hypoxia-inducible factor activation and tumorigenesis. Mol Cell Biol 28:718–31.

Hägerhäll C. (1997). Succinate:quinone oxidoreductases. variations on a censerved theme. Biochim Biophys Acta 1320:107–41.

Hall RE, Henriksson KG, Lewis SF, *et al*. (1993). Mitochondrial myopathy with succinate dehydrogenase and aconitase deficiency. Abnormalities of several iron-sulfur proteins. J Clin Invest 92:2660–6.

Hao HX, Khalimonchuk O, Schraders M, *et al*. (2009). SDH5, a gene required for flavination of succinate dehydrogenase, is mutated in paraganglioma. Science 325:1139–42.

Hoekstra AS, Bayley J-P. (2013). The role of complex II in disease. Biochim Biophys Acta Bioenergetics 1827:543–51.

Horváth R, Abicht A, Holinski-Feder E, *et al*. (2006). Leigh syndrome caused by mutations in the flavoprotein (Fp) subunit of succinate dehydrogenase (SDHA). J Neurol Neurosurg Psychiatry 77:74–6.

Imlay JA. (2006). Iron-sulphur clusters and the problem with oxygen. Mol Microbiol 59:1073–82.

Ishii T, Yasuda K, Akatsuka A, *et al*. (2005). A mutation in the SDHC gene of complex II increases oxidative stress, resulting in apoptosis and tumorigenesis. Cancer Res 65:203–9.

DOI: 10.3109/10409238.2014.990556

Jackson CB, Nuoffer J-M, Hahn D, *et al*. (2014). Mutations in SDHD lead to autosomal recessive encephalomyopathy and isolated mitochondrial complex II deficiency. J Med Genet 51:170–5.

Jain-Ghai S, Cameron JM, Al Maawali A, *et al*. (2013). Complex II deficiency – a case report and review of the literature. Am J Med Genet A 161A:285–94.

Janeway KA, Kim SY, Lodish M, *et al*. (2011). Defects in succinate dehydrogenase in gastrointestinal stromal tumors lacking KIT and PDGFRA mutations. Proc Natl Acad Sci USA 108:314–18.

Jensen LT, Culotta VC. (2000). Role of *Saccharomyces cerevisiae* ISA1and ISA2 in iron homeostasis. Mol Cell Biol 20:3918–27.

Johansson C, Roos AK, Montano SJ, *et al*. (2011). The crystal structure of human GLRX5: iron-sulfur cluster co-ordination, tetrameric assembly and monomer activity. Biochem J 433:303–11.

Kennedy MC, Emptage MH, Dreyer JL, Beinert H. (1983). The role of iron in the activation-inactivation of aconitase. J Biol Chem 258: 11098–105.

Kim HJ, Jeong MY, Na U, Winge DR. (2012). Flavinylation and assembly of succinate dehydrogenase are dependent on the C-terminal tail of the flavoprotein subunit. J Biol Chem 287:40670–9.

Kim HJ, Winge DR. (2013). Emerging concepts in the flavinylation of succinate dehydrogenase. Biochim Biophys Acta 1827:627–36.

Kounosu A. (2014). Analysis of covalent flavinylation using thermostable succinate dehydrogenase from *Thermus thermophilus* and *Sulfolobus tokodaii* lacking SdhE homologs. FEBS Lett 588:1058–63.

Lemarie A, Huc L, Pazarentzos E, *et al*. (2011). Specific disintegration of complex II succinate: ubiquinone oxidoreductase links pH changes to oxidative stress for apoptosis induction. Cell Death Differ 18: 338–49.

Lemire BD, Oyedotun KS. (2002). The *Saccharomyces cerevisiae* mitochondrial succinate: ubiquinone oxidoreductase. Biochim Biophys Acta 1553:102–16.

Li H, Outten CE. (2012). Monothiol CGFS glutaredoxins and BolA-like proteins: [2Fe-2S] binding partners in iron homeostasis. Biochemistry 51:4377–89.

Lill R, Hoffmann B, Molik S, *et al*. (2012). The role of mitochondria in cellular iron-sulfur protein biogenesis and iron metabolism. Biochim Biophys Acta 1823:1491–508.

Lim SC, Friemel M, Marum JE, *et al*. (2013). Mutations in LYRM4, encoding iron-sulfur cluster biogenesis factor ISD11, cause deficiency of multiple respiratory chain complexes. Hum Mol Genet 22:4460–73.

Maio N, Singh A, Uhrigshardt H, *et al*. (2014). Cochaperone binding to LYR motifs confers specificity of iron sulfur cluster delivery. Cell Metab 19:445–57.

Majewska J, Ciesielski SJ, Schilke B, *et al*. (2013). Binding of the chaperone Jac1 protein and cysteine desulfurase Nfs1 to the iron-sulfur cluster scaffold Isu protein is mutually exclusive. J Biol Chem 288:29134–42.

Mashkevich G, Repetto B, Glerum DM, *et al*. (1997). SHY1, the yeast homolog of the mammalian SURF-1 gene, encodes a mitochondrial protein required for respiration. J Biol Chem 272:14356–64.

Messner KR, Imlay JA. (2002). Mechanism of superoxide and hydrogen peroxide formation by fumarate reductase, succinate dehydrogenase, and aspartate oxidase. J Biol Chem 277:42563–71.

Muhlenhoff U, Richter N, Pines O, *et al*. (2011). Specialized function of yeast Isa1 and Isa2 proteins in the maturation of mitochondrial [4Fe-4S] proteins. J Biol Chem 286:41205–16.

Na U, Yu W, Cox JE, *et al*. (2014). The LYR factors SDHAF1 and SDHAF3 mediate maturation of the iron-sulfur subunit of succinate dehydrogenase. Cell Metab 20:253–66.

Navarro-Sastre A, Tort F, Stehling O, *et al*. (2011). A fatal mitochondrial disease is associated with defective NFU1 function in the maturation of a subset of mitochondrial Fe-S proteins. Am J Hum Genet 89: 656–67.

Nihei C, Nakayashiki T, Nakamura K, *et al*. (2001). Abortive assembly of succinate-ubiquinone reductase (complex II) in a ferrochelatase-deficient mutant of *Escherichia coli*. Mol Genet Genomics 265: 394–404.

Ohlenbusch A, Edvardson S, Skorpen J, *et al*. (2012). Leukoencephalopathy with accumulated succinate is indicative of SDHAF1 related complex II deficiency. Orphanet J Rare Dis 7:69.

Oyedotun KS, Lemire BD. (2001). The Quinone-binding sites of the *Saccharomyces cerevisiae* succinate-ubiquinone oxidoreductase. J Biol Chem 276:16936–43.

Oyedotun KS, Sit CS, Lemire BD. (2007). The *Saccharomyces cerevisiae* succinate dehydrogenase does not require heme for ubiquinone reduction. Biochim Biophys Acta 1767:1436–45.

Pandey A, Golla R, Yoon H, *et al*. (2012). Persulfide formation on mitochondrial cysteine desulfurase: enzyme activation by a eukaryote-specific interacting protein and Fe-S cluster synthesis. Biochem J 448: 171–87.

Pandey A, Gordon DM, Pain J, *et al*. (2013). Frataxin directly stimulates mitochondrial cysteine desulfurase by exposing substrate-binding sites, and a mutant Fe-S cluster scaffold protein with frataxin-bypassing ability acts similarly. J Biol Chem 288:36773–86.

Pantaleo MA, Astolfi A, Indio V. (2011). SDHA loss-of-function mutations in KIT-PDGFRA wild-type gastrointestinal stromal tumors identified by massively parallel sequencing. J Natl Cancer Inst 103: 983–7.

Pantaleo MA, Astolfi A, Urbini M, *et al*. (2014). Analysis of all subunits, SDHA, SDHB, SDHC, SDHD, of the succinate dehydrogenase complex in KIT/PDGFRA wild-type GIST. Eur J Hum Genet 22:32–9.

Peczkowska M, Cascon A, Prejbisz A, *et al*. (2008). Extra-adrenal and adrenal pheochromocytomas associated with a germline SDHC mutation. Nat Clin Pract End Met 4:111–15.

Pierrel F, Bestwick ML, Cobine PA, *et al*. (2007). Coa1 links the Mss51 post-translational function to Cox1 cofactor insertion in cytochrome c oxidase assembly. EMBO J 26:4335–46.

Pierrel F, Khalimonchuk O, Cobine PA, *et al*. (2008). Coa2 is an assembly factor for yeast cytochrome c oxidase biogenesis that facilitates the maturation of Cox1. Mol Cell Biol 28:4927–39.

Py B, Gerez C, Angelini S, *et al*. (2012). Molecular organization, biochemical function, cellular role and evolution of NfuA, an atypical Fe-S carrier. Mol Microbiol 86:155–71.

Quinlan CL, Goncalves RL, Hey-Mogensen M, *et al*. (2014). The 2-oxoacid dehydrogenase complexes in mitochondria can produce superoxide/hydrogen peroxide at much higher rates than complex I. J Biol Chem 289:8312–25.

Robinson KM, Lemire BD. (1996). Covalent attachment of FAD to the yeast succinate dehydrogenase flavoprotein requires import into mitochondria, presequence removal, and folding. J Biol Chem 271: 4055–60.

Robinson KM, Rothery RA, Weiner JH, Lemire BD. (1994). The covalent attachment of FAD to the flavoprotein of *Saccharomyces cerevisiae* succinate dehydrogenase is not necessary for import and assembly into mitochondria. Eur J Biochem 222:983–90.

Rodriguez-Manzaneque MAT, Tamarit J, Bellí G, *et al*. (2002). Grx5 is a mitochondrial glutaredoxin required for the activity of iron/sulfur enzymes. Mol Biol Cell 13:1109–21.

Rutter J, Winge DR, Schiffman JD. (2010). Succinate dehydrogenase – assembly, regulation and role in human disease. Mitochondrion 10: 393–401.

Santos MAA, Jiménez A, Revuelta J. (2000). Molecular characterization of FMN1, the structural gene for the monofunctional flavokinase of *Saccharomyces cerevisiae*. J Biol Chem 275:28618–24.

Schmucker S, Martelli A, Colin F, *et al*. (2011). Mammalian frataxin: an essential function for cellular viability through an interaction with a preformed ISCU/NFS1/ISD11 iron-sulfur assembly complex. PLoS One 6:e16199.

Sheftel AD, Stehling O, Pierik AJ, *et al*. (2010). Humans possess two mitochondrial ferredoxins, Fdx1 and Fdx2, with distinct roles in steroidogenesis, heme, and Fe/S cluster biosynthesis. Proc Natl Acad Sci USA 107:11775–80.

Sheftel AD, Wilbrecht C, Stehling O, *et al*. (2012). The human mitochondrial ISCA1, ISCA2, and IBA57 proteins are required for [4Fe-4S] protein maturation. Mol Biol Cell 23:1157–66.

Silkin Y, Oyedotun KS, Lemire BD. (2007). The role of Sdh4p Tyr-89 in ubiquinone reduction by the Saccharomyces cerevisiae succinate dehydrogenase. Biochim Biophys Acta 1767:143–50.

Sun F, Huo X, Zhai Y, *et al*. (2005). Crystal structure of mitochondrial respiratory membrane protein complex II. Cell 121:1043–57.

Torchetti EM, Brizio C, Colella M, *et al*. (2010). Mitochondrial localization of human FAD synthetase isoform 1. Mitochondrion 10: 263–73.

Tsai CL, Barondeau DP. (2010). Human frataxin is an allosteric switch that activates the Fe-S cluster biosynthetic complex. Biochemistry 49: 9132–9.

Tzagoloff A, Jang J, Glerum DM, Wu M. (1996). FLX1 codes for a carrier protein involved in maintaining a proper balance of flavin nucleotides in yeast mitochondria. J Biol Chem 271:7392–7.

Uzarska MA, Dutkiewicz R, Freibert SA, *et al*. (2013). The mitochondrial Hsp70 chaperone Ssq1 facilitates Fe/S cluster transfer from Isu1 to Grx5 by complex formation. Mol Biol Cell 24: 1830–41.

Van Vranken JG, Bricker DK, Dephoure N, *et al*. (2014). SDHAF4 promotes mitochondrial succinate dehydrogenase activity and prevents neurodegeneration. Cell Metab 20:241–52.

Vanharanta S, Buchta M, Mcwhinney SR, *et al*. (2004). Early-onset renal cell carcinoma as a novel extraparaganglial component of SDHB-associated heritable paraganglioma. Am J Hum Genet 74:153–9.

Wu M, Repetto B, Glerum DM, Tzagoloff A. (1995). Cloning and characterization of FAD1, the structural gene for flavin adenine dinucleotide synthetase of *Saccharomyces cerevisiae*. Mol Cell Biol 15:264–71.

Yankovskaya V, Horsefield R, Tornroth S, *et al*. (2003). Architecture of succinate dehydrogenase and reactive oxygen species generation. Science 299:700–4.

CHAPTER 3

SDHAF4 PROMOTES MITOCHONDRIAL SUCCINATE DEHYDROGENASE ACTIVITY AND PREVENTS NEURODEGENERATION

Jonathan G. Van Vranken, Daniel K. Bricker, Noah Dephoure, Steven P. Gygi, James E. Cox, Carl S. Thummel, and Jared Rutter

Reprinted with permission from Cell Metabolism, vol. 20, pp. 241-52

Cell Metabolism
Article

SDHAF4 Promotes Mitochondrial Succinate Dehydrogenase Activity and Prevents Neurodegeneration

Jonathan G. Van Vranken,[1,5] Daniel K. Bricker,[2,5] Noah Dephoure,[3] Steven P. Gygi,[3] James E. Cox,[4] Carl S. Thummel,[2,*] and Jared Rutter[1,*]
[1]Department of Biochemistry
[2]Department of Human Genetics
University of Utah School of Medicine, Salt Lake City, UT 84112, USA
[3]Department of Cell Biology, Harvard University Medical School, Boston, MA 02115, USA
[4]Metabolomics Core Research Facility, University of Utah School of Medicine, Salt Lake City, UT 84112, USA
[5]Co-first authors
*Correspondence: carl.thummel@genetics.utah.edu (C.S.T.), rutter@biochem.utah.edu (J.R.)
http://dx.doi.org/10.1016/j.cmet.2014.05.012

SUMMARY

Succinate dehydrogenase (SDH) occupies a central place in cellular energy production, linking the tricarboxylic cycle with the electron transport chain. As a result, a subset of cancers and neuromuscular disorders result from mutations affecting any of the four SDH structural subunits or either of two known SDH assembly factors. Herein we characterize an evolutionarily conserved SDH assembly factor designated Sdh8/SDHAF4, using yeast, *Drosophila*, and mammalian cells. Sdh8 interacts specifically with the catalytic Sdh1 subunit in the mitochondrial matrix, facilitating its association with Sdh2 and the subsequent assembly of the SDH holocomplex. These roles for Sdh8 are critical for preventing motility defects and neurodegeneration in *Drosophila* as well as the excess ROS generated by free Sdh1. These studies provide insights into the mechanisms by which SDH is assembled and raise the possibility that some forms of neuromuscular disease may be associated with mutations that affect this SDH assembly factor.

INTRODUCTION

Mitochondria are dynamic organelles that are essential for many cellular processes including metabolism, signal transduction, and apoptosis. Consistent with these broad cellular functions, mitochondrial dysfunction is associated with a wide range of human diseases, including diabetes, neurodegeneration, and cancer. These important roles have led to comprehensive characterization of the mitochondrial proteome, identifying more than 1,000 nuclear-encoded proteins (Sickmann et al., 2003; Pagliarini et al., 2008). In spite of these efforts, however, many mitochondrial proteins remain uncharacterized, including proteins that are conserved throughout eukaryotic evolution. We are studying this subset of proteins as part of a systematic effort to comprehensively understand mitochondrial physiology. Herein, we describe the function of one of these evolutionarily conserved proteins and demonstrate that it is essential for proper succinate dehydrogenase (SDH) complex assembly and activity in yeast, flies, and mammalian cells.

SDH is unique in that it functions in both the tricarboxylic acid (TCA) cycle and the electron transport chain (ETC), wherein it is referred to as Complex II. SDH links the oxidation of succinate to fumarate in the TCA cycle with the reduction of ubiquinone to ubiquinol in the ETC, which contributes to the establishment of the mitochondrial membrane potential and ATP synthesis. SDH is a heterotetrameric protein complex that is embedded in the inner mitochondrial membrane (IMM), with its catalytic domain facing the mitochondrial matrix. The complex is anchored to the IMM by two integral membrane proteins, Sdh3 (SDHC in humans) and Sdh4 (SDHD). The Sdh3/Sdh4 dimer binds the peripheral membrane protein Sdh2 (SDHB), which tethers the catalytic Sdh1 (SDHA) subunit to the complex. Sdh1 harbors a covalently bound FAD cofactor that is required for the oxidation of succinate (Robinson et al., 1994). The two electrons that result from succinate oxidation are channeled through the three iron-sulfur clusters in Sdh2 to ubiquinone, which interacts with SDH via the Sdh3/Sdh4 membrane anchor (Rutter et al., 2010).

The assembly of complexes like SDH presents the cell with the problem of coordinating the synthesis and stepwise interactions of individual subunits to form an intricate membrane-bound complex. This problem is exacerbated in the case of ETC complexes, as individual subunits contain redox-active cofactors that can perform inappropriate and deleterious reactions when they are not properly secluded within the native complex. As a result, a number of dedicated factors assist the assembly of these complexes by facilitating cofactor insertion, preventing nonproductive interactions, and stabilizing assembly intermediates. While the importance of assembly factors for Complexes I and IV are well established (Fernández-Vizarra et al., 2009; Diaz et al., 2011), dedicated SDH assembly factors have only recently begun to emerge with the discovery of SDHAF1 (Sdh6 in yeast) and SDHAF2 (Sdh5; Ghezzi et al., 2009; Hao et al., 2009). Human

patients with loss-of-function mutations in *SDHAF1* or *SDHAF2* display reduced SDH complex levels and activity and present with infantile leukoencephalopathy and neuroendocrine tumors, respectively (Ghezzi et al., 2009; Hao et al., 2009). This is consistent with the spectrum of diseases that associate with mutations affecting the core subunits of SDH—*SDHA*, *SDHB*, *SDHC*, and *SDHD* (Rutter et al., 2010) and with a series of additional diseases that are characterized by loss of SDH activity, but which lack mutations in known SDH genes (Jain-Ghai et al., 2013). Disruption of the yeast orthologs for *SDHAF1* or *SDHAF2* (*SDH6* or *SDH5*) prevents respiratory-dependent growth, with a clear defect in SDH activity. While the precise mechanism by which Sdh6 supports SDH biogenesis has remained elusive, Sdh5 was shown to be required for the covalent attachment of the FAD cofactor to Sdh1 (Ghezzi et al., 2009; Hao et al., 2009). The current model proposes that Sdh1 is flavinated by Sdh5 and binds iron-sulfur-loaded Sdh2, which then docks onto the preassembled membrane-bound Sdh3-Sdh4 dimer to form the holocomplex (Rutter et al., 2010). We hypothesized that the complexity of this assembly process likely necessitates the action of additional dedicated assembly factors and that the genes encoding these factors may contribute to the currently idiopathic SDH-associated genetic diseases.

With the goal of discovering new human disease genes and gaining a better understanding of SDH assembly and activity, we have focused on our ongoing functional elucidation of uncharacterized mitochondrial proteins. These studies led us to identify an evolutionarily conserved SDH assembly factor, Ybr269, which we have renamed Sdh8 in yeast and SDHAF4 in higher organisms. Utilizing yeast, flies, and mammalian cells, we have defined the molecular function of the SDHAF4 protein family in SDH assembly and an important role for SDHAF4 in metazoan physiology.

RESULTS

Yeast Sdh8 Is a Conserved Mitochondrial Matrix Protein Required for Maximal SDH Activity

Sdh8 is a small protein of approximately 15 kDa that belongs to a pan-eukaryotic protein family, which we have named the SDHAF4 family (Figure S1A available online). N- and C-terminal Sdh8 fusion proteins were unable to complement the phenotype of an *sdh8*Δ mutant strain and were therefore deemed to be nonfunctional. Efficient rescue was seen, however, when either a tandem affinity tag (His_6HA_3) or GFP was fused into a predicted unstructured region within Sdh8, between residues N82 and S83. These constructs, which were subsequently named Sdh8-His_6HA_3 and Sdh8-GFP, respectively, were expressed under the control of the native *SDH8* promoter and terminator and determined to be fully functional (See Figures 1A and S1E). As expected, we found that Sdh8 localizes exclusively to mitochondria and determined it to be a soluble matrix protein (Figures S1B–S1D). To begin to assess the role of Sdh8 in mitochondrial function, an *sdh8*Δ mutant was established in two strains (BY4741 and W303), both of which were used for key experiments to control for genetic background. While *sdh8*Δ mutants grew normally in glucose medium, growth was impaired on glycerol and acetate, demonstrating a defect in mitochondrial respiration (Figures 1A and S1E). Interestingly, the growth impairment was exacerbated on acetate-containing medium, which is a hallmark of mutants that affect SDH activity. Consistent with this possibility, metabolomic analysis of *sdh8*Δ mutants revealed an apparent block in the TCA cycle at SDH, with an accumulation of succinate and depletion of the two TCA cycle intermediates downstream of SDH: fumarate and malate (Figures 1B and S1F–S1H). We also measured the enzymatic activity of SDH in mitochondria harvested from wild-type (WT) and *sdh8*Δ cells. SDH activity in *sdh8*Δ cells was decreased 60% relative to WT (Figure 1C), while malate dehydrogenase (MDH) activity was unaffected (Figure 1D). Finally, the steady-state level of the SDH holocomplex was assessed by blue native polyacrylamide gel electrophoresis (BN-PAGE). Mitochondria purified from either WT or *sdh8*Δ cells were solubilized in digitonin, resolved by BN-PAGE, and probed by immunoblot. We observed a marked decrease in assembled SDH and demonstrated that re-expression of Sdh8-His_6HA_3 (see Supplemental Information) in *sdh8*Δ cells was sufficient to rescue the defect in SDH assembly (Figures 1E and S1I). Taken together, these data demonstrate that Sdh8 is required for the stability and activity of SDH.

As a first step toward determining if its function is conserved across eukaryotic species, the human and *Drosophila* orthologs of *SDH8* (*SDHAF4* and *dSdhaf4*, respectively) were expressed in the *sdh8*Δ mutant under the control of the native *SDH8* promoter and terminator. Both orthologs complement the *sdh8*Δ growth defects (Figure 1F), suggesting that the role of Sdh8 in SDH assembly is an evolutionarily conserved feature of the SDHAF4 family.

Mammalian SDHAF4 Is Required for Maximal SDH Activity

To assess a possible role for mammalian SDHAF4 in SDH function, we transfected C2C12 mouse myoblasts with a nontargeting control siRNA (control) or either of two siRNAs targeting mouse SDHAF4 (si1 and si2). Knockdown of *SDHAF4* mRNA was confirmed (Figure 2A), and mitochondria were harvested from cells transfected with control, si1, and si2 siRNAs. Immunoblot of the isolated mitochondria revealed that depletion of SDHAF4 did not affect the steady-state abundance of SDHA or SDHB (Figure S2A). We detected, however, a decrease in SDH enzymatic activity in *SDHAF4* knockdown cells (Figure 2B) with no significant change in MDH activity (Figure S2B). In addition, cells transfected with si1 or si2 showed a reproducible and specific decrease in steady-state SDH complexes as assayed by BN-PAGE of a magnitude similar to that seen in SDH activity (Figure 2C). We conclude that SDHAF4 is required for the proper assembly and activity of SDH in both yeast and mammalian cells.

Drosophila Sdhaf4 Is Required for Maximal SDH Activity

To further define the function of Sdh8 in a multicellular organism, we extended our analysis to *Drosophila*. Three null alleles were generated in the *Drosophila* ortholog of *SDH8* (*CG7224*) that we have renamed *Drosophila Sdhaf4* (*dSdhaf4*) (Figure S3A). Similar to our findings in yeast, metabolomic analysis of *dSdhaf4* mutants compared to genetically matched controls revealed a significant accumulation of succinate and depletion of malate and fumarate (Figure 3A). Acetyl-CoA was also elevated, while citrate and isocitrate were reduced in the mutants (Figure 3A). These effects may be due to a reduction in oxaloacetate that is

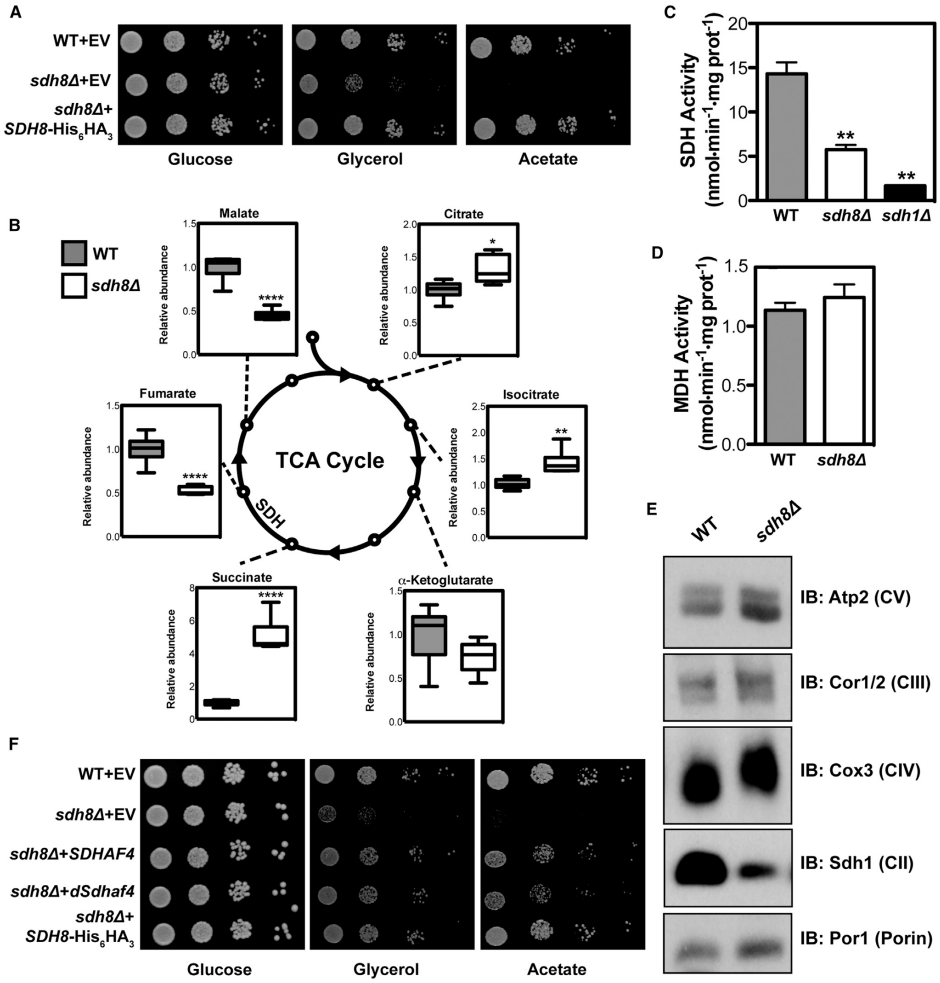

Figure 1. Yeast Sdh8 Is a Conserved Mitochondrial Matrix Protein Required for Maximal SDH Activity and Assembly

(A) Ten-fold serial dilutions of WT yeast transformed with an empty vector (EV) or *sdh8*Δ mutants transformed with either EV or a plasmid expressing SDH8-His_6HA_3, all in a BY4741 background.

(B) GC/MS was used to measure the abundance of metabolites in WT and *sdh8*Δ yeast (BY4741 background. n = 6 biological replicates. ****$p < 0.0001$; **$p < 0.005$; *$p < 0.05$).

(C and D) (C) SDH and (D) MDH enzyme assays were performed on mitochondrial extracts of WT, *sdh8*Δ, and *sdh1*Δ strains, normalized to total protein (±SEM. n = 3 biological replicates. **$p < 0.005$).

(E) WT and *sdh8*Δ mitochondria were solubilized in digitonin, fractionated by BN-PAGE, and analyzed by immunoblotting to detect Atp2 (complex V), Cor1/2 (complex III), Cox3 (complex IV), Sdh1 (complex II), or Porin.

(F) Ten-fold serial dilutions of the indicated strains were grown as in (A). *SDHAF4* and *dSdhaf4* are the human and *Drosophila* orthologs of *SDH8*, respectively, and were each expressed under the control of the endogenous *SDH8* promoter and terminator.

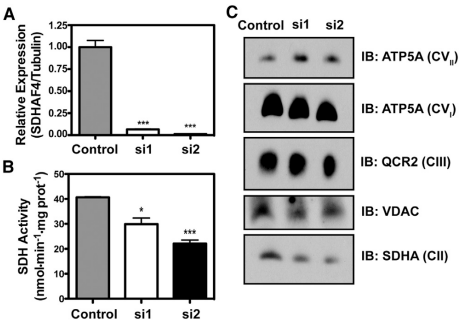

Figure 2. Mammalian SDHAF4 Is Required for Maximal SDH Activity

(A) C2C12 cells were transfected with either a control nontargeting siRNA or either of two siRNAs directed against *SDHAF4* (si1 and si2), and *SDHAF4* mRNA abundance was assayed by quantitative RT-PCR and normalized to tubulin mRNA (±SEM. n = 3 biological replicates. ***$p < 0.0005$).

(B) SDH enzyme activity was measured in mitochondria harvested from C2C12 cells treated as in (A) (±SEM. n = 3 biological replicates. ***$p < 0.0005$; *$p < 0.05$).

(C) Mitochondria extracted from C2C12 cells treated as in (A) were solubilized in digitonin, fractionated by BN-PAGE, and analyzed by immunoblotting for ATP5A (complex V monomers [CV_I] or dimers [CV_{II}], QCR2 [complex III], VDAC, or SDHA [complex II]).

required for the formation of citrate from acetyl-CoA. Consistent with this, aspartate, which is interconvertible with oxaloacetate, is depleted in *dSdhaf4* mutants (Figure S3C). Similar changes were observed upon metabolomic analysis of flies carrying a *dSdhaf4* TALEN-induced allele over an independently derived imprecise excision, indicating that these results remain constant across genetic backgrounds (Figures S3B and S3C). Consistent with this metabolomic profile, *dSdhaf4* mutant mitochondria displayed an 85% reduction in SDH activity (Figure 3B) while citrate synthase (CS) activity was unaffected (Figure 3C). Based on these data, we conclude that, like yeast *sdh8*Δ mutants, *dSdhaf4* mutants have a specific impairment in SDH function.

Drosophila Sdhaf4 Is Required for the Stability of SdhA and SdhB

The decrease in SDH activity in *dSdhaf4* mutants is greater than that seen in yeast *sdh8*Δ mutants, suggesting that there might be a more profound effect on the steady-state level of SDH. Consistent with this, the SDH holocomplex was undetectable by BN-PAGE, whereas the levels of Complex V were unaffected (Figure 4A). This lack of SDH holocomplex was accompanied by an apparent reduction in the stability of the SdhA and SdhB subunits in *dSdhaf4* mutants (Figures 4B, S4A, and S4B). In contrast, *dSdhaf4* heterozygous mutants displayed similar SDH activity to controls (Figure S4C), and *dSdhaf4* overexpression had no effect on SDH activity or SDH subunit protein levels (Figures S4D and S4E).

The reduced levels of SDH subunits in the *dSdhaf4* mutant suggest that we might see genetic interactions between *dSdhaf4* alleles and mutations in SDH subunit-encoding genes. Consistent with this, we found that *dSdhaf4* mutant flies heterozygous for a strong loss-of-function mutation in *SdhA* or homozygous for a hypomorphic mutation in *SdhB* displayed reduced viability compared to controls (Figures 4C and S4F). This genetic interaction is specific for SDH subunit-encoding genes, as *dSdhaf4* mutants heterozygous for a null allele of *CoVa* (Mandal et al., 2005) displayed normal viability (Figure 4C). Taken together, these biochemical and genetic studies indicate that dSdhaf4 is required for SDH assembly and activity.

dSdhaf4 Mutants Display Neurodegeneration, Early-Adult Lethality, and Sensitivity to Oxidative Stress

Consistent with their metabolic defects, *dSdhaf4* mutants died significantly earlier than controls, with a median lifespan of 12 days compared to a median lifespan of 69 days for control flies (Figure 5A). Interestingly, these mutants also displayed two phenotypes that are hallmarks of mitochondrial dysfunction: bang sensitivity and erect wings (Figures 5B, 5C, S5A, and S5B) (Greene et al., 2003; Fergestad et al., 2006). In addition, *dSdhaf4* mutant retinas displayed a marked disorganization of retinal architecture (Figure 5D, asterisks), consistent with the known association between bang sensitivity and neurodegeneration (Celotto et al., 2006a; Gnerer et al., 2006; Liu et al., 2007). The photoreceptors were also highly vesicularized (Figure 5D, arrows) (Kiselev et al., 2000), with aberrant mitochondrial morphology (Figure 5D, arrowheads). The bang sensitivity of *dSdhaf4* mutants can be rescued by specific expression of WT *dSdhaf4* in neurons, suggesting that it is associated with the neurodegeneration (Figures 5E, S5C, and S5D). Moreover, global expression of human *Sdhaf4* in *dSdhaf4* mutants partially rescued the bang-sensitivity of these animals, providing further evidence of a conserved function for *Sdhaf4* (Figures 5E, S5C, and S5D). Taken together, these results demonstrate that dSdhaf4 is required in neurons to maintain tissue architecture and function.

Defects in mitochondrial ATP production and reactive oxygen species (ROS) homeostasis have been previously shown to cause neurodegenerative phenotypes similar to those observed in *dSdhaf4* mutants (Fergestad et al., 2006; Liu et al., 2007; Celotto et al., 2012). Since loss of *dSdhaf4* does not appear to affect steady state ATP levels (Figures 3A and S3B), we hypothesized that dSdhaf4 may be required to protect against ROS toxicity. Consistent with this, *dSdhaf4* mutants were highly sensitive to oxidative stress induced by hyperoxia (Figure 5F) but showed no sensitivity to starvation, which is unassociated with ROS production (Figure S5E). These data suggest a connection between the role of dSdhaf4 in SDH assembly and oxidative stress resistance.

Yeast Sdh8 Is a Chaperone for Soluble and Covalently Flavinated Sdh1

Data from three distinct eukaryotic systems indicate that the SDHAF4 protein family plays an evolutionarily conserved role in SDH assembly and activity. Turning back to yeast, we sought to understand the mechanism by which Sdh8 supports SDH biogenesis. To identify proteins interacting with Sdh8, we performed a large-scale HA immunoprecipitation from either WT or Sdh8-His_6HA_3 containing mitochondria. The final eluates were resolved by SDS-PAGE, revealing a band of ~70 kDa that was present only in the Sdh8-His_6HA_3 immunoprecipitation.

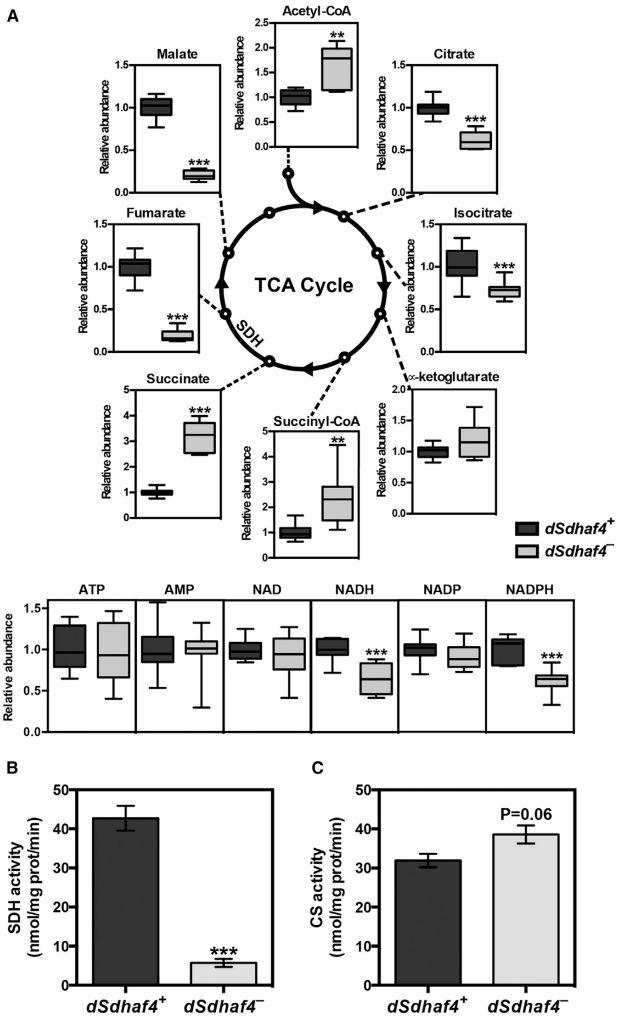

Figure 3. *Drosophila Sdhaf4* Is Required for SDH Activity

(A) Either LC/MS (acetyl-CoA, succinyl-CoA, ATP, AMP, NAD, NADH, NADP, and NADPH) or GC/MS (citrate, isocitrate, alpha-ketoglutarate, succinate, fumarate, and malate) was used to measure the abundance of metabolites in *trans*-heterozygous $dSdhaf4^{1/2}$ ($dSdhaf4^{-}$) mutants compared to genetically matched w^{1118} controls ($dSdhaf4^{+}$). Eight to twelve biological replicates from two independent experiments were combined per genotype.

(B and C) (B) SDH or (C) CS enzymatic activity was measured in extracts from mitochondria isolated from either control or *dSdhaf4* mutant flies (±SEM. n = 4–6 biological replicates. **p < 0.01 and ***p < 0.001). Two independent experiments were performed with similar results.

Using mass spectrometry, we found that this band contained Sdh1, the catalytic subunit of SDH (Figure S6A). The putative Sdh8/Sdh1 interaction was confirmed by immunoprecipitation of Sdh8 followed by identification of Sdh1 in the eluate using an Sdh1-specific antibody (Figure 6A, lanes 1 and 6 versus 2 and 7). Interestingly, it appears that Sdh2 is not a member of this complex as it is undetectable in the eluate (Figure 6A).

Since Sdh8 binds Sdh1 independent of Sdh2, we hypothesized that Sdh8 may be acting as a chaperone for a free soluble pool of Sdh1 in the mitochondrial matrix. If this is true, then deletion of *SDH2* might shift Sdh1 to a free soluble form, which would increase the demand for Sdh8 function. Consistent with this possibility, *sdh2*Δ mutant mitochondria exhibit an accumulation of Sdh8-His_6HA_3 (Figure 6B, lane 1 versus 3), while *sdh1*Δ mutant mitochondria exhibit a depletion of Sdh8-His_6HA_3 (Figure 6B, lane 1 versus 2). Furthermore, this accumulation of Sdh8-His_6HA_3 results in enhanced Sdh1-Sdh8 association in the *sdh2*Δ mutant (Figure 6A, lanes 2 and 7 versus 3 and 8) despite an approximately 2-fold decrease in steady-state Sdh1 levels (Figure 6B, lane 1 versus 3).

Although the stability of Sdh8 depends on Sdh1, Sdh1 abundance is unaffected by the deletion of *SDH8* (Figure 6B, lane 1 versus 4). However, Sdh2 levels are reduced in an *sdh8*Δ mutant, likely due to decreased Sdh1 competence for interaction with Sdh2 (Figure 6B, lane 1 versus 4). This is further supported by the observation that the formation of the Sdh1-Sdh2 soluble dimer, which is readily apparent in a mutant lacking the Sdh4 membrane anchor, is impaired in an *sdh8*Δ mutant (Figure S6F). Interpretation of this experiment is complicated by the decreased Sdh2 steady-state level in the *sdh8*Δ mutant, but the data are most consistent with the hypothesis that Sdh8 is required to maintain Sdh1 in a state that is fully competent to bind Sdh2 and assemble in the SDH holocomplex.

Sdh1 is known to be covalently flavinated at H90 in a reaction that requires the activity of Sdh5 (Hao et al., 2009). Initially, we found that deletion of *SDH8* does not impact the flavination of Sdh1 (Figure S6B). We reasoned, however, that Sdh8 might act specifically on the flavinated form of free Sdh1. Accordingly,

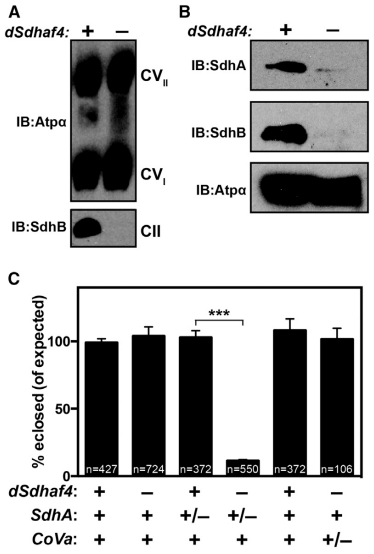

Figure 4. *Drosophila Sdhaf4* Is Required for SdhA and SdhB Stability

(A) Mitochondrial extracts from either w^{1118} controls (*dSdhaf4*$^{+}$) or *dSdhaf4*$^{1/2}$ mutants (*dSdhaf4*$^{-}$) were fractionated by BN-PAGE and analyzed by immunoblotting to detect Atpα (Complex V) or SdhB (Complex II).

(B) Total protein from mitochondria isolated from either control or *dSdhaf4* mutant flies was resolved using SDS-PAGE, followed by immunoblotting to detect SdhA, SdhB, or Atpα.

(C) Flies carrying either control or *dSdhaf4* mutant chromosomes over a balancer chromosome were crossed to flies carrying a strong loss-of-function allele for either *SdhA* or *Cytochrome c oxidase Va subunit* (*CoVa*) over a balancer. The resulting progeny were scored for the absence or presence of the marker linked to the balancer chromosome. The proportion of the expected progeny that eclosed, based on Mendelian ratios of the indicated genotypes, is shown. (±SEM. n = number of progeny assayed from each cross. ***$p < 0.001$ (Student's t test).

we immunoprecipitated Sdh8-His$_6$HA$_3$ from mitochondria that express WT Sdh1, Sdh1^{H90A}, or Sdh1^{H90S}, which are Sdh1 mutants that cannot covalently bind FAD. Indeed, Sdh1^{H90A} and Sdh1^{H90S} both failed to copurify with Sdh8-His$_6$HA$_3$ (Figures 6A, lanes 2 and 7 versus 4 and 9, and S6C), even in the absence of Sdh2 (Figure 6A, lanes 3 and 8 versus 5 and 10). In further support of this hypothesis, we found that Sdh1 failed to interact with Sdh8-His$_6$HA$_3$ in *sdh5*Δ mutant cells (Figure S6D), which lack covalent Sdh1 flavination (Figure S6B) (Hao et al., 2009). Furthermore, Sdh8-His$_6$HA$_3$ was destabilized in the *sdh5*Δ mutant as was observed for the *sdh1*Δ mutant (Figure S6E, lane 1 versus 6).

Finally, Sdh8-His$_6$HA$_3$ is not present in the SDH holocomplex, as assayed by BN-PAGE (Figure 6C, lane 1). We also observed that deletion of *SDH2* or *SDH4*, which ablates the SDH holocomplex, causes the emergence of a subcomplex of ~150 kDa, which lacks Sdh2 but clearly contains both Sdh1 and Sdh8 (Figure 6C, lanes 2 and 5). This is not coincidental comigration as loss of either Sdh1 or Sdh8 causes this subcomplex to disappear from *sdh2*Δ and *sdh4*Δ mutant strains (Figure 6C, lanes 3, 4, 6, and 7). The Sdh1-Sdh8 subcomplex can also be detected in WT cells, albeit at lower steady-state levels than in *sdh2*Δ and *sdh4*Δ mutants (Figure S6G). Taken together, these data demonstrate that Sdh8 interacts specifically with flavo-Sdh1, independent of other components of the SDH complex, and its stability depends upon this interaction.

Sdh8 Protects the Cell from Oxidative Stress

The data presented thus far demonstrate that Sdh8 acts as a chaperone for Sdh1 to promote formation of the Sdh1-Sdh2 dimer. We found that overexpression of Sdh1 does not rescue the growth defects of *sdh8*Δ mutants but, rather, is toxic to both WT and *sdh8*Δ cells on respiratory carbon sources, with the *sdh8*Δ mutant being particularly sensitive (Figures 7A and S7A). This observation raises the possibility that free Sdh1 is toxic and that Sdh8 may alleviate this toxicity. To test this, we co-overexpressed Sdh8 with Sdh1 and observed a significant rescue of the Sdh1 toxicity in WT cells (Figure 7B). We conclude that, in addition to promoting assembly of the Sdh1-Sdh2 dimer, Sdh8 also prevents the toxicity associated with free Sdh1.

In considering possible mechanisms for toxicity of free Sdh1, we hypothesized that the exacerbated *sdh8*Δ phenotype on acetate compared to glycerol medium (Figure 1A) may be the result of increased oxidative stress. This is consistent with previous reports using acetate to trigger ROS-dependent cell death in yeast (Carmona-Gutierrez et al., 2010), as well as the sensitivity of *dSdhaf4* mutant to hyperoxia (Figure 5F). In support of this hypothesis, we found that the *sdh8*Δ mutant is profoundly hypersensitive to paraquat in glycerol media relative to WT cells (Figure 7C). To test this hypothesis directly, we sought to quantify the levels of ROS in the *sdh8*Δ mutant. We observed a significant decrease in aconitase activity in *sdh8*Δ cells, consistent with an accumulation of ROS in the mutant strain (Figure 7D). We also established a system for measuring the redox state of yeast mitochondria using a mitochondrially targeted redox-sensitive GFP construct (mito-roGFP) (McFaline-Figueroa et al., 2011; Vevea et al., 2013). This construct has been engineered to contain two surface exposed cysteines that are capable of forming a disulfide bond. Mito-roGFP exhibits two excitation peaks at ~400nm and ~480nm with a single emission peak at ~510nm. Oxidation of the surface-exposed cysteines promotes excitation at 400 nm, while reduction of these residues favors excitation at 480 nm (Figures S7B and S7C) (McFaline-Figueroa et al., 2011; Vevea et al., 2013). Thus, the excitation ratio of mito-roGFP is a measure of the redox state of yeast mitochondria in live cells. To quantify the redox state of the matrix, we transformed WT cells, *sdh8*Δ cells, and *sdh8*Δ cells expressing Sdh8-His$_6$HA$_3$ with mito-roGFP (Figure S7D). Cells were grown in the presence of 2% acetate and analyzed by flow cytometry. Consistent with the aconitase activity data, we observed an increase in the ratio of oxidized/reduced mito-roGFP in the *sdh8*Δ strain that was fully rescued by re-expressing Sdh8-His$_6$HA$_3$ (Figures 7E and 7F). If this impaired growth of the *sdh8*Δ mutant is the result of the elevated ROS seen in these cells, then overexpression of genes involved in ROS detoxification might suppress the growth phenotype. Consistent with this, overexpression of *YAP1*, a transcription factor that stimulates the expression of many genes

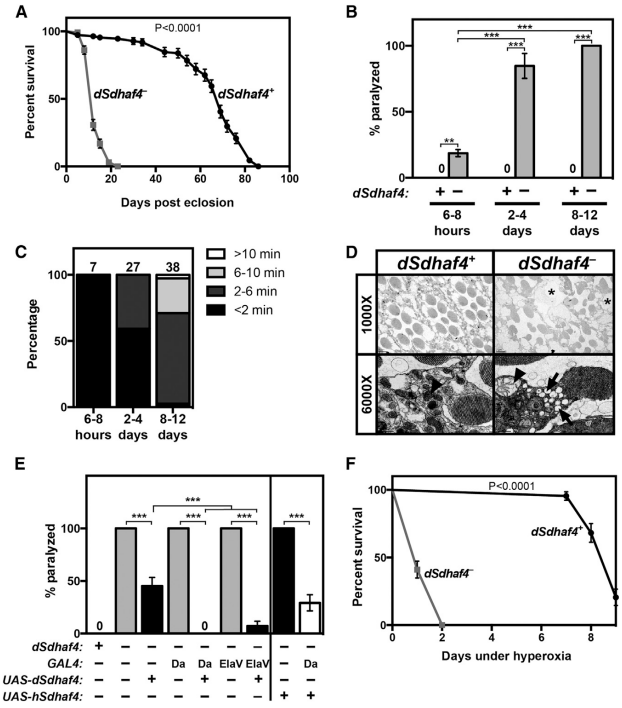

Figure 5. *Drosophila Sdhaf4* Mutants Display Neurodegenerative Phenotypes, Early-Adult Lethality, and Sensitivity to Oxidative Stress

(A) The number of surviving w^{1118} control (*dSdhaf4*$^{+}$) or *dSdhaf4*$^{1/2}$ mutant (*dSdhaf4*$^{-}$) females maintained on standard laboratory food at normoxia was assayed at 2–4 day intervals. Each data point is the percentage of surviving flies ±SEM, with at least 110 flies assayed per genotype.

(B) Control or *dSdhaf4* mutant females aged 6–8 hr, 2–4 days, or 8–12 days were vortexed for 15 s, and the percentage of paralyzed flies was counted as described (Ganetzky and Wu, 1982). (±SEM. n > 32 flies per age per genotype. **p < 0.01 and ***p < 0.001 [ANOVA].)

(C) The length of time required for the *dSdhaf4* mutant flies in (A) to recover from paralysis is presented as a bar graph, with the number of paralyzed *dSdhaf4* mutants analyzed from each age group depicted above the bar.

(D) Cross-sections of compound eyes from 8- to 12-day-old control or *dSdhaf4* mutant flies visualized by transmission electron microscopy. Arrows point to aberrant vesicularization of *dSdhaf4* mutant photoreceptors, arrowheads point to mitochondria, and asterisks denote vacuoles.

(E) control or *dSdhaf4* mutant flies at 8–12 days of age carrying either the ubiquitous *Daughterless-Gal4* (*Da-GAL4*) driver, the pan-neuronal *Elav*-Gal4 driver, or no driver, in the presence or absence of either a *UAS-dSdhaf4* transgene or a *UAS-human Sdhaf4* (*hSdhaf4*) transgene, were vortexed as in (A). Note that *UAS-dSdhaf4* alone has leaky *dSdhaf4* activity since it partially rescues in the absence of a GAL4 driver. (±SEM. n = 15–40. ***p < 0.001 [ANOVA].)

(F) Control or *dSdhaf4* mutant females at 2–4 days of age were transferred to 100% oxygen, and the number of surviving animals was counted each day. The median lifespan after transfer to hyperoxia is 9 days for controls and 1 day for *dSdhaf4* mutants. Data are shown as the percentage of surviving flies ±SEM. At least 40 flies were assayed per genotype. p values for both survival curves ([A] and [F]) were calculated using a log rank test.

important for oxidative stress defense (including *TRR1*, *TRX2*, *GSH1*, and *GLR1*), as well as the mitochondrial superoxide dismutase *SOD2*, completely or partially rescued the growth phenotype of *sdh8*Δ cells (Figures 7G and S7E). Interestingly, despite a profound ability to rescue the growth phenotype associated with *sdh8*Δ cells, *YAP1* overexpression has no effect on SDH activity (Figure 7H), SDH assembly (Figure S7F), or Sdh2 steady-state levels (Figure S7G). Thus, we conclude that the ability of *YAP1* to rescue the *sdh8*Δ mutant phenotype is not related to SDH activity and likely due to an amelioration of oxidative stress in the mutant cells.

DISCUSSION

The critical role of SDH in primary cellular metabolism is reflected by the variety of diseases associated with its dysfunction. Unlike other ETC complexes, which require multiple factors for their assembly, only two factors, SDHAF1 and SDHAF2, have been identified to date that are required for the assembly of the SDH holocomplex within the IMM (Ghezzi et al., 2009; Hao et al., 2009). Herein we use three distinct eukaryotic model systems, yeast, *Drosophila*, and mammalian cells, to demonstrate that the SDHAF4 protein family consists of evolutionarily conserved SDH assembly factors. We show that Sdh8 binds directly to flavinated Sdh1, blocking the generation of excess ROS and facilitating its interaction with Sdh2 and the subsequent assembly of the SDH holocomplex. These functions for SDHAF4 appear to be conserved in metazoans and suggest a role for this factor in disease, as *Drosophila Sdhaf4* mutants display muscular and neuronal dysfunction as well as neurodegeneration.

Yeast *sdh8*Δ and *Drosophila Sdhaf4* mutants exhibit the classic metabolomic phenotype of SDH deficiency, with an apparent block in the TCA cycle that results in an accumulation of succinate and a depletion of fumarate and malate, the two TCA cycle intermediates downstream of SDH. Consistent with these effects, the yeast and fly mutants display a reduction in the steady-state levels of the SDH holocomplex and reduced SDH enzyme activity, indicating an important role for SDHAF4 in SDH stability and activity. siRNA-mediated knockdown of SDHAF4 in mammalian cells leads to similar defects. Moreover,

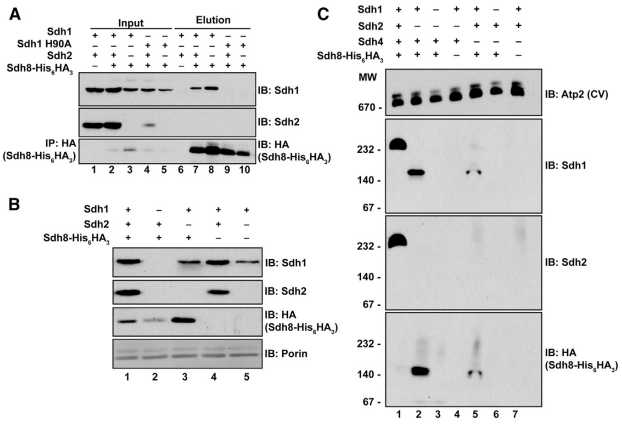

Figure 6. Yeast Sdh8 Is a Cochaperone for Unbound and Covalently Flavinated Sdh1

(A) Sdh8-His_6HA_3 was immunoprecipitated from digitonin-solubilized mitochondria isolated from the yeast strains described as follows: lanes 1 and 6, WT cells; lanes 2 and 7, *sdh8*Δ cells expressing Sdh8-His_6HA_3; lanes 3 and 8, *sdh2*Δ *sdh8*Δ cells expressing Sdh8-His_6HA_3; lanes 4 and 9, *sdh1*Δ *sdh8*Δ cells expressing Sdh8-His_6HA_3 and $Sdh1^{H90A}$; and lanes 5 and 10, *sdh1*Δ *sdh2*Δ *sdh8*Δ cells expressing Sdh8-His_6HA_3 and $Sdh1^{H90A}$.

(B) Mitochondrial lysates isolated from the following strains were fractionated by SDS-PAGE. Lane 1, *sdh8*Δ cells expressing Sdh8-His_6HA_3; lane 2, *sdh1*Δ *sdh8*Δ cells expressing Sdh8-His_6HA_3; lane 3, *sdh2*Δ *sdh8*Δ cells expressing Sdh8-His_6HA_3; lane 4, *sdh8*Δ cells; lane 5, *sdh2*Δ *sdh8*Δ cells (BY4741 background). Steady-state protein abundance was assessed by immunoblot using antibodies against Sdh1, Sdh2, and HA (Sdh8-His_6HA_3).

(C) Mitochondria isolated from the following yeast strains were solubilized in digitonin and fractionated by BN-PAGE: lane 1, *sdh8*Δ cells expressing Sdh8-His_6HA_3; lane 2, *sdh2*Δ *sdh8*Δ cells expressing Sdh8-His_6HA_3; lane 3, *sdh1*Δ *sdh2*Δ *sdh8*Δ cells expressing Sdh8-His_6HA_3; lane 4, *sdh2*Δ *sdh8*Δ; lane 5, *sdh4*Δ *sdh8*Δ cells expressing Sdh8-His_6HA_3; lane 6, *sdh1*Δ *sdh4*Δ *sdh8*Δ cells expressing Sdh8-His_6HA_3; and lane 7, *sdh4*Δ *sdh8*Δ cells. Immunoblotting was used to detect Atp2 (complex V) as a control and complexes containing Sdh1, Sdh2, and HA (Sdh8-His_6HA_3). SDH complex (~232 kDa), Sdh1-Sdh8 subcomplex (~150 kDa).

expression of either fly or human SDHAF4 is sufficient to rescue the growth defects of an *sdh8*Δ mutant yeast strain. Taken together, these results demonstrate that the central requirement for SDHAF4 in SDH assembly has been conserved through evolution, from yeast to mammals.

Our biochemical studies in yeast provide a mechanistic context for understanding the role of SDHAF4 in SDH assembly. An unbiased proteomic analysis of Sdh8-associated proteins revealed a physical interaction between Sdh8 and Sdh1, the catalytic subunit of SDH. We confirmed the specificity of this interaction by coimmunoprecipitation and demonstrated that an Sdh1-Sdh8 subcomplex of ~150 kDa can be detected in unstressed WT cells, albeit at very low levels. Increased levels of this subcomplex, however, become readily detectable upon genetic disruption of the SDH complex through deletion of either Sdh2 or Sdh4. Taken together, these results support the model that Sdh8 interacts with a soluble pool of Sdh1 prior to the formation of the Sdh1-Sdh2 soluble dimer and assembly of the holocomplex. Moreover, Sdh8 interacts specifically with the flavinated form of Sdh1, indicating that this association follows Sdh1 flavination by Sdh5/SDHAF2 (Hao et al., 2009). This model is consistent with the localization of Sdh8 to the matrix where it can readily access free flavo-Sdh1, which is subsequently tethered to the IMM through its association with Sdh2 and the membrane-bound Sdh3/Sdh4 dimer.

We observed that Sdh8 stability directly relates to its association with Sdh1, further supporting the centrality of its role as an Sdh1 chaperone. Thus, deletion of Sdh1 leads to a dramatic reduction in Sdh8 levels while deletion of Sdh2, which causes greatly increased availability of free Sdh1, leads to an increase in Sdh8. Although Sdh1 protein levels are unperturbed in *sdh8*Δ cells, we observed considerable destabilization of Sdh2, which is consistent with impaired formation of Sdh1-Sdh2 dimers. Therefore, we hypothesize that the occupation of free Sdh1 by Sdh8 facilitates the formation of Sdh1-Sdh2 dimers. This dimer fails to form efficiently in the absence of Sdh8, and Sdh2 is destabilized as it is in mutants lacking Sdh1 altogether.

Interestingly, the loss of SDHAF4 appears to have more severe consequences in *Drosophila* than in yeast or mammalian cells. *dSdhaf4* mutants display a profound reduction in SDH enzyme activity, destabilization of both SdhA and SdhB, and a significant loss of SDH holocomplexes. In contrast, yeast *sdh8*Δ mutants and C2C12 mouse myoblasts treated with SDHAF4 siRNA maintain ~40%–50% of WT SDH activity and preserve a similar fraction of assembled SDH holocomplexes. While yeast *sdh8*Δ mutants have relatively normal levels of Sdh1, *dSdhaf4* mutants have greatly reduced levels of SdhA, which probably underlies the nearly complete loss of SDH holocomplexes. It is possible that yeast and mammalian cells express an additional SDHA chaperone that can function in the absence of SDHAF4, maintaining the levels of SDHA to support holocomplex assembly. It is also possible that growth in rich culture medium provides a buffer against oxidative stress in yeast that is not present in the more complex *Drosophila* system. Identification of the mechanism that underlies this discrepancy, however, will require further study of SDH assembly in both yeast and flies. Regardless, it is important to note that *dSdhaf4* mutants retain some SDH activity (~15%) and that this is sufficient to support limited viability, albeit with both muscular (erect wings) and behavioral (neurodegeneration) dysfunction. In contrast, *SdhA* null mutants are lethal, demonstrating that a further reduction in SDH activity cannot be tolerated (Mast et al., 2008). Thus, while the SDHAF4 protein family is clearly involved in SDH stability and activity, it

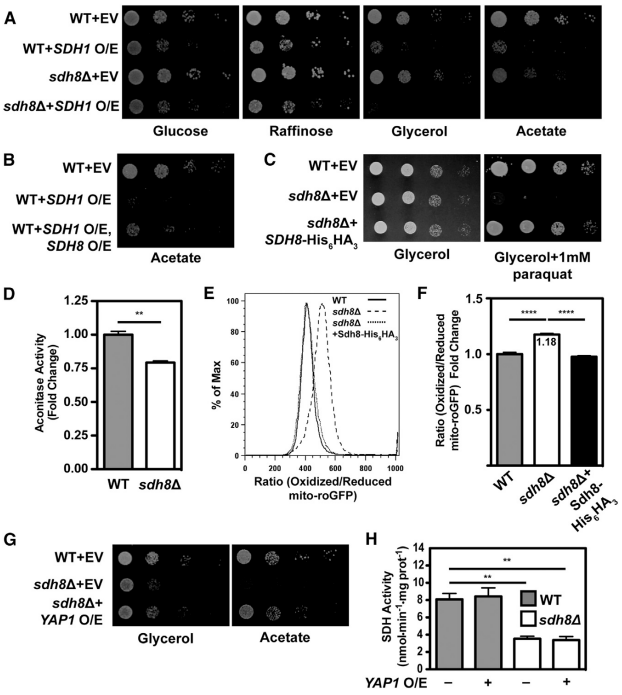

Figure 7. Sdh8 Protects the Cell from Oxidative Stress

(A) Ten-fold serial dilutions of WT and *sdh8*Δ yeast either transformed with an empty vector or overexpressing Sdh1 were plated on media containing the indicated carbon source (W303 background).

(B) Ten-fold serial dilutions of WT yeast transformed with an empty vector, WT yeast overexpressing Sdh1, and WT yeast overexpressing Sdh1 and Sdh8-His_6HA_3 were plated on media containing acetate (W303 background).

(C) Ten-fold serial dilutions of WT yeast transformed with an empty vector, *sdh8*Δ cells transformed with an empty vector, and *sdh8*Δ cells expressing Sdh8-His_6HA_3 were plated on media containing glycerol with and without 1 mM paraquat and incubated at 30°C (W303 background) as in (A).

(D) Aconitase activity was measured in WT and *sdh8*Δ cells grown to stationary phase in synthetic complete media containing 2% glucose and normalized to total protein (±SEM; n =4 biological replicates. $^{**}p < 0.005$).

(E) WT cells (solid line), *sdh8*Δ cells (dashed line), and *sdh8*Δ cells expressing Sdh8-His_6HA_3 (dotted line) transformed with mito-roGFP were plated on synthetic media containing 2% acetate, allowed to grow for 48 hr, and analyzed by flow cytometry. Shown are representative histograms measuring the ratio of oxidized/reduced mito-roGFP in 30,000 cells (BY4741 background).

(F) The median value of the ratio of oxidized/reduced mito-roGFP is plotted for WT cells, *sdh8*Δ cells, and *sdh8*Δ cells expressing Sdh8-His_6HA_3 (±SEM; n = 4 biological replicates. $^{****}p < 0.0001$).

(G) Ten-fold serial dilutions of WT yeast transformed with an empty vector, *sdh8*Δ cells transformed with an empty vector, and *sdh8*Δ cells overexpressing *YAP1* were plated on media containing the indicated carbon source and incubated at 30°C (BY4741 background) as in (A).

(H) SDH activity enzyme assays were performed using mitochondria harvested from WT and *sdh8*Δ cells carrying an empty vector or overexpressing *YAP1*. Activity was normalized to total protein (±SEM; n = 3 biological replicates. $^{**}p < 0.005$).

does not appear to be an absolute requirement, as some level of SDH activity remains in the absence of the respective SDHAF4 ortholog in all three model systems.

Our demonstration that Sdh8 acts through Sdh1 to facilitate formation of the Sdh1/Sdh2 dimer, and subsequently the SDH holocomplex, further emphasizes the importance of dedicated chaperones for ETC complex assembly. We propose that this unique demand might relate to the need to protect the redox-active cofactors present in many ETC complex subunits (Messner and Imlay, 2002). Prior to assembly, these cofactors are exposed to solvent and are, therefore, susceptible to damaging chemical reactions. The susceptibility of free cofactors to damaging chemical reactions is exemplified by our data suggesting that free flavinated Sdh1 is toxic and that this toxicity is alleviated by Sdh8. Overexpression of Sdh1 causes growth defects in WT cells, but this phenotype is exacerbated in *sdh8*Δ mutants and ameliorated by co-overexpression of Sdh8. Thus, we conclude that the chaperone activity of Sdh8 protects the cell from potentially damaging effects of unbound Sdh1, which are likely due to the generation of ROS enabled by solvent-accessible FAD. Sdh1, which contains a covalently bound, redox active, FAD cofactor is capable of oxidizing succinate to fumarate independent of the SDH complex. This oxidation of succinate leads to the reduction of FAD, which is then auto-oxidized by molecular oxygen to yield superoxide (Messner and Imlay, 2002; Guzy et al., 2008). The observation that Sdh8 interacts specifically with covalently flavinated Sdh1, but not with apo-Sdh1, is consistent with Sdh8 acting to prevent this mechanism of oxidative stress. Further, *sdh8*Δ mutant cells were unable to grow on respiratory medium in the presence of the superoxide producer paraquat and demonstrate a marked accumulation of ROS as determined by two independent assays. Similarly, *dSdhaf4* mutant flies are highly sensitive to oxidative stress induced by hyperoxia. Importantly, overexpression of two genes involved in the detoxification of ROS —*YAP1* and *SOD2*—rescued the *sdh8*Δ growth defects in yeast without affecting the SDH activity, SDH assembly, or steady-state Sdh2 levels. We conclude that, in addition to promoting

Sdh2 binding and holocomplex assembly, Sdh1 protects the redox-active FAD cofactor from potentially deleterious solvent interactions.

These biochemical aberrations resulted in profound physiological defects in *Drosophila* lacking *dSdhaf4*, all of which are hallmarks of mitochondrial dysfunction and which suggest possible links to human disease. Most notably, *dSdhaf4* mutants display bang sensitivity, a phenotype characterized by a susceptibility to mechanically induced paralytic seizures, which is commonly elicited by defects in mitochondrial function (Fergestad et al., 2006; Liu et al., 2007). *dSdhaf4* mutants also display neurodegeneration and reduced lifespan, which often accompany bang sensitivity (Fergestad et al., 2008). In addition, we observed abnormal wing posture in *dSdhaf4* mutants, which is characteristic of muscular dysfunction (Greene et al., 2003). Similar phenotypes have been reported in flies harboring mutations in several known disease-causing genes that impact mitochondrial function. For example, *Pink* and *Parkin* mutants display abnormal wing posture, and *mtATP6* mutants are bang sensitive (Celotto et al., 2006b; Fernandes and Rao, 2011). Human mutations in *Pink*/*Parkin* and *mtATP6* are known to cause familial Parkinson's disease and mitochondrial encephalopathy, respectively (Schapira, 2012). Moreover, as described in more detail below, some neurodegenerative diseases such as Leigh's syndrome are known to be associated with a loss of SDH activity. Our studies of *dSdhaf4* thus provide a genetic model for better understanding the pathophysiology of neurodegenerative disorders that are caused by SDH deficiency (Rutter et al., 2010; Hoekstra and Bayley, 2013).

Similar to *dSdhaf4* mutants, *SdhB* hypomorphic mutants that retain ~40% of normal SDH activity are sensitive to oxidative stress and display a reduced lifespan (Walker et al., 2006). The *SdhB* hypomorphs, however, were not reported to undergo mechanically induced paralytic seizures or display neurodegenerative phenotypes (Walker et al., 2006). This lack of neuronal phenotypes in *SdhB* mutants could be due to the higher overall SDH activity seen in these partial loss-of-function mutants relative to a complete loss of *dSdhaf4* activity. It is also possible, however, that the neurodegeneration phenotype is driven by increased ROS production rather than a defect in mitochondrial ATP production. In support of this model, clones generated using a lethal null allele of *SdhA* in the eye display retinal degeneration similar to that seen in *dSdhaf4* mutants, which was shown to be specifically caused by increased ROS production (Mast et al., 2008). This is also consistent with our finding that *dSdhaf4* mutants are not depleted of ATP, possibly enabled by metabolic compensation (Celotto et al., 2011). Thus, our study of *dSdhaf4*, and other work characterizing *SdhA*, *SdhB*, and *dSdhaf3* mutants in *Drosophila*, suggests that tissue dysfunction induced by a loss of SDH appears to be largely driven by increased ROS production. This is consistent with our hypothesis that SDH assembly factors may have evolved as a mechanism to protect cells and organisms from ROS production during SDH assembly.

Mutations in all genes encoding previously published SDH subunits and assembly factors have been shown to cause human disease. These include neurodegenerative diseases (Leigh's Syndrome, leukodystrophy, and leukoencephalopathy), which have been linked to mutations in *SDHA*, *SDHB*, and *SDHAF1* (Horváth et al., 2006; Ghezzi et al., 2009; Alston et al., 2012; Ohlenbusch et al., 2012). Mutations in *SDHA*, *SDHB*, *SDHC*, *SDHD*, and *SDHAF2* have also been shown to cause paragangliomas and pheochromocytomas—two classes of neuroendocrine tumors (Astuti et al., 2001; Hao et al., 2009; Fishbein and Nathanson, 2012). Recently, several cases of WT gastrointestinal stromal tumors (WT GIST) have been linked to germline loss-of-function mutations in *SDHA* and *SDHB* (Janeway et al., 2011; Celestino et al., 2012; Italiano et al., 2012; Oudijk et al., 2013). This wealth of evidence linking SDH dysfunction to disease raises the possibility that damaging mutations in *SDHAF4* may cause human disease. In fact, several cases of SDH-deficient diseases, including Leigh's Syndrome and WT GIST, lack mutations in the genes encoding all known SDH subunits (Horváth et al., 2006; Janeway et al., 2011; Jain-Ghai et al., 2013). Our phenotypic studies raise the important possibility that *SDHAF4* is a candidate gene for these and other diseases characterized by SDH deficiency. Our future efforts will focus on determining the incidence of these possible causative *SDHAF4* mutations.

On the basis of the data presented in this report, we conclude that the SDHAF4 gene family encodes an SDH assembly factor. Insights gained in our studies of this protein have allowed us to propose a more complete model of SDH assembly (Figure S7H). Upon import into the matrix by TOM and TIM, apo-Sdh1 is flavinated in a reaction that requires Sdh5 (Hao et al., 2009). Free flavo-Sdh1 is then bound by Sdh8 to form a ~150 kDa subcomplex. This subcomplex occupies Sdh1, preventing autooxidation and supporting its ability to dimerize with Sdh2. The Sdh1-Sdh2 soluble dimer is then recruited to the IMM via interactions with Sdh3 and Sdh4 to form the SDH holocomplex. This model highlights the importance of subunit-specific chaperones in the process of assembly. Indeed, failure of SDHAF4 to occupy free SdhA prevents normal SDH assembly in three eukaryotic systems and has profound physiological consequences. The identification and characterization of the SDHAF4 protein family thus provides important new insights into the process of SDH assembly, the mechanisms by which SDH subunits are protected for generating ROS, and a new candidate gene to understand human disease associated with a loss of SDH activity.

EXPERIMENTAL PROCEDURES

Drosophila Metabolomic Analysis and Enzyme Activity Assays

Adult male flies were aged 5–7 days, washed with PBS, and snap frozen in liquid nitrogen. Metabolites were extracted from frozen flies, and gas chromatography-mass spectrometry (GC/MS) was performed as previously described (Bricker et al., 2012). SDH activity was measured in mitochondrial extracts, as previously described, by examining the reduction of iodonitrotetrazolium at 500 nm in the presence of succinate (Celotto et al., 2011). CS activity was measured in mitochondrial extracts by examining the reduction of 5,5′-5 dithiobis-2-nitrobenzoic acid in the presence of oxaloacetate and acetyl-CoA, as previously described (Tang et al., 2009). Enzyme activity per gram of mitochondrial protein was calculated.

Drosophila Paralytic Assays

Bang sensitivity was measured as previously described (Ganetzky and Wu, 1982). Flies were collected in groups of five to eight females per vial and allowed to recover from CO_2 anesthesia for at least 2 hr. Flies were then vortexed for 15 s, and the time it takes to return to a standing position was assayed. At least three vials were assayed per condition in each experiment,

and all experiments were repeated at least twice. Experiments on female flies are presented, but similar results were observed when assaying males (data not shown).

Electron Microscopy

Heads were removed from 8- to 12-day-old female flies, the proboscis was removed, and EM was performed as described in the Supplemental Experimental Procedures.

Mito-roGFP and Flow Cytometry

The protocol used in this investigation has been adapted from Vevea et al., 2013. For each experiment, an equal number of cells transformed with mito-roGFP were plated thinly on synthetic media containing 2% acetate or 2% glycerol. Cells were allowed to incubate for approximately 48 hr before being harvested and analyzed by flow cytometry. Data was collected at the University of Utah Flow Cytometry Core Facility. Cells were acquired on a BD FACSCanto II by collecting emission wavelengths of 530/30 from a violet (405 nm) and blue (488 nm) laser. Postacquisition analysis was accomplished in Flowjo (Treestar, Inc). After single cells were selected using FSC-W and FSC-H parameters, GFP+ cells were gated on for further analysis. The fluorescence intensity was expressed as a ratio of oxidized (405 nm excitation) to reduced (488 nm excitation) mito-roGFP.

BN-PAGE

BN-PAGE was performed as described previously (Wittig et al., 2006). Mitochondria were resuspended in lysis buffer (50 mM NaCl, 5 mM 6-aminocaproic acid, 50 mM imidazole, 1 mM AEBSF, and protease inhibitor cocktail). Yeast and *Drosophila* mitochondria were solubilized with 1% digitonin and mammalian mitochondria with 2% digitonin. Lysates were resolved on a 3%–13% gradient native gel using a PROTEAN II xi Cell gel running system (Bio-Rad). Western blot performed as described elsewhere using a Trans-blot transfer cell (Bio-Rad) and PVDF membranes.

Statistics

PRISM software was used to graph all quantitative data and perform statistical analyses. p values for pairwise comparisons were determined using a Student's t test, and p values for multiple comparisons were calculated using one-way ANOVA with a Bonferroni correction. Metabolomics data are presented in box-plot form, where the box represents the 25^{th}–75^{th} percentile, the line is the median, and the whiskers represent the range of the data. All other quantitative data are shown as the mean ±SEM. p values for Kaplan-Meier survival curves in Figures 5 and S5 were calculated using a log rank test.

SUPPLEMENTAL INFORMATION

Supplemental Information includes seven figures, one table, and Supplemental Experimental Procedures and can be found with this article online at http://dx.doi.org/10.1016/j.cmet.2014.05.012.

AUTHOR CONTRIBUTIONS

J.G.V., D.K.B., C.S.T., and J.R. designed the research and prepared the manuscript. J.G.V. performed all experiments in yeast and mammalian cells and BN-PAGE experiments. D.K.B. performed all the experiments in *Drosophila*. N.D. and S.P.G. performed protein mass spectroscopy. J.E.C. performed the metabolomics analysis.

ACKNOWLEDGMENTS

We thank Tim Dahlem at the University of Utah Mutation and Detection Core for generating the TALEN gene-targeting constructs, Linda Nikolova at the University of Utah Electron Microscopy core for assistance performing TEM, the Bloomington Stock Center for providing stocks, FlyBase for critical information that made these studies possible, Dennis Winge for providing antibodies and other reagents, James Marvin at the University of Utah Flow Cytometry core for help in establishing the mito-roGFP system, and Liza Pon (Columbia University) for providing the mito-roGFP construct. This research was supported by NIH grant NIH 1R01 GM094232 (J.R. and C.S.T.) and NIH 1RO1 GM110755, and we acknowledge support of funds in conjunction with the grant P30CA042014 awarded to the Huntsman Cancer Institute. D.K.B. was supported by the NIH Genetics Predoctoral Training Grant T32 GM007464. J.G.V. was supported by the Huntsman Cancer Institute Multidisciplinary Cancer Research Training Program (T32 CA093247).

Received: January 7, 2014
Revised: March 28, 2014
Accepted: April 28, 2014
Published: June 19, 2014

REFERENCES

Alston, C.L., Davison, J.E., Meloni, F., van der Westhuizen, F.H., He, L., Hornig-Do, H.T., Peet, A.C., Gissen, P., Goffrini, P., Ferrero, I., et al. (2012). Recessive germline SDHA and SDHB mutations causing leukodystrophy and isolated mitochondrial complex II deficiency. J. Med. Genet. *49*, 569–577.

Astuti, D., Latif, F., Dallol, A., Dahia, P.L., Douglas, F., George, E., Sköldberg, F., Husebye, E.S., Eng, C., and Maher, E.R. (2001). Gene mutations in the succinate dehydrogenase subunit SDHB cause susceptibility to familial pheochromocytoma and to familial paraganglioma. Am. J. Hum. Genet. *69*, 49–54.

Bricker, D.K., Taylor, E.B., Schell, J.C., Orsak, T., Boutron, A., Chen, Y.C., Cox, J.E., Cardon, C.M., Van Vranken, J.G., Dephoure, N., et al. (2012). A mitochondrial pyruvate carrier required for pyruvate uptake in yeast, *Drosophila*, and humans. Science *337*, 96–100.

Carmona-Gutierrez, D., Eisenberg, T., Büttner, S., Meisinger, C., Kroemer, G., and Madeo, F. (2010). Apoptosis in yeast: triggers, pathways, subroutines. Cell Death Differ. *17*, 763–773.

Celestino, R., Lima, J., Faustino, A., Máximo, V., Gouveia, A., Vinagre, J., Soares, P., and Lopes, J.M. (2012). A novel germline SDHB mutation in a gastrointestinal stromal tumor patient without bona fide features of the Carney-Stratakis dyad. Fam. Cancer *11*, 189–194.

Celotto, A.M., Frank, A.C., McGrath, S.W., Fergestad, T., Van Voorhies, W.A., Buttle, K.F., Mannella, C.A., and Palladino, M.J. (2006a). Mitochondrial encephalomyopathy in *Drosophila*. J. Neurosci. *26*, 810–820.

Celotto, A.M., Frank, A.C., Seigle, J.L., and Palladino, M.J. (2006b). *Drosophila* model of human inherited triosephosphate isomerase deficiency glycolytic enzymopathy. Genetics *174*, 1237–1246.

Celotto, A.M., Chiu, W.K., Van Voorhies, W., and Palladino, M.J. (2011). Modes of metabolic compensation during mitochondrial disease using the *Drosophila* model of ATP6 dysfunction. PLoS ONE *6*, e25823.

Celotto, A.M., Liu, Z., Vandemark, A.P., and Palladino, M.J. (2012). A novel *Drosophila* SOD2 mutant demonstrates a role for mitochondrial ROS in neurodevelopment and disease. Brain Behav. *2*, 424–434.

Diaz, F., Kotarsky, H., Fellman, V., and Moraes, C.T. (2011). Mitochondrial disorders caused by mutations in respiratory chain assembly factors. Semin. Fetal Neonatal Med. *16*, 197–204.

Fergestad, T., Bostwick, B., and Ganetzky, B. (2006). Metabolic disruption in *Drosophila* bang-sensitive seizure mutants. Genetics *173*, 1357–1364.

Fergestad, T., Olson, L., Patel, K.P., Miller, R., Palladino, M.J., and Ganetzky, B. (2008). Neuropathology in *Drosophila* mutants with increased seizure susceptibility. Genetics *178*, 947–956.

Fernandes, C., and Rao, Y. (2011). Genome-wide screen for modifiers of Parkinson's disease genes in *Drosophila*. Mol. Brain *4*, 17.

Fernández-Vizarra, E., Tiranti, V., and Zeviani, M. (2009). Assembly of the oxidative phosphorylation system in humans: what we have learned by studying its defects. Biochim. Biophys. Acta *1793*, 200–211.

Fishbein, L., and Nathanson, K.L. (2012). Pheochromocytoma and paraganglioma: understanding the complexities of the genetic background. Cancer Genet. *205*, 1–11.

Ganetzky, B., and Wu, C.F. (1982). Indirect suppression involving behavioral mutants with altered nerve excitability in *Drosophila* melanogaster. Genetics *100*, 597–614.

Ghezzi, D., Goffrini, P., Uziel, G., Horvath, R., Klopstock, T., Lochmüller, H., D'Adamo, P., Gasparini, P., Strom, T.M., Prokisch, H., et al. (2009). SDHAF1, encoding a LYR complex-II specific assembly factor, is mutated in SDH-defective infantile leukoencephalopathy. Nat. Genet. *41*, 654–656.

Gnerer, J.P., Kreber, R.A., and Ganetzky, B. (2006). wasted away, a *Drosophila* mutation in triosephosphate isomerase, causes paralysis, neurodegeneration, and early death. Proc. Natl. Acad. Sci. USA *103*, 14987–14993.

Greene, J.C., Whitworth, A.J., Kuo, I., Andrews, L.A., Feany, M.B., and Pallanck, L.J. (2003). Mitochondrial pathology and apoptotic muscle degeneration in *Drosophila* parkin mutants. Proc. Natl. Acad. Sci. USA *100*, 4078–4083.

Guzy, R.D., Sharma, B., Bell, E., Chandel, N.S., and Schumacker, P.T. (2008). Loss of the SdhB, but Not the SdhA, subunit of complex II triggers reactive oxygen species-dependent hypoxia-inducible factor activation and tumorigenesis. Mol. Cell. Biol. *28*, 718–731.

Hao, H.X., Khalimonchuk, O., Schraders, M., Dephoure, N., Bayley, J.P., Kunst, H., Devilee, P., Cremers, C.W., Schiffman, J.D., Bentz, B.G., et al. (2009). SDH5, a gene required for flavination of succinate dehydrogenase, is mutated in paraganglioma. Science *325*, 1139–1142.

Hoekstra, A.S., and Bayley, J.P. (2013). The role of complex II in disease. Biochim. Biophys. Acta *1827*, 543–551.

Horváth, R., Abicht, A., Holinski-Feder, E., Laner, A., Gempel, K., Prokisch, H., Lochmüller, H., Klopstock, T., and Jaksch, M. (2006). Leigh syndrome caused by mutations in the flavoprotein (Fp) subunit of succinate dehydrogenase (SDHA). J. Neurol. Neurosurg. Psychiatry *77*, 74–76.

Italiano, A., Chen, C.L., Sung, Y.S., Singer, S., DeMatteo, R.P., LaQuaglia, M.P., Besmer, P., Socci, N., and Antonescu, C.R. (2012). SDHA loss of function mutations in a subset of young adult wild-type gastrointestinal stromal tumors. BMC Cancer *12*, 408.

Jain-Ghai, S., Cameron, J.M., Al Maawali, A., Blaser, S., MacKay, N., Robinson, B., and Raiman, J. (2013). Complex II deficiency—a case report and review of the literature. Am. J. Med. Genet. A. *161A*, 285–294.

Janeway, K.A., Kim, S.Y., Lodish, M., Nosé, V., Rustin, P., Gaal, J., Dahia, P.L., Liegl, B., Ball, E.R., Raygada, M., et al.; NIH Pediatric and Wild-Type GIST Clinic (2011). Defects in succinate dehydrogenase in gastrointestinal stromal tumors lacking KIT and PDGFRA mutations. Proc. Natl. Acad. Sci. USA *108*, 314–318.

Kiselev, A., Socolich, M., Vinós, J., Hardy, R.W., Zuker, C.S., and Ranganathan, R. (2000). A molecular pathway for light-dependent photoreceptor apoptosis in *Drosophila*. Neuron *28*, 139–152.

Liu, W., Gnanasambandam, R., Benjamin, J., Kaur, G., Getman, P.B., Siegel, A.J., Shortridge, R.D., and Singh, S. (2007). Mutations in cytochrome c oxidase subunit VIa cause neurodegeneration and motor dysfunction in *Drosophila*. Genetics *176*, 937–946.

Mandal, S., Guptan, P., Owusu-Ansah, E., and Banerjee, U. (2005). Mitochondrial regulation of cell cycle progression during development as revealed by the tenured mutation in *Drosophila*. Dev. Cell *9*, 843–854.

Mast, J.D., Tomalty, K.M., Vogel, H., and Clandinin, T.R. (2008). Reactive oxygen species act remotely to cause synapse loss in a *Drosophila* model of developmental mitochondrial encephalopathy. Development *135*, 2669–2679.

McFaline-Figueroa, J.R., Vevea, J.D., Swayne, T.C., Zhou, C., Liu, C., Leung, G., Boldogh, I.R., and Pon, L.A. (2011). Mitochondrial quality control during inheritance is associated with lifespan and mother-daughter age asymmetry in budding yeast. Aging Cell *10*, 885–895.

Messner, K.R., and Imlay, J.A. (2002). Mechanism of superoxide and hydrogen peroxide formation by fumarate reductase, succinate dehydrogenase, and aspartate oxidase. J. Biol. Chem. *277*, 42563–42571.

Ohlenbusch, A., Edvardson, S., Skorpen, J., Bjornstad, A., Saada, A., Elpeleg, O., Gärtner, J., and Brockmann, K. (2012). Leukoencephalopathy with accumulated succinate is indicative of SDHAF1 related complex II deficiency. Orphanet J. Rare Dis. *7*, 69.

Oudijk, L., Gaal, J., Korpershoek, E., van Nederveen, F.H., Kelly, L., Schiavon, G., Verweij, J., Mathijssen, R.H., den Bakker, M.A., Oldenburg, R.A., et al. (2013). SDHA mutations in adult and pediatric wild-type gastrointestinal stromal tumors. Mod. Pathol. *26*, 456–463.

Pagliarini, D.J., Calvo, S.E., Chang, B., Sheth, S.A., Vafai, S.B., Ong, S.E., Walford, G.A., Sugiana, C., Boneh, A., Chen, W.K., et al. (2008). A mitochondrial protein compendium elucidates complex I disease biology. Cell *134*, 112–123.

Robinson, K.M., Rothery, R.A., Weiner, J.H., and Lemire, B.D. (1994). The covalent attachment of FAD to the flavoprotein of Saccharomyces cerevisiae succinate dehydrogenase is not necessary for import and assembly into mitochondria. Eur. J. Biochem. *222*, 983–990.

Rutter, J., Winge, D.R., and Schiffman, J.D. (2010). Succinate dehydrogenase - Assembly, regulation and role in human disease. Mitochondrion *10*, 393–401.

Schapira, A.H. (2012). Mitochondrial diseases. Lancet *379*, 1825–1834.

Sickmann, A., Reinders, J., Wagner, Y., Joppich, C., Zahedi, R., Meyer, H.E., Schönfisch, B., Perschil, I., Chacinska, A., Guiard, B., et al. (2003). The proteome of Saccharomyces cerevisiae mitochondria. Proc. Natl. Acad. Sci. USA *100*, 13207–13212.

Tang, S., Le, P.K., Tse, S., Wallace, D.C., and Huang, T. (2009). Heterozygous mutation of Opa1 in *Drosophila* shortens lifespan mediated through increased reactive oxygen species production. PLoS ONE *4*, e4492.

Vevea, J.D., Wolken, D.M., Swayne, T.C., White, A.B., and Pon, L.A. (2013). Ratiometric biosensors that measure mitochondrial redox state and ATP in living yeast cells. J. Vis. Exp. *77*, e50633.

Walker, D.W., Hájek, P., Muffat, J., Knoepfle, D., Cornelison, S., Attardi, G., and Benzer, S. (2006). Hypersensitivity to oxygen and shortened lifespan in a *Drosophila* mitochondrial complex II mutant. Proc. Natl. Acad. Sci. USA *103*, 16382–16387.

Wittig, I., Braun, H.P., and Schägger, H. (2006). Blue native PAGE. Nat. Protoc. *1*, 418–428.

Cell Metabolism, Volume *20*

Supplemental Information

SDHAF4 Promotes Mitochondrial Succinate Dehydrogenase Activity and Prevents Neurodegeneration

Jonathan G. Van Vranken, Daniel K. Bricker, Noah Dephoure, Steven P. Gygi, James E. Cox, Carl S. Thummel, and Jared Rutter

Supplemental Material for:

SDHAF4 promotes mitochondrial succinate dehydrogenase activity and prevents neurodegeneration

Jonathan G. Van Vranken[1†], Daniel K. Bricker[2†], Noah Dephoure[3], Steven P. Gygi[3], James E. Cox[4], Carl S. Thummel[2*], and Jared Rutter[1*]

Inventory of Supplemental Material

Supplemental Figures

Figure S1, related to Figure 1. Yeast Sdh8 is a conserved matrix protein required for maximal SDH activity.

(A) Sequence alignment of the SDHAF4 protein family (Clustal Omega). (B) The *sdh8*Δ mutant expressing Sdh8-GFP and MitoRFP were grown to early log phase and imaged by fluorescence microscopy. Sdh8-GFP exhibits a complete co-localization with MitoRFP confirming the previously annotated mitochondrial localization (Reinders et al., 2006). (C) Intact mitochondria, hypotonic-swollen mitoplasts, and Triton X-100-solubilized mitochondria of an *sdh8*Δ strain expressing Sdh8-His_6HA_3 were treated either with (+) or without (-) proteinase K and analyzed by immunoblot along with the whole-cell lysate (WCL) and post-mitochondrial supernatant (PMS). Fzo1, Cyb2, and Mge1 are outer mitochondrial membrane, inner-membrane space, and matrix proteins, respectively. Upon biochemical fractionation Sdh8-His_6HA_3 was readily detected in the whole cell lysate but was undetectable in the post-mitochondrial supernatant. Sdh8-His_6HA_3 was present in purified mitochondria and protected from Proteinase K except in the presence of Triton X-100, consistent with localization to the mitochondrial matrix. (D) Mitochondria isolated from *sdh8*Δ mutant cells expressing Sdh8-His_6HA_3 were separated into soluble and membrane fractions. Each fraction was assessed by SDS-PAGE and immunoblot. Sdh5 and Porin are used as controls and represent soluble and membrane bound proteins, respectively. Sdh8-His_6HA_3 can be readily detected in the soluble fraction but is excluded from the membrane fraction. (E) Ten-fold serial dilutions of wild-type (WT) yeast transformed with an empty vector (EV), *sdh8*Δ mutants transformed with EV, or *sdh8*Δ transformed with SDH8-His_6HA_3, all in a W303 background, were grown on different carbon sources and incubated at 30°C. (F-H) GC/MS was used to measure the abundance of metabolites in WT and *sdh8*Δ yeast (W303 background). The data is depicted in box plot format, with the box representing the lower and upper quartiles, the horizontal line representing the median, and the bars representing the minimum and maximum data points. (N=6 biological replicates. $^{**}p<0.005$; $^{*}p<0.05$). (I) Mitochondria isolated from either WT yeast or *sdh8*Δ yeast expressing Sdh8-His_6HA_3 were solubilized in digitonin and the resulting extract was fractionated by BN-PAGE.

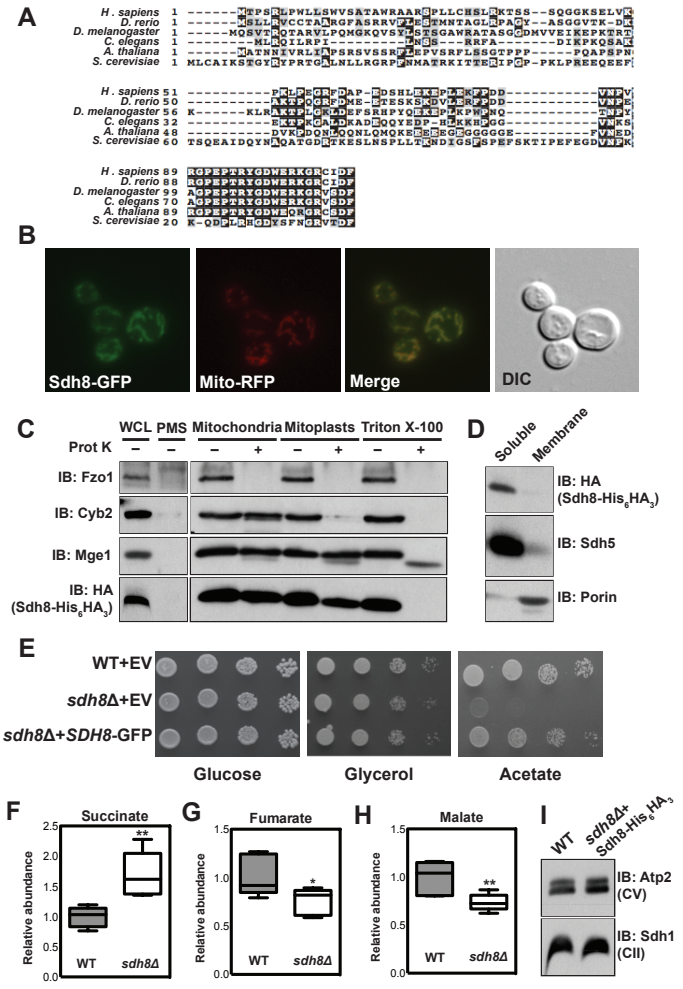

Supplemental Figure 1

Figure S2, related to figure 2. Mammalian SDHAF4 is required for maximal SDH activity.

(A) Mitochondria extracted from C2C12 cells transfected with AS, si1, or si2 were subjected to SDS-PAGE and analyzed by immunoblot of SDHA, SDHB, ATP5A, and VDAC. (B) MDH enzyme activity was measured in mitochondria harvested from C2C12 cells transfected with AS, si1, or si2 (±SEM. N=3 biological replicates).

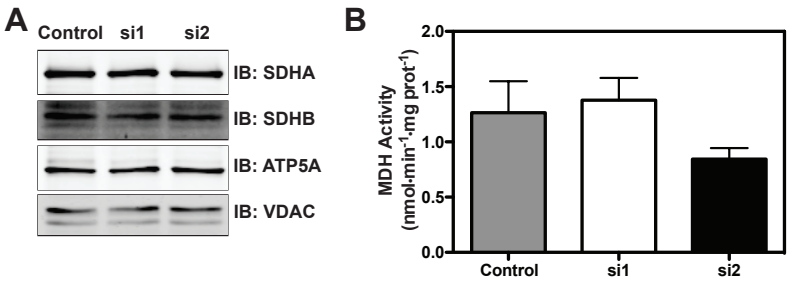

Supplemental Figure 2

Figure S3, related to Figure 3: Metabolomic analysis of multiple *dSdhaf4* mutants reveals changes in several metabolic pathways

(A) *dSdhaf4* alleles generated and used in this study. TALEN induced alleles (*dSdhaf4*^{1} and *dSdhaf4*^{2}) are shown in red, while the deletion generated by imprecise excision (*dSdhaf4*^{3}) of the p*CG7224*$^{[KG07581]}$ P element, is shown in blue. The *dSdhaf4*^{3} allele contains a remnant of the p*CG7224*$^{[KG07581]}$ element that was not excised. Another strain in which the p*CG7224*$^{[KG07581]}$ element was precisely excised (*Ex32+*) was generated, confirmed by PCR, and used as a control for all studies with the *dSdhaf4*^{3} allele. (B) Either LC/MS or GC/MS was used to measure the abundance of metabolites in transheterozygous *dSdhaf4*$^{1/3}$ mutants compared to genetically matched *dSdhaf4*$^{+/Ex32+}$ controls. (C) Changes in non-TCA cycle metabolites in *dSdhaf4*$^{1/2}$ or *dSdhaf4*$^{1/3}$ flies compared to their respective controls measured using GC/MS. The data is depicted in box plot format, with the box representing the lower and upper quartiles, the horizontal line representing the median, and the bars representing the minimum and maximum data points. 8-12 biological replicates from two independent experiments were combined per genotype. *p<0.05, **p<0.01 and ***p<0.001. The reduced levels of glutamate, which is interconvertible with alpha-ketoglutarate, as well as aspartate and 2-methylcitrate, which can be produced using oxaloacetate as a substrate (Gerike et al., 1998; (Jafari et al., 2013) suggest that *dSdhaf4* mutant cells are utilizing aspartate and glutamate for anapleurosis. Conversely, elevated levels of homocysteine and GABA could reflect their interconvertibility with succinyl-CoA and succinate, respectively.

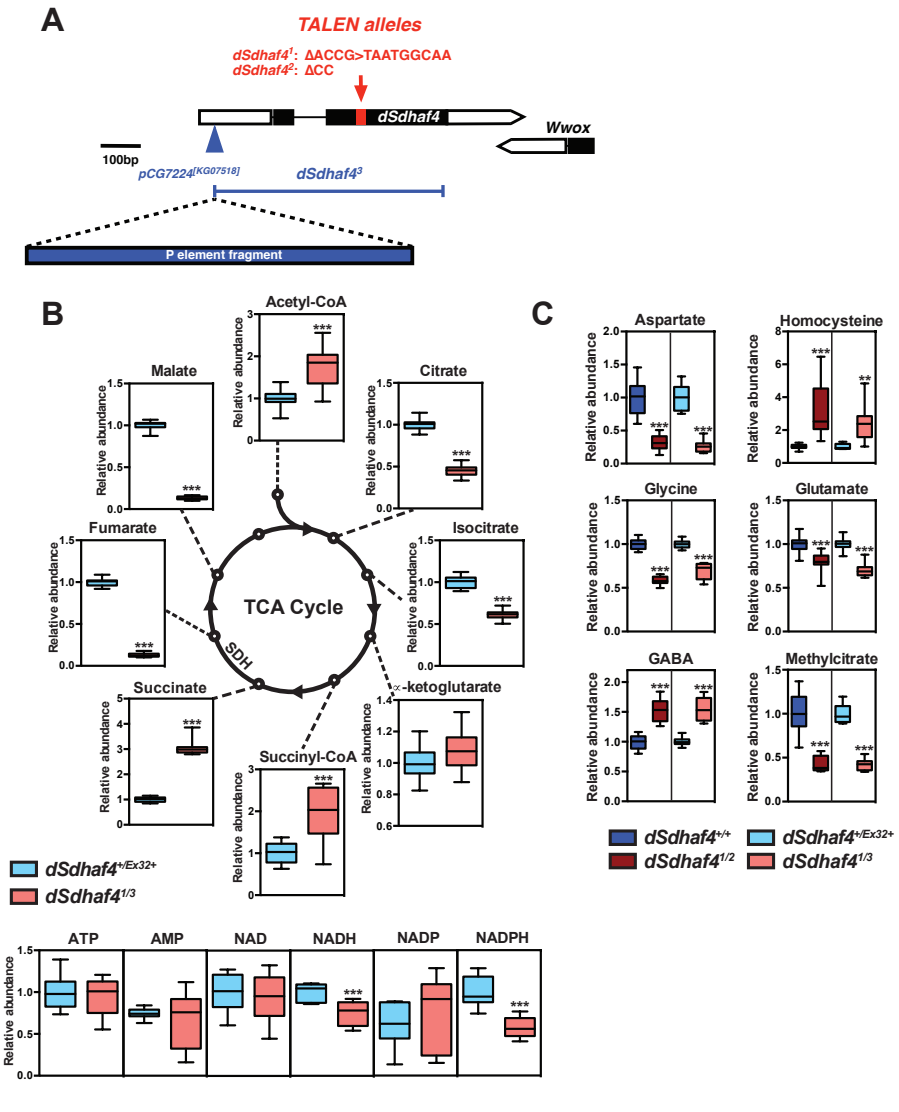

Supplemental Figure 3

Figure S4, related to Figure 4: *dSdhaf4* is required for the stability of SdhA and SdhB, but is not a rate limiting factor in SDH assembly

(A) Mitochondrial extracts from w^{1118} control (*dSdhaf4*$^{+}$) or *dSdhaf4*$^{1/2}$ (*dSdhaf4*$^{-}$) flies were resolved by SDS-PAGE, the gel was washed, and then either exposed to ultraviolet light to visualize flavinated SdhA (top), or stained with Coomassie Blue (bottom) to visualize total protein. Two biological replicates are shown. The reduction in flavinated SdhA reflects the overall reduction in SdhA protein levels (Figure 4B), indicating little if any effect of the mutation on flavination. (B) Protein from whole-fly homogenates was resolved by SDS-PAGE followed by immunoblotting to detect SdhB or tubulin. The asterisk denotes a non-specific band. Two biological replicates are shown. (C) Mitochondria were isolated from either control w^{1118} (*dSdhaf4*$^{+/+}$) or heterozygous *dSdhaf4*$^{+/1}$ (*dSdhaf4*$^{+/-}$) flies and SDH enzymatic activity was assayed. (D) Mitochondria were isolated from flies carrying a ubiquitous *Tubulin-GAL4* driver or a *UAS-dSdhaf4* element alone or in combination, and SDH enzymatic activity was assayed. (E) Mitochondria were isolated from flies carrying a ubiquitous *Tubulin-GAL4* driver or a *UAS-dSdhaf4* element alone or in combination, and SdhA, SdhB or ATP∝ subunit levels were assayed by western blot analysis. (F) Flies harboring either control (*dSdhaf4*$^{+}$) or *dSdhaf4*$^{1/2}$ (*dSdhaf4*$^{-}$) mutant chromosomes linked to a hypomorphic *SdhB* allele or wild type *SdhB* locus over a balancer were crossed to each other in various combinations. The resulting progeny from these crosses were then assayed for the absence or presence of the marker linked to the balancer chromosome. The proportion of the expected progeny eclosed based on Mendelian ratios of the indicated genotype is shown. The n values displayed in parentheses in the graph represent the total number of progeny assayed resulting from each cross. The mean±SEM is shown in D-F.

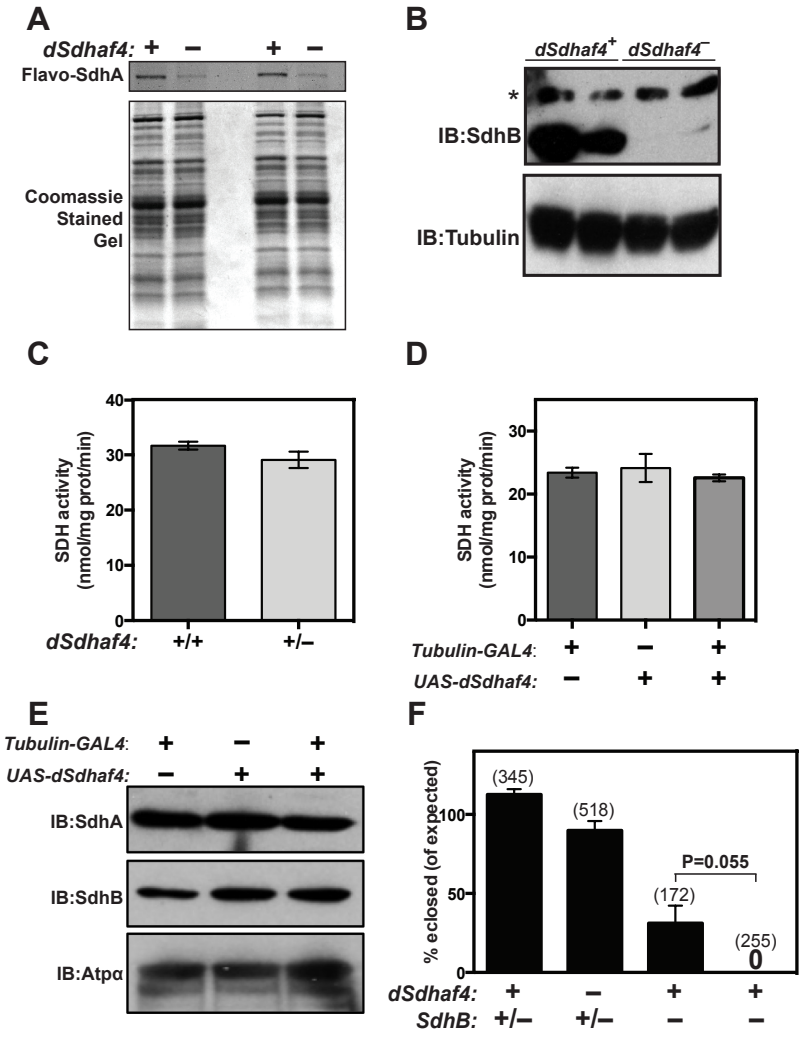

Supplemental Figure 4

Figure S5, related to Figure 5: *dSdhaf4* mutants are sensitive to bang-induced paralysis, but not starvation

(A) Adult *dSdhaf4*$^{+/Ex32+}$ (*dSdhaf4*$^{+}$) or *dSdhaf4*$^{1/3}$ (*dSdhaf4*$^{-}$) females aged 6-8 hours, 2-4 days, or 8-12 days were vortexed for 15 seconds and the percentage of paralyzed flies was counted. N>35 flies at each age per genotype. ***p<0.001 (ANOVA). (B) The percentage of 3-7 day old *w*^{1118} control or *dSdhaf4*$^{1/2}$ females that hold their wings in an upright position is shown. N>180 flies per genotype. ***p<0.001 (Student's t test). The mean±SEM is shown in A and B. (C) Controls or *dSdhaf4* mutant flies carrying the ubiquitous *Daughterless* driver (*Da-GAL4*) or no driver in the presence or absence of either a *UAS-dSdhaf4* transgene or a *UAS-human Sdhaf4* (*hSdhaf4*) transgene were homogenized. Proteins from these homogenates were resolved by SDS-PAGE followed by immunoblotting to detect either SdhB or tubulin. Note that *UAS-dSdhaf4* is leaky since it partially rescues in the absence of a GAL4 driver. (D) The amount of time 8-12 day old flies paralyzed in Figure 5E take to recover from paralysis was quantified. The percentage of flies paralyzed < 2 minutes, 2-6 minutes, 8-10 minutes or >10 minutes are shown. The number above each bar represents the total number of flies of the indicated genotype paralyzed and is the sample size from which each data set is based. (E) 2-4 day old controls or *dSdhaf4* mutant females were starved and the number of surviving animals was counted every 12 hours. The median lifespan under starvation 3.5 days for controls and 3.25 days for *dSdhaf4* mutants. Data shown as the percentage of surviving flies±SEM. At least 90 flies were assayed per genotype. P value calculated using a log-rank test.

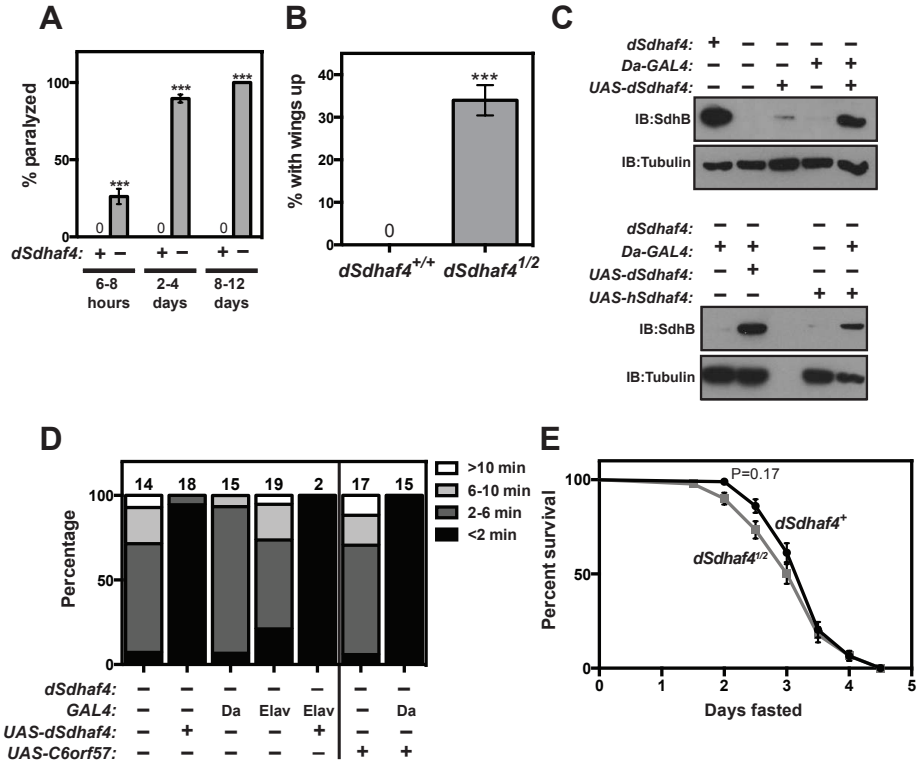

Supplemental Figure 5

Figure S6, related to Figure 6. Yeast Sdh8 is a co-chaperone for unbound and covalently flavinated Sdh1.

(A) A large scale HA immunoprecipitation of mitochondria isolated from *sdh8*Δ cells expressing Sdh8-His_6HA_3 and WT cells as a control. The final eluates were resolved by SDS-PAGE and visualized by silver stain (Thermo Scientific). The proteins present in each band were identified by mass-spectroscopy. (B) WT, *sdh8*Δ, and *sdh5*Δ mitochondria were resolved by SDS-PAGE and imaged for covalent FAD (ultra-violet light) or immunoblotted for Sdh1. (C) Sdh8-His_6HA_3 was immunoprecipitated using anti-HA conjugated agarose from digitonin-solublilized mitochondria. Mitochondria were extracted from *sdh8*Δ cells expressing Sdh8-His_6HA_3 or *sdh1*Δ*sdh8*Δ cells expressing Sdh8-His_6HA_3 and $Sdh1^{H90S}$ mutant (BY4741 background). (D) Sdh8-His_6HA_3 was immunoprecipitated from WT and *sdh5*Δ mitochondria using anti-HA conjugated agarose (W303 background). (E) Mitochondrial lysates isolated from control cells (WT), *sdh8*Δ cells expressing Sdh8-His_6HA_3, *sdh1*Δ*sdh8*Δ cells expressing Sdh8-His_6HA_3, *sdh2*Δ*sdh8*Δ cells expressing Sdh8-His_6HA_3, *sdh8*Δ cells, *sdh2*Δ*sdh8*Δ cells, and *sdh5*Δ*sdh8*Δ cells expressing Sdh8-His_6HA_3 were fractionated by SDS-PAGE. Levels of each protein was assessed by immunoblot for Sdh1, Sdh2, and HA (Sdh8-His_6HA_3). Immunoblot of Porin was used as a loading control (W303 background). (F) Sdh2- His_6HA_3 was immunoprecipitated from digitonin-solubilized mitochondria. Mitochondria were extracted from control cells (WT), *sdh2*Δ*sdh4*Δ cells expressing Sdh2-His_6HA_3, or *sdh2*Δ*sdh4*Δ*sdh8*Δ cells expressing Sdh2-His_6HA_3 (BY4741 background). (G) Mitochondria isolated from *sdh8*Δ cells expressing Sdh8-His_6HA_3 or *sdh2*Δ*sdh8*Δ cells expressing Sdh8-His_6HA_3 were solubilized in digintonin and the resulting extract was fractionated by BN-PAGE. The left and right panels represent the same western blot with a high and low exposure, respectively. The arrowheads highlight the Sdh1-Sdh8 subcomplex.

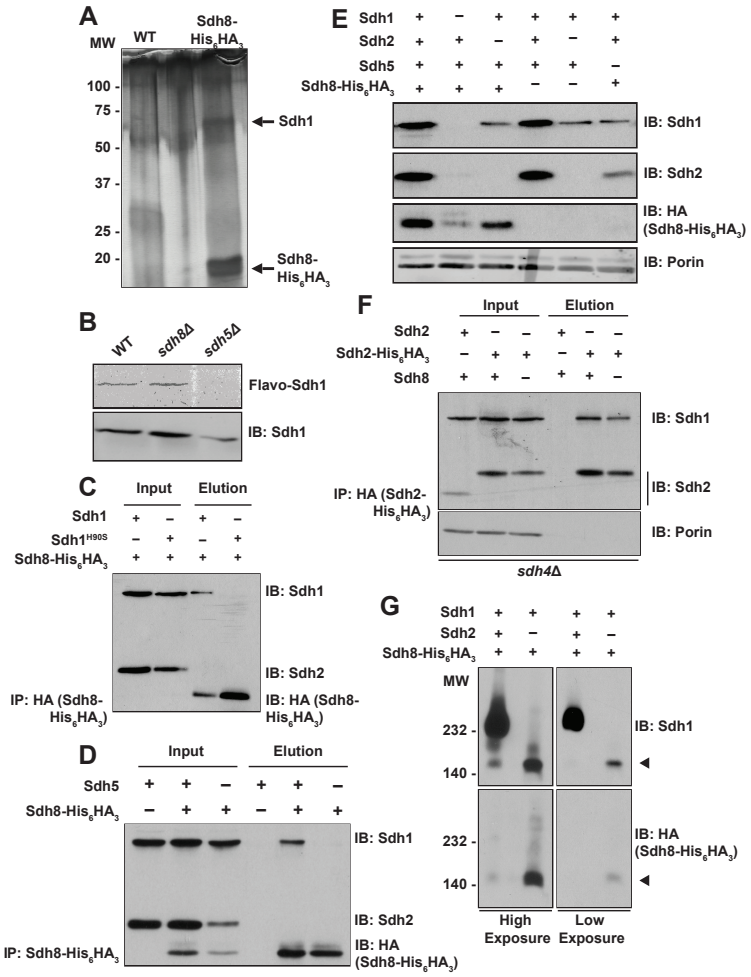

Supplemental Figure 6

Figure S7, related to Figure 7. Sdh8 protects the cell from oxidative stress

(A) Ten-fold serial dilutions of WT yeast transformed with an empty vector, WT yeast over-expressing SDH1, *sdh8*Δ cells transformed with an empty vector, and *sdh8*Δ cells over-expressing SDH1 were plated on media containing the indicated carbon source and incubated at 30°C (BY4741 background). (B) WT yeast cells (W303 background) were grown in synthetic media containing 2% glycerol. Two hours before analysis by flow cytometry the cells were either treated with 10mM H_2O_2 or 10mM DTT or left untreated (NT). Shown are representative histograms of the measurement of the ratio of oxidized/reduced mito-roGFP in 30,000 cells from each group. (C) The median value of the ratio of oxidized/reduced mito-roGFP is plotted for WT cells experiencing each treatment. (±SEM; N=3 biological replicates. $^{**}p < 0.01$). (D) WT and *sdh8*Δ cells were transformed with mito-roGFP and imaged by fluorescence microscopy. (E) Ten-fold serial dilutions of WT yeast transformed with an empty vector, sdh8Δ cells transformed with an empty vector, and *sdh8*Δ cells over-expressing *SOD2* were plated on media containing the indicated carbon source and incubated at 30°C (BY4741 background). (F) Mitochondria harvested from WT and *sdh8*Δ cells carrying an empty vector or overexpressing *YAP1* were solubilized in digitonin and separated by BN-PAGE. (G) Mitochondria harvested from WT and *sdh8*Δ cells carrying an empty vector or overexpressing *YAP1* were subjected to western blot analysis to detect Sdh1, Sdh2, and Porin. (H) A model for the assembly of SDH is depicted. (1) Upon entry into the mitochondrial matrix, apo-Sdh1 is rapidly flavinated in a reaction that requires Sdh5 (Hao et al., 2009). (2) Acting as a co-chaperone, Sdh8 binds to flavinated Sdh1 forming an intermediate sub-complex that prevents Sdh1 autoxidation. (3) Sdh8 may also facilitate the formation of Sdh1-Sdh2 soluble dimers. (4) Finally, the Sdh1-Sdh2 dimer can dock on the IMM via interactions with Sdh3 and Sdh4 that have previously assembled in the IMM.

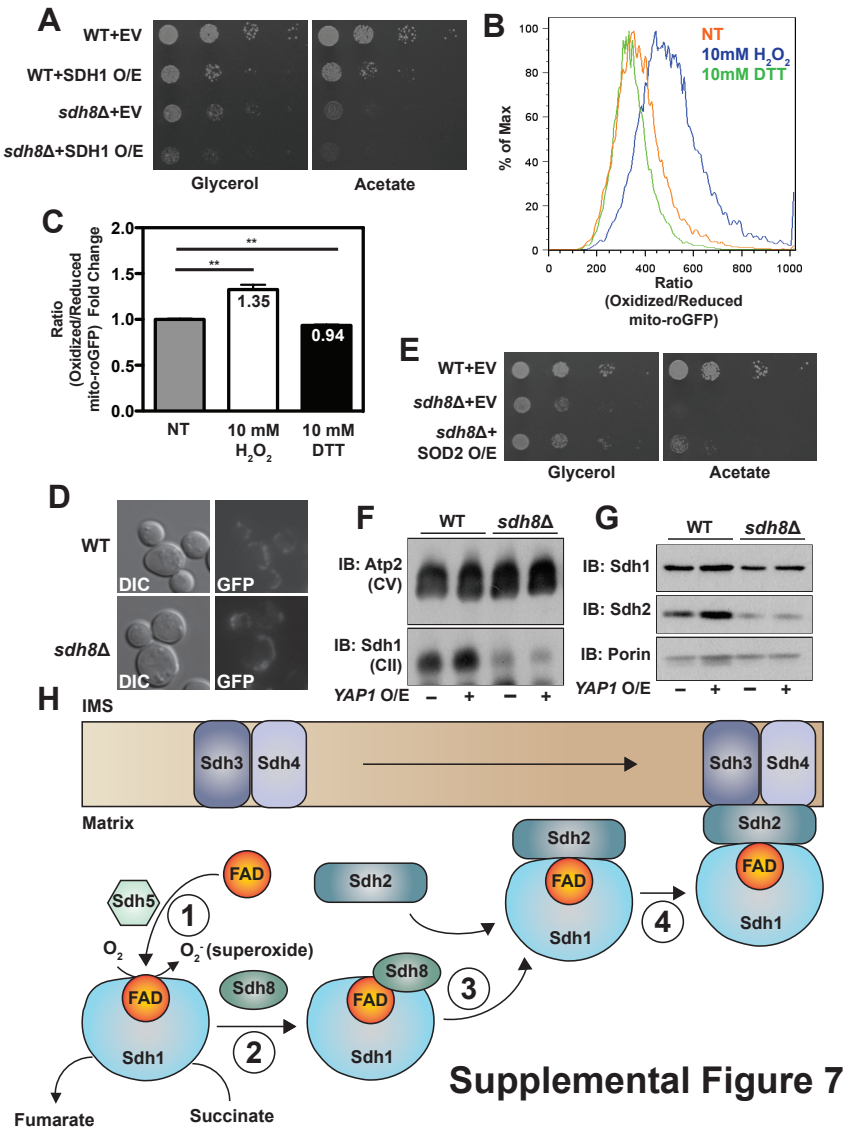

Supplemental Figure 7

Table S1, related to Figure 1. Description of the yeast strains used in this investigation.

Strain	Genotype	Source
WT (BY4741)	*Mat A his3 leu2 ura3 met15*	Open Biosystems
*sdh1*Δ	*Mat A his3 leu2 ura3 met15 sdh1::his3MX*	This Study
*sdh2*Δ	*Mat A his3 leu2 ura3 met15 sdh2::kanMX*	This Study
*sdh4*Δ	*Mat A his3 leu2 ura3 met15 sdh4::natMX*	This Study
*sdh8*Δ	*Mat A his3 leu2 ura3 met15 sdh8::hygMX*	This Study
*sdh1*Δ*sdh2*Δ	*Mat A his3 leu2 ura3 met15 sdh1::his3MX sdh2::kanMX*	This Study
*sdh1*Δ*sdh4*Δ	*Mat A his3 leu2 ura3 met15 sdh1::his3MX sdh4::natMX*	This Study
*sdh1*Δ*sdh8*Δ	*Mat A his3 leu2 ura3 met15 sdh1::his3MX sdh8::hygMX*	This Study
*sdh2*Δ*sdh4*Δ	*Mat A his3 leu2 ura3 met15 sdh2::kanMX sdh4::natMX*	This Study
*sdh2*Δ*sdh8*Δ	*Mat A his3 leu2 ura3 met15 sdh2::kanMX sdh8::hygMX*	This Study
*sdh4*Δ*sdh8*Δ	*Mat A his3 leu2 ura3 met15 sdh4::natMX sdh8::hygMX*	This Study
*sdh1*Δ*sdh2*Δ*sdh4*Δ	*Mat A his3 leu2 ura3 met15 sdh1::his3MX sdh2::kanMX sdh4::natMX*	This Study
*sdh1*Δ*sdh2*Δ*sdh8*Δ	*Mat A his3 leu2 ura3 met15 sdh1::his3MX sdh2::kanMX sdh8::hygMX*	This Study
*sdh1*Δ*sdh4*Δ*sdh8*Δ	*Mat A his3 leu2 ura3 met15 sdh1::his3MX sdh4::natMX sdh8::hygMX*	This Study
*sdh2*Δ*sdh4*Δ*sdh8*Δ	*Mat A his3 leu2 ura3 met15 sdh2::kanMX sdh4::natMX sdh8::hygMX*	This Study
*sdh1*Δ*sdh2*Δ*sdh4*Δ*sdh8*Δ	*Mat A his3 leu2 ura3 met15 sdh1::his3MX sdh2::kanMX sdh4::natMX sdh8::hygMX*	This Study
WT (W303)	*Mat A his3 leu2 ura3 met15 trp1*	David Stillman
*sdh1*Δ	*Mat A his3 leu2 ura3 met15 trp1 sdh1::kanMX*	This Study
*sdh2*Δ	*Mat A his3 leu2 ura3 met15 trp1 sdh2::kanMX*	This Study
*sdh5*Δ	*Mat A his3 leu2 ura3 met15 trp1 sdh5::kanMX*	This Study
*sdh8*Δ	*Mat A his3 leu2 ura3 met15 trp1 sdh8::hygMX*	
*sdh1*Δ*sdh8*Δ	*Mat A his3 leu2 ura3 met15 trp1 sdh1::kanMX sdh8::hygMX*	This Study
*sdh2*Δ*sdh8*Δ	*Mat A his3 leu2 ura3 met15 trp1 sdh2::kanMX sdh8::hygMX*	This Study
*sdh5*Δ*sdh8*Δ	*Mat A his3 leu2 ura3 met15 trp1 sdh5::kanMX sdh8::hygMX*	This Study

Supplemental Experimental Procedures

***Drosophila* strains**

The following stocks were obtained from the Bloomington Stock Center: *ElaV-Gal4 (Luo et al., 1994), Daughterless-Gal4* (Wodarz et al., 1995), *Frt82B,CoVa^{tend}/TM6B* (Mandal et al., 2005), *SdhB$^{[120811]}$/CyO* (Walker et al., 2006) and *SdhA$^{[HP21216]}$/CyO* . *Sdhaf4* mutants and transgenic lines were generated as described below. All fly stocks were maintained at 25°C on standard cornmeal/molasses/agar food ambient O_2 concentrations unless otherwise noted.

Generation of *dSdhaf4* mutant lines

DSdhaf4 mutants were generated by targeting the second exon of *dSdhaf4* using TALENs, as described (Cermak et al., 2011; Dahlem et al., 2012; Hu et al., 2013). The specificity of potential TALEN target sequences was determined using Target Finder (https://tale-nt.cac.cornell.edu) and a BLAST analysis. TALEN pairs were designed and constructed by the Mutation Generation and Detection Core Research Facility at the University of Utah (http://www.cores.utah.edu/) with the following specifications: Left binding site – 5'-CGAGATCAAGGAACCAAA-3'; Right binding site – 5'-AATGGCCTTCCAGAAGA-3'; Spacer – 5'-GACGCGCACCGAGAAGCT-3'. The TALEN Golden Gate kit described by Cermak et al was used with modifications and TALENs were assembled as described by Dahlem *et al* and Hu *et al*. Plasmid DNAs carrying the *dSdhaf4* TALEN construct were then purified with a Qiagen maxi-prep kit and concentrated by ethanol precipitation. RNAs were generated by digesting the TALEN construct with NotI, repurifying, and directing in vitro transcription using the AmpliScribe SP6 High Yield Transcription Kit (Epicentre), followed by the ScriptCap m7G Capping System (Epicentre). The TALEN RNAs were concentrated and 250 μg/ml of each RNA was combined in 0.1X PBS. We used the obligate heterodimer architecture DDD/RRR and injected ~200 *Canton S* embryos. ~35 surviving injected G_0 animals were crossed individually to a strain carrying a *CyO* balancer. ~5 F_1 progeny males from each cross were then outcrossed to a strain carrying a *CyO* balancer marked with GFP, and individual strains were isolated. Flies were screened for mutations in *dSdhaf4* by high

resolution melt analysis (Dahlem et al., 2012). Two putative mutant strains (*dSdhaf4*^{1} and *dSdhaf4*^{2}) were verified by DNA sequencing. Flies carrying a wild type *dSdhaf4* locus derived from the same G_0 animals as the *dSdhaf4*^{1} and *dSdhaf4*^{2} alleles were carried through the same series of crosses and used as genetically matched controls. This control is labeled *dSdhaf4*$^{+}$ or *dSdhaf4*$^{+/+}$ in all figures. The transposable P-element insertion p*CG7224*^{KG07581} was also used to generate a *dSdhaf4* allele by imprecise excision. The *dSdhaf4*^{3} allele, which was verified by Southern blotting, PCR and DNA sequencing, contains an unexcised fragment of the p*CG7224*^{KG07581} element (Supplemental Figure 3A). A precise excision was also isolated (*dSdhaf4*$^{Ex32+}$) and is used as a control for *dSdhaf4*^{3} in all relevant experiments. All mutant and control genotypes analyzed are in a w^{1118} background.

Generation of transgenic fly lines

To generate *UAS-dSdhaf4* rescue construct, the *CG7224* cDNA (GH 06541) was excised using XhoI and BglII and inserted into a pUAST vector. To generate the *UAS-hSdhaf4* construct, the *hSdhaf4* cDNA was PCR amplified from pJR3455A, which contains an *hSdhaf4* cDNA amplified from HepG2 cells using the primers 5'-CGAGATCTATGACCCCATCGAGGCTT-3' and 5'-CGCTCGAGTTAAAAATCAATACAGCGTCCTTTT-3'. This amplicon was then cut with BglII and XhoI and cloned into an pUAST-AttB plasmid. All plasmids used to generate transgenic lines were verified by restriction digestion and DNA sequencing. *UAS-dShdaf4* transgenic lines were generated using standard P-element mediated transformation, and *UAS-hSdhaf4* transgenic lines were targeted to AttP2 by site-directed transformation (Bateman et al., 2006; Pfeiffer et al., 2010). *elav-Gal4*, *UAS-dSdhaf4* and *UAS-hSdhaf4* on the third chromosome were crossed into the *dSdhaf4*^{1} or *dSdhaf4*^{2} background using balanced crossing schemes. *Da-Gal4* on the third chromosome was recombined onto the same chromosome as the *dSdhaf4*^{2} allele. The presence of the *dSdhaf4* mutant alleles in transgenic lines was verified by DNA sequencing and complementation tests.

***Drosophila* genetic interactions**

To assay whether combining the lethal allele of *SdhA* or the viable hypomorphic allele of *SdhB* with *dSdhaf4* mutations affects viability, the $SdhA^{[HP21216]}$ or $SdhB^{[12081]}$ insertions were recombined with the either $dSdhaf4^{1}$ or $dSdhaf4^{2}$ alleles. Flies carrying these recombinant chromosomes, $dSdhaf4^{1}$ allele alone, *Sdh* allele alone, or a wild type chromosome over an SM5 balancer marked with Cy^{-} were intercrossed in various combinations. All crosses were performed in triplicate. The number of expected progeny resulting from these crosses was calculated based on mendelian ratios. To determine if the expected number of progeny of non-SM5 chromosomes reached adulthood, the total number of eclosed Cy^{+} adult flies was counted, and that number was compared to 1/2 or 1/3 of the total number of progeny depending on whether a 1:1 or 1:2 ratio was expected. The N values shown in Figure 4C and Supplemental figure 4F concerning the genetic interactions between *dSdhaf4* and *SdhA/B* represent the total number of progeny counted from the pertinent cross. Since $CoVa^{[tend]}$ mutation is on the third chromosome, $dSdhaf4^{1}/SM5;CoVa^{[tend]}/TM3$ or $dSdhaf4^{+}/SM5;CoVa^{[tend]}/TM3$ flies were crossed to $dSdhaf4^{2}/dSdhaf4^{2}$ or $dSdhaf4^{+}/dSdhaf4^{+}$ flies, respectively. A normal 1:1 distribution of $Cy^{-}:Cy^{+}$ flies were observed (Data not shown), so only the Cy^{+} flies were counted. Since TM3 is marked with Sb^{-}, the total number of $Cy^{+};Sb^{-}$ or $Cy^{+};Sb^{+}$ flies was counted and compared to the 1:1 ratio expected. The N values shown in Figure 4C concerning the lack of a genetic interaction between *dSdhaf4* and *CoVa* represent the total number of Cy^{+} progeny assayed.

***Drosophila* lifespan analyses**

For lifespan measurements, flies were allowed to eclose for one day, and were separated into vials containing ~20 flies. Every 2-4 days dead flies were counted/removed and surviving flies transferred to new food vials. >100 flies were assayed for each genotype. For starvation assays, 2-4 day old females were transferred to starvation media (1% agar in H_2O) and the number of surviving flies was assayed every 12 hours. >90 flies were assayed per genotype. To measure sensitivity to hyperoxia, vials containing 2-4 day old females were placed in polyethylene bags (Scienceware 12”x16”), which were subsequently filled with 100% O_2 and sealed using a Quick Seal bag sealer. Bags were refilled with fresh O_2 2-3 times daily and the number of surviving flies was assayed every

24 hours. >40 flies were assayed per genotype. A similar degree of hyperoxia sensitivity was observed in *dSdhaf* mutants placed in a styrofoam box with a continuous flow of 100% O_2 as described (Walker et al., 2006), however, we could not maintain this experimental paradigm long enough to assay the full lifespan of controls (data not shown). Survival during hyperoxia was assayed at room temperature, whereas flies for all other lifespan experiments were kept at 25˚C. Experiments on female flies are presented for all survival curves, but similar results were observed when assaying males (data not shown).

Electron microscopy

Heads were removed from 8-12 day old female flies, the was proboscis removed, and heads were fixed overnight in EM grade 3% glutaraldehyde/3% paraformaldehyde in PBS at 4˚C. After fixation, heads were rinsed three times in 10mM cacodylate buffer and postfixed in 2% OsO_4 for 2 hours at room temperature. The heads were then washed in the same buffer, followed by a wash in dH2O, and then post stained in 1% uranyl acetate for 1 hour at room temperature. After washing with dH2O, heads were dehydrated in a graded series of acetone (25%, 50%, 75%, 90% and 3x100% for 20 min each step), and then infiltration was conducted over 3 days followed by embedding in epoxy resin (Embed 812, Electron Microscopy Sciences). For the infiltration step, specimens were incubated in 30% resin and acetone for 6 hours, then in placed in 70% resin and acetone overnight. The next day, the specimens were placed into 90% resin and acetone for 8 hrs and 100% resin for another overnight incubation. On the following day, after two incubations in freshly prepared 100% resin over 6 hrs, specimens were embedded and polymerized at 60°C for 48 hrs. Ultrathin (70nm) sections were obtained with diamond knife (Diatome) and an ultratome Leica UC6 (Leica Microsystems, Bannockburn,IL). Grids with sections were post stained with saturated uranyl acetate in dH2O for 20 min and with lead citrate for 10 min and imaged at 120kV using a Technai T 12 electron microscope. N=3 flies assayed per genotype.

Immunoblotting

Antibodies used for immunoblotting: anti-SdhA (Abcam 137756; rabbit polyclonal to human SdhA), anti-SdhB (Abcam 14714; mouse monoclonal to human SdhB), anti-Atp synthase a (Abcam 14748; mouse monoclonal to bovine Atp5) and anti-beta Tubulin (Chemicon MAB380; mouse monoclonal), anti-VDAC (Abcam 15895), anti-Sdh1 (rabbit polyclonal to yeast Sdh1; was a generous gift from Dennis Winge), anti-Sdh2 (rabbit polyclonal to yeast Sdh2; was a generous gift from Dennis Winge), anti-Porin (Abcam 110326).

SdhA/Sdh1 flavination assay

To visualize flavinated SdhA, mitochondrial extracts were fractionated by SDS-PAGE and the gel was incubated for 20 minutes in 10% acetic acid. Auto-fluorescent flavo-SdhA was imaged using an ethidium bromide filter, as previously described (Hao et al., 2009). The gel was stained with Coomassie Blue to visualize total protein as a control for loading in Drosophila experiments. In yeast experiments, immunoblot for Sdh1 was used to control for loading.

Yeast strains and growth conditions

Saccharomyces cerevisiae (BY4741 *MATa, his3 leu2 met15 ura3*) and *Saccharomyces cerevisiae* (W303a *MATa, his3 leu2 met15 trp1 ura3*) were used as the wild-type strains where indicated. Each mutant was derived from a BY4741 or W303 diploid using a standard PCR-based homologous recombination method. Each haploid was generated by sporulation and tetrad dissection. The genotypes of all strains used in this study are listed in Supplemental Table 1. Yeast transformation was performed by the standard TE/LiAc method and transformed cells were recovered and grown in synthetic complete glucose (SD) medium lacking the appropriate amino acid(s) for selection purposes. Medium used in this study includes YPA and synthetic minimal medium supplemented with 2% glucose, 2% raffinose, 2% glycerol, 2% ethanol, or 2% acetate.

Growth assays were performed using synthetic minimal media supplemented with the appropriate amino acids and indicated carbon source. Overnight cultures were back-diluted equivalent ODs and spotted as 10-fold serial dilutions.

Plasmid construction

The plasmids expressing internal His_6HA_3 or GFP tagged Sdh8 were generated by PCR amplification of SDH8 (NC_001134.8) flanked by its upstream promoter and downstream terminator regions off genomic DNA. The untagged gene along with its regulatory elements was ligated into pRS415 using XhoI and SpeI. Sewing PCR was used to add NheI and SalI restriction sites between the codons encoding residues N82 and S83 of SDH8. The His_6HA_3 tag, which was chemically synthesized, and the GFP tag, which was amplified by PCR, were each ligated between N82 and S83 using the NheI and SalI yielding the final SDH8-His_6HA_3 and SDH8-GFP constructs. The sequence of each construct was confirmed by sequencing (Genewiz).

Human and *Drosophila SDHAF4* were cloned such that the expression of each gene was under the control of the SDH8 promoter. Sewing PCR was used to clone the SDH8 promoter and terminator separated by NheI and SalI restriction sites into pRS415. SDHAF4 from each species was PCR amplified from cDNA and ligated between the SDH8 promoter and terminator using NheI and SalI.

$Sdh1^{H90A}$ and $Sdh1^{H90S}$ constructs were generated by sewing PCR. The mutants were ligated into pRS416 using XhoI and XmaI. Both constructs were expressed under the control of the native *SDH1* promoter and terminator.

Isolation of Yeast Mitochondria

Yeast cells were harvested in mid-log phase. Preparation of crude mitochondria was as described previously .(Boldogh and Pon, 2007) Cell pellet was washed once with ddH_2O and incubated in TD buffer (100 mM Tris-SO_4, pH 9.4 and 100 mM DTT) for 15 min at 30°C. Spheroplasts were obtained by incubating cells in SP buffer (1.2 M Sorbitol and 20 mM potassium phosphate, pH 7.4) supplemented with 0.3 mg/mL lyticase for 1 hour

at 30°C to remove the cell wall. Spheroplasts were gently washed once and homogenized in ice-cold SEH buffer (0.6 M sorbitol, 20 mM HEPES-KOH, pH 7.4, 2 mM $MgCl_2$, 1mM EGTA) using a dounce homogenizer applied with 30-40 strokes. Crude mitochondria were further purified using differential centrifugation. When needed, pure mitochondria were isolated by ultracentrifugation through a continuous nycodenz gradient.

Fluorescence Microscopy

The sdh8 mutant strain transformed with plasmids expressing Sdh8-GFP and MtRFP was grown in SD medium overnight. Cells were back-diluted in fresh media to 0.1 OD and allowed to grow for several hours. Images wee captured using a Zeiss Axioplan 2 Imaging microscope (Carl Zeiss).

Steady-State Protein Analysis

Yeast mitochondria were solubilized in Laemmli buffer. Samples were resolved by SDS-PAGE and assessed by immunoblot. *Drosophila* extracts from either 20 μg isolated mitochondria or the equivalent of ½ of a fly were analyzed in each lane of a Western blot.

Immunoprecipitation of Sdh8-His_6HA_3 and Sdh2-His_6HA_3

Crude mitochondria were isolated and resuspended to a concentration of 5 mg/mL in XWA buffer. Soluble proteins were extracted by sonication and centrifugation at 20,000 x g for 20 mins. Membrane proteins were extracted in buffer containing 0.7% digitonin for 1 hr. and and centrifugation at 20,000 x g for 20 mins. Cleared mitochondrial lysates were incubated with anti-HA antibody conjugated agarose (Sigma) for 2 hrs. at 4°C. The agarose was washed 3-5 times and eluted in buffer containing 1 mg/mL HA peptide. Elution samples were precipitated in 20% TCA, resolved by SDS-PAGE, and assessed by mass spectroscopy and/or immunoblot.

Assessment of Submitochondrial Localization and Solubility

Submitochondrial fractionation was performed using a protocol adapted from (Boldogh and Pon, 2007). Mitochondria were incubated in the isotonic SH buffer (20mM HEPES-

KOH, pH 7.4, 0.6M Sorbitol) of hypotonic H buffer (20mM HEPES-KOH, pH 7.4) with and without 1% Tritin-X100. Samples were treated with Protease K (New England BioLabs) on ice for 30 min. Addition of PMSF to each sample was used to terminate protease digestion. Samples were resolved by SDS-PAGE and assessed by immunoblot.

Solubility of Sdh8 was assessed by ultracentrifugation. Mitochondria was suspended in SH buffer and subjected to sonication. Mitochondrial membranes were isolated by ultracentrifugation at 100,000 x g for 30 min (MLA-130, Beckman Coulter). The membrane (membrane fraction) was resuspended in 2X Laemmli buffer. The supernatant (soluble fraction) was precipitated in 20% TCA and resuspended in 2X Laemmli buffer. Samples were resolved by SDS-PAGE and assessed by immunoblot.

Yeast Enzyme Activity Assays

SDH and MDH activity assays were performed as described in Hao *et al.,* 2009.

Aconitase Activity Assay

Yeast cells were grown in SD medium well into stationary phase and resuspended in lysis buffer (50 mM Tris-HCl, 50 mM KCl, 2 mM sodium citrate dihydrate, 10% glycerol, 1 mM PMSF, and 7 mM β-mercaptoethanol), and stored at –80°C overnight. After thawing on ice, cells were homogenized by vortexing with glass beads and cleared lysate was collected by centrifugation. Aconitase activity was measured by coupling with NADP+-dependent isocitrate dehydrogenase activity. 30 µl of crude lysate was mixed with 150 µl of reaction mixture (1 M Tris-Cl pH 8.0, 10 mM MgCl2, 10 mM NADP+, 0.32 units of NADP+- dependent Isocitrate Dehydrogenase), and 10 µl of 50 mM citrate. The reaction mixture was recorded at 340nm for 2 minutes (15 sec intervals). Aconitase activity was normalized to total protein concentration.

Yeast Metabolomic Analysis

Metabolomic analysis was carried out in the Metabolomics Core Research Facility at the University of Utah School of Medicine. Yeast cultures were grown to an OD of 1 in synthetic media containing 2% glycerol and 2% ethanol.

Mammalian Cell Culture

C2C12 myoblasts (ATCC CLR-1772) were maintained in DMEM with 10% FBS, 2mM Glutamax (Gibco), and 1% Primocin (Invitrogen). All knockdowns were performed by treating cells with 5 nM total siRNA, using the Lipofectamine RNAiMax tranfection reagent (Invitrogen). The All-Stars non-targeting siRNA (Qiagen) was used as a control for siRNAs targeting *SDHAF4* (NM_026503) which were designed using Dharmacon siDesign Center tool (http://www.dharmacon.com/designcenter/DesignCenterPage.aspx). Sequences of the sense strands of targeting siRNAs, which include a 3' tt DNA overhang, are as follows: (si1) UGAGUUAUCAGGAAGGAAA and (si3) UCUCACAACUGCAGAAUCA. Cells were subjected to knockdown on day 0, again on day 3, and harvested for analysis on day 6. Total RNA was isolated with the RNeasy Mini Kit (Qiagen) and reverse transcribed to cDNA using the High Capacity cDNA Reverse Transcriptase Kit (Applied Biosystems). Quantitative PCR was performed on cDNA with a Roche 480 LightCycler using LightCycler 480 SYBR Green 1 Master Mix (Roche) to confirm knockdown.

Isolation of Mammalian Mitochondria

The procedure was adapted from (Bozidis et al., 2007). C2C12 cells were trypsinized, washed twice with ice cold PBS and pelleted. The cell pellet was resuspended in 2 mL ice cold MTE buffer and lysed by sonication (Branson Model 250, continuous pulse, power setting 3.5, 3 cycle, 10 s. each). Cell debris and nuclei were pelleted at 1,400 x g for 10 min. Mitochondria were recovered from the supernatant by centrifugation at 10,000 x g for 10 min. Mitochondria were resuspended in MTE. Protein concentration was determined by Advanced Protein Assay Reagent (Cytoskeleton).

Supplemental References

Bateman, J.R., Lee, A.M., and Wu, C.T. (2006). Site-specific transformation of Drosophila via phiC31 integrase-mediated cassette exchange. Genetics *173*, 769-777.
Boldogh, I.R., and Pon, L.A. (2007). Purification and subfractionation of mitochondria from the yeast Saccharomyces cerevisiae. Methods Cell Biol *80*, 45-64.
Bozidis, P., Williamson, C.D., and Colberg-Poley, A.M. (2007). Isolation of endoplasmic reticulum, mitochondria, and mitochondria-associated membrane fractions from

transfected cells and from human cytomegalovirus-infected primary fibroblasts. Curr Protoc Cell Biol *Chapter 3*, Unit 3 27.
Cermak, T., Doyle, E.L., Christian, M., Wang, L., Zhang, Y., Schmidt, C., Baller, J.A., Somia, N.V., Bogdanove, A.J., and Voytas, D.F. (2011). Efficient design and assembly of custom TALEN and other TAL effector-based constructs for DNA targeting. Nucleic Acids Res *39*, e82.
Dahlem, T.J., Hoshijima, K., Jurynec, M.J., Gunther, D., Starker, C.G., Locke, A.S., Weis, A.M., Voytas, D.F., and Grunwald, D.J. (2012). Simple methods for generating and detecting locus-specific mutations induced with TALENs in the zebrafish genome. PLoS Genet *8*, e1002861.
Hao, H.X., Khalimonchuk, O., Schraders, M., Dephoure, N., Bayley, J.P., Kunst, H., Devilee, P., Cremers, C.W., Schiffman, J.D., Bentz, B.G., *et al*. (2009). SDH5, a gene required for flavination of succinate dehydrogenase, is mutated in paraganglioma. Science *325*, 1139-1142.
Herrmann, W., and Obeid, R. (2011). Homocysteine: a biomarker in neurodegenerative diseases. Clin Chem Lab Med *49*, 435-441.
Hu, R., Wallace, J., Dahlem, T.J., Grunwald, D.J., and O'Connell, R.M. (2013). Targeting human microRNA genes using engineered Tal-effector nucleases (TALENs). PLoS One *8*, e63074.
Jafari, P., Braissant, O., Zavadakova, P., Henry, H., Bonafe, L., and Ballhausen, D. (2013). Brain damage in methylmalonic aciduria: 2-methylcitrate induces cerebral ammonium accumulation and apoptosis in 3D organotypic brain cell cultures. Orphanet J Rare Dis *8*, 4.
Luo, L., Liao, Y.J., Jan, L.Y., and Jan, Y.N. (1994). Distinct morphogenetic functions of similar small GTPases: Drosophila Drac1 is involved in axonal outgrowth and myoblast fusion. Genes Dev *8*, 1787-1802.
Mandal, S., Guptan, P., Owusu-Ansah, E., and Banerjee, U. (2005). Mitochondrial regulation of cell cycle progression during development as revealed by the tenured mutation in Drosophila. Dev Cell *9*, 843-854.
Pearl, P.L., Gibson, K.M., Cortez, M.A., Wu, Y., Carter Snead, O., 3rd, Knerr, I., Forester, K., Pettiford, J.M., Jakobs, C., and Theodore, W.H. (2009). Succinic semialdehyde dehydrogenase deficiency: lessons from mice and men. J Inherit Metab Dis *32*, 343-352.
Pfeiffer, B.D., Ngo, T.T., Hibbard, K.L., Murphy, C., Jenett, A., Truman, J.W., and Rubin, G.M. (2010). Refinement of tools for targeted gene expression in Drosophila. Genetics *186*, 735-755.
Reinders, J., Zahedi, R., Pfanner, N., Meisinger, C., and Sickmann, A. (2006). Toward the Complete Yeast Mitochondrial Proteome: Multidimensional Separation Techniques for Mitochondrial Proteomics, Journal of Proteome Research *5*, 1543-1554.
Walker, D.W., Hajek, P., Muffat, J., Knoepfle, D., Cornelison, S., Attardi, G., and Benzer, S. (2006). Hypersensitivity to oxygen and shortened lifespan in a Drosophila mitochondrial complex II mutant. Proc Natl Acad Sci U S A *103*, 16382-16387.
Wodarz, A., Hinz, U., Engelbert, M., and Knust, E. (1995). Expression of crumbs confers apical character on plasma membrane domains of ectodermal epithelia of Drosophila. Cell *82*, 67-76.

CHAPTER 4

THE MITOCHONDRIAL ACYL CARRIER PROTEIN (ACP) COORDINATES MITOCHONDRIAL FATTY ACID SYNTHESIS WITH IRON SULFUR CLUSTER BIOGENESIS

Jonathan G. Van Vranken, Mi-Young Jeong, Peng Wei, Yu-Chan Chen, Steven P. Gygi, Dennis R. Winge, and Jared Rutter

Reprinted with permission from eLife, vol. 5, e17828

eLIFE elifesciences.org

SHORT REPORT

The mitochondrial acyl carrier protein (ACP) coordinates mitochondrial fatty acid synthesis with iron sulfur cluster biogenesis

Jonathan G Van Vranken[1†], Mi-Young Jeong[1,2†], Peng Wei[1], Yu-Chan Chen[1‡], Steven P Gygi[3], Dennis R Winge[1,2*], Jared Rutter[1,4*]

[1]Department of Biochemistry, University of Utah School of Medicine, Salt Lake City, United States; [2]Department of Medicine, University of Utah School of Medicine, Salt Lake City, United States; [3]Department of Cell Biology, Harvard University School of Medicine, Boston, United States; [4]Howard Hughes Medical Institute, University of Utah School of Medicine, Salt Lake City, United States

Abstract Mitochondrial fatty acid synthesis (FASII) and iron sulfur cluster (FeS) biogenesis are both vital biosynthetic processes within mitochondria. In this study, we demonstrate that the mitochondrial acyl carrier protein (ACP), which has a well-known role in FASII, plays an unexpected and evolutionarily conserved role in FeS biogenesis. ACP is a stable and essential subunit of the eukaryotic FeS biogenesis complex. In the absence of ACP, the complex is destabilized resulting in a profound depletion of FeS throughout the cell. This role of ACP depends upon its covalently bound 4'-phosphopantetheine (4-PP)-conjugated acyl chain to support maximal cysteine desulfurase activity. Thus, it is likely that ACP is not simply an obligate subunit but also exploits the 4-PP-conjugated acyl chain to coordinate mitochondrial fatty acid and FeS biogenesis.
DOI: 10.7554/eLife.17828.001

***For correspondence:** dennis.winge@hsc.utah.edu (DRW); rutter@biochem.utah.edu (JR)

[†]These authors contributed equally to this work

Present address: [‡]Department of Biology, Stanford University, Stanford, United States

Competing interests: The authors declare that no competing interests exist.

Funding: See page 10

Received: 13 May 2016
Accepted: 22 July 2016
Published: 19 August 2016

Reviewing editor: J Wade Harper, Harvard Medical School, United States

Introduction

The mitochondrial acyl carrier protein (ACP; ***Figure 1—figure supplement 1***) plays a critical role in the evolutionarily conserved type II fatty acid biosynthesis pathway (FASII; ***Figure 1—figure supplement 2A***). Unlike the cytosolic fatty acid biosynthesis pathway (FASI), the mitochondrial FASII system, which is homologous to the prokaryotic fatty acid biosynthesis pathway, utilizes a set of monofunctional enzymes that interact transiently with ACP to catalyze the initiation and elongation of nascent acyl chains (***Hiltunen et al., 2010***). To facilitate FASII, ACP utilizes a 4'-phosphopantetheine prosthetic group (4-PP), which is covalently bound to an invariant Ser residue (***Majerus et al., 1965***; ***Stuible et al., 1998***). As such, ACP serves as a soluble scaffold for acyl intermediates during the stepwise process of *de novo* fatty acid synthesis. Currently, it is thought that the primary product of ACP-dependent FASII is octanoate, which is cleaved from ACP and further processed to generate lipoic acid. Lipoic acid is an obligate cofactor of the pyruvate dehydrogenase and α-ketoglutarate dehydrogenase complexes as well as the branched chain α-keto acid dehydrogenase and glycine cleavage complex (***Hiltunen et al., 2010***; ***Brody et al., 1997***). In addition, a FASII-derived acyl chain other than lipoic acid is required for RNase P function in tRNA maturation (***Schonauer et al., 2008***).

Biochemical analyses of mammalian FASII enzymes demonstrate that this pathway is capable of generating ACP-bound acyl chains as long as fourteen carbons (***Zhang et al., 2005***). Since lipoic acid biosynthesis requires an acyl chain of just eight carbons, it is likely that these extended FASII-synthesized fatty acids serve an alternative function in mitochondria (***Brody et al., 1997***). Indeed,

eLife digest Like animals and plants, yeast cells contain structures called mitochondria. These structures are commonly referred to as the powerhouses of the cell because they provide much of the energy that cells need to survive. All mitochondria contain a protein called acyl carrier protein (ACP), which cells need in order to live. The ACP protein has a number of known roles including manufacturing the molecules that make up certain fats and helping to organise other proteins that are important for energy production. However, neither of these roles explain why yeast cells require ACP because the other proteins required for these processes are not required for survival.

Mitochondria are also the sites where iron and sulfur atoms are joined together to make the iron sulfur clusters that many proteins need in order to carry out their roles. Van Vranken, Jeong et al. now show that the ACP protein associates with a molecular machine that makes iron sulfur clusters in the mitochondria of budding yeast cells. The experiments show that this interaction is needed to produce iron sulfur clusters, and without it the other proteins involved in the process are not able to work together. Since iron sulfur clusters are essential for life, this could explain why cells cannot survive without ACP. Van Vranken et al. also showed that ACP is only able to efficiently produce iron sulfur clusters when a chemical called a "4-PP-conjugated acyl chain" is attached to it.

It is possible to separate the activity of ACP in making iron sulfur clusters from its previously known roles. Van Vranken et al. suggest that the addition of the 4-PP-conjugated acyl chain to ACP may help to balance the use of ACP between its different activities. Moving forward, Van Vranken et al. hope to determine the structure of ACP in more detail to understand how it contributes to iron sulfur cluster formation, and why this single protein has evolved to perform so many distinct roles.

DOI: 10.7554/eLife.17828.002

proteomic and structural studies have demonstrated that ACP is a stable accessory subunit of mitochondrial respiratory Complex I (CI) (***Sackmann et al., 1991***; ***Angerer et al., 2014***). Furthermore, the pool of ACP associated with CI contains a 4-PP-conjugated 3-hydroxymyristic acid, however, the functional importance of this 14-carbon acyl chain has never been investigated in the context of CI activity or assembly (***Carroll et al., 2003***).

In *Saccharomyces cerevisiae, ACP1*, the gene encoding ACP, is essential for cell viability in multiple strain backgrounds, while the genes required for lipoic acid biosynthesis and ligation are not (***Figure 1A***, ***Figure 1—figure supplement 2B,C***) (***Schonauer et al., 2008***; ***Brody et al., 1997***). This is consistent with reports demonstrating that ACP is essential for viability in *Yarrowia lipolytica* (***Dobrynin et al., 2010***) and in mammalian cells (***Yi and Maeda, 2005***; ***Feng et al., 2009***). Moreover, *S. cerevisiae* mitochondria do not have CI or any structurally similar analog of it. Since neither known function explains the essentiality of *ACP1*, we reasoned that ACP must perform a distinct, unknown, and essential mitochondrial function.

Results and conclusions

To begin to define the essential function of Acp1, we purified endogenously expressed and fully functional Acp1-HA (***Figure 1A***) from purified mitochondria to discover interacting proteins that might explain the *acp1*Δ phenotype. We were particularly intrigued by the co-purification of three subunits of the ISU complex—Nfs1, Isd11, and Isu1—each of which is required for FeS biogenesis and essential for viability. The cysteine desulfurase (Nfs1) and Isd11 form the core of the ISU complex and catalyze the conversion of cysteine to alanine thereby generating a persulfide intermediate, which is the source of sulfide ions that combine with ferrous iron on the Isu1 scaffold protein to form [2Fe-2S] clusters (***Garland et al., 1999***; ***Mühlenhoff et al., 2004***; ***Adam et al., 2006***; ***Wiedemann et al., 2006***). To confirm these interactions, we immunoprecipitated Acp1-HA from isolated mitochondria and analyzed the eluates by immunoblot. Indeed, Nfs1, Isd11, and Isu1 all specifically co-immunoprecipitate with Acp1, although Isu1 appears to interact less avidly than Nfs1 or Isd11 (***Figure 1B***). In addition to SDS-PAGE, the resultant eluates were also resolved by blue native (BN)-PAGE, which demonstrated that Acp1 co-purifies with the intact core Nfs1-Isd11 complex (***Figure 1B***). Finally, Nfs1-V5 and Isd11-V5 were each immunoprecipitated from isolated

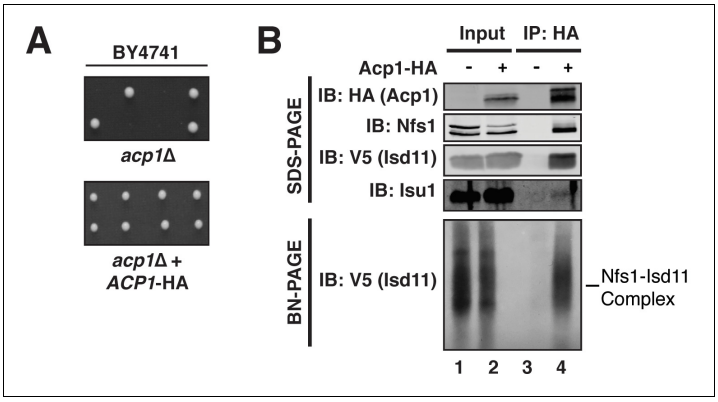

Figure 1. Acp1 is a stable subunit of the ISU complex. (**A**) *acp1Δ* heterozygous diploids were dissected with and without a plasmid expressing Acp1-HA (BY4741) and spores were grown on YPAD medium for 2 days. Sporulation of the heterozygous deletion strain failed to generate haploid *ACP1* deletion strains unless a vector borne *ACP1* gene was present. (**B**) Purified mitochondria from cells either expressing Acp1-HA or not were solubilized by digitonin (input) and then subjected to anti-HA immunoprecipitation. The resulting eluates and input samples were subjected to SDS-PAGE and BN-PAGE and immunoblot.

DOI: 10.7554/eLife.17828.003

The following figure supplements are available for figure 1:

Figure supplement 1. Protein sequence alignment of ACP from eukaryotes.

DOI: 10.7554/eLife.17828.004

Figure supplement 2. Eukarotic mitochondrial fatty acid biosynthesis (FASII) pathway.

DOI: 10.7554/eLife.17828.005

Figure supplement 3. Acp1 is a stable subunit of the ISU complex.

DOI: 10.7554/eLife.17828.006

mitochondria. As expected, Acp1-HA was detected in the eluates of each immunoprecipitation (***Figure 1—figure supplement 3***). These results are further supported by proteomics-based interaction studies, which identify human ACP, NFS1, and ISD11 as mutually interacting proteins in mammalian cells (***Huttlin et al., 2015***). Taken together these data demonstrate that Acp1 is a stable and evolutionarily conserved subunit of the ISU complex with Nfs1, Isd11, and Isu1.

FeS biogenesis is an essential function of mitochondria and is absolutely dependent on the ISU complex with which Acp1 stably interacts (***Lill et al., 1999***). Thus, we hypothesized that the essential function of Acp1 might relate to FeS biogenesis. We engineered inducible *ACP1* knockdown strains ($Acp1^{KD}$) using two distinct strategies and strain backgrounds—$TetO_7$-*ACP1* in the BY4741 background and Gal-*ACP1* in the DY150 background, in which *ACP1* expression is suppressed by doxycycline and galactose withdrawal, respectively. As expected, $Acp1^{KD}$ cells from each background displayed attenuated growth upon *ACP1* shutdown, which is particularly evident on respiration-requiring glycerol medium (***Figure 2—figure supplement 1A–C***). Importantly, viability could be restored in each of these strains by episomal expression of the Acp1-HA at endogenous levels. In addition to the expected loss of lipoic acid-containing subunits of pyruvate dehydrogenase and α-ketoglutarate dehydrogenase in the $Acp1^{KD}$ cells, we also observed a specific destabilization of the FeS-containing subunits of Complex II (Sdh2) and Complex III (Rip1) and loss of those assembled respiratory complexes (***Figure 2A*** and ***Figure 2—figure supplement 2A***). A similar destabilization of these complexes occurs in cells depleted for Nfs1 and Isu1 (***Adam et al., 2006***; ***Wiedemann et al., 2006***). Importantly, Complex III biogenesis stalls in $Acp1^{KD}$ cells at the final stage of assembly – incorporation of the Rieske FeS protein (Rip1) (***Figure 2A***; IB: Rip1)–resulting in the accumulation of a stable assembly intermediate of Complex III lacking Rip1 (***Figure 2A***; III_2*; IB:

Qcr7). The presence of the late stage intermediate III_2* indicates that mitochondrial translation of the Cob cytochrome b subunit is normal in $Acp1^{KD}$ cells (***Atkinson et al., 2011***; ***Cui et al., 2012***). Likewise, translation of the mitochondrial subunits of ATP synthase is normal as seen by the assembled F_1F_0 complex (***Figure 2A***). We also observed a loss of activity of aconitase, a mitochondrial enzyme with an obligate FeS cofactor (***Figure 2B*** and ***Figure 2—figure supplement 2B***).

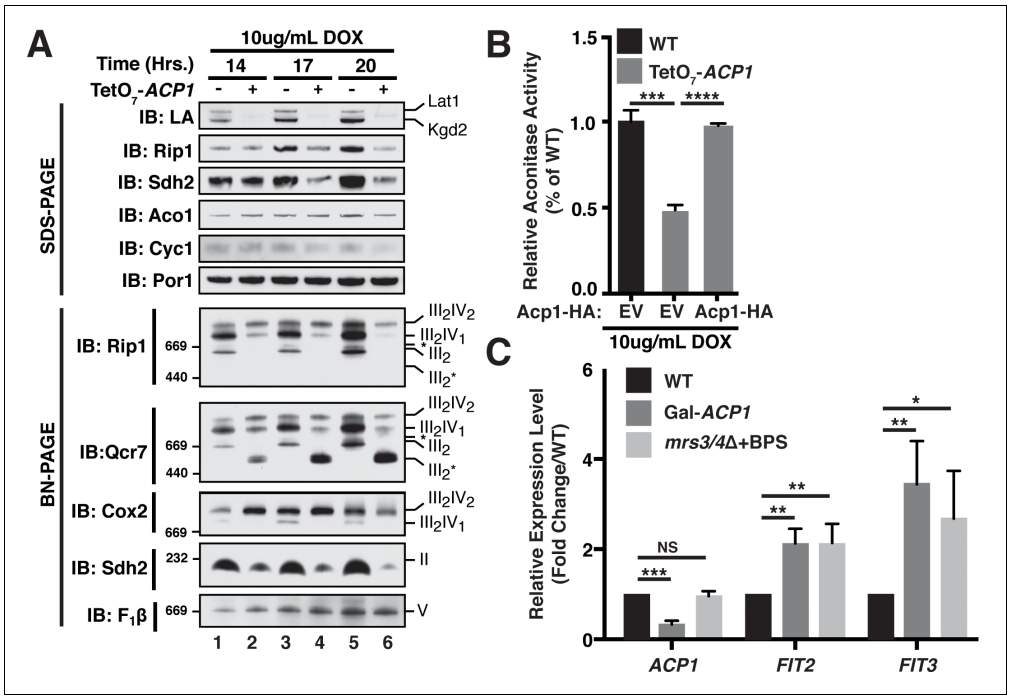

Figure 2. Acp1 is required for FeS biogenesis. (**A**) Isolated mitochondria from the indicated strains were resolved by SDS-PAGE (upper panel) or solubilized in 1% digitonin and resolved by BN-PAGE (lower panel). The time course indicates the time following addition of 10 µg/mL doxycycline to the cultures, which suppresses expression from the $TetO_7$-*ACP1* allele. The indicated proteins and protein complexes were assessed by immunoblot. LA indicates lipoic acid-conjugated Lat1 (PDH complex subunit; upper band) and Kgd2 (α-ketoglutarate dehydrogenase complex subunit; lower band). (**B**) Aconitase activity was measured in whole cell lysates from the indicated strains containing the indicated plasmids 18 hr post-addition of 10 µg/mL doxycycline (± SEM; N = 3 biological replicates. ***p<0.0005, ****p<0.00005). (**C**) qPCR was used to measure the expression of *ACP1, FIT2,* and *FIT3* in the indicated strains. The Gal-*ACP1* strain was harvested at 28 hr post-transfer to raffinose medium to suppress *ACP1* expression. The *mrs3/4*Δ strain lacks both Mrs3 and Mrs4 mitochondrial iron transporters. BPS (80 µM) is a Fe(II) chelator that causes depletion of bioavailable iron. *FIT2* and *FIT3* are components of the iron regulon that is induced upon loss of cytosolic FeS (± SEM; N = 3 biological replicates. *p<0.05, **p<0.005, ***p<0.0005).

DOI: 10.7554/eLife.17828.007

The following source data and figure supplements are available for figure 2:

Source data 1. Source data for ***Figure 2***.

DOI: 10.7554/eLife.17828.008

Figure supplement 1. *ACP1* expression is required for cell proliferation.

DOI: 10.7554/eLife.17828.009

Figure supplement 2. Acp1 is essential for FeS biogenesis.

DOI: 10.7554/eLife.17828.010

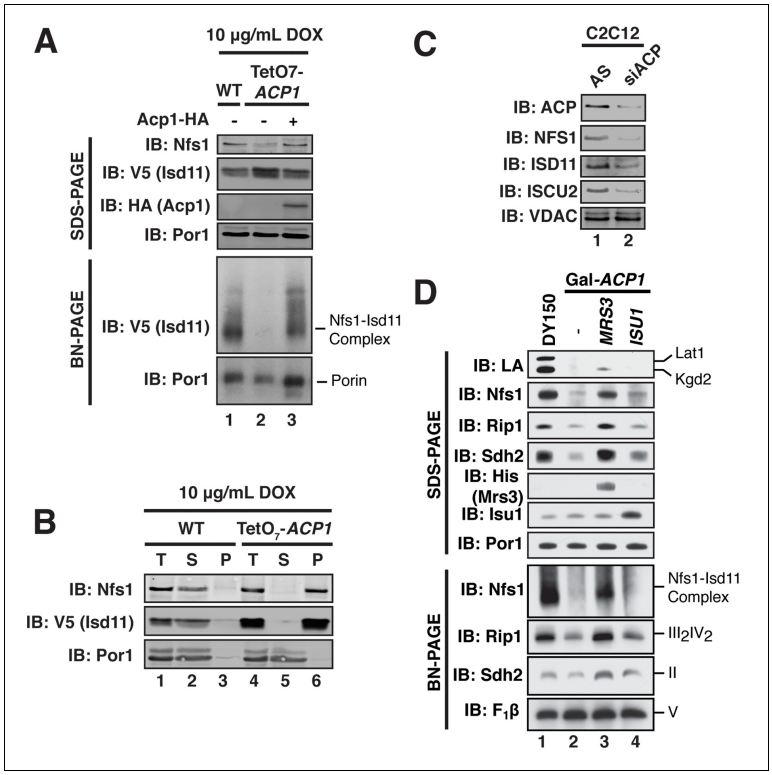

Figure 3. ACP promotes FeS biogenesis by maintaining the stability of the ISU (Nfs1-Isd11) complex. (**A**) Purified mitochondria from the indicated strains were either resolved by SDS-PAGE (lower panels) or solubilized in 1% digitonin and resolved by BN-PAGE (upper panels). Cells were grown for 18 hr in the presence of 10 µg/mL doxycycline. The indicated proteins and protein complexes were assessed by immunoblot. (**B**) Mitochondria purified from the indicated strains 18 hr post-addition of 10 µg/mL doxycycline were solubilized with 1% Triton X-100. Soluble (S) and pellet (P) fractions were separated by centrifugation at 100,000 *g*. The fractions, along with the total input (T) were resolved by SDS-PAGE and assessed by immunoblot. (**C**) C2C12 mouse myoblasts were transfected with a pool of siRNA targeting *NDUFAB1* (ACP) or a scrambled control. Isolated mitochondria was resolved by SDS-PAGE and assessed by immunoblot. (**D**) Isolated mitochondria from the WT and Gal-*ACP1* strains expressing the indicated gene via a 2 µ plasmid at 28 hr post-transfer to raffinose-containing medium were either resolved by SDS-PAGE (lower panels) or solubilized in 1% digitonin and resolved by BN-PAGE (upper panels). The indicated proteins and protein complexes were assessed by immunoblot.

DOI: 10.7554/eLife.17828.011

The following source data and figure supplement are available for figure 3:

Source data 1. Source data for ***Figure 3***.

DOI: 10.7554/eLife.17828.012

Figure supplement 1. ACP promotes FeS biogenesis by maintaining the stability of the ISU (Nfs1-Isd11) complex.

DOI: 10.7554/eLife.17828.013

The mitochondrial ISU complex is essential for the production of FeS that act in the cytosol as well as ribosome assembly (***Kispal et al., 2005***). In addition, mitochondrial FeS synthesis is important to attenuate the transcriptional activity of two partially redundant iron-responsive factors Aft1 and Aft2. In Acp1^{KD} cells the expression of Aft1-target genes *FIT2* and *FIT3* was elevated consistent with impaired mitochondrial FeS synthesis (***Figure 2C***) (***Chen et al., 2004***; ***Rutherford et al., 2005***).

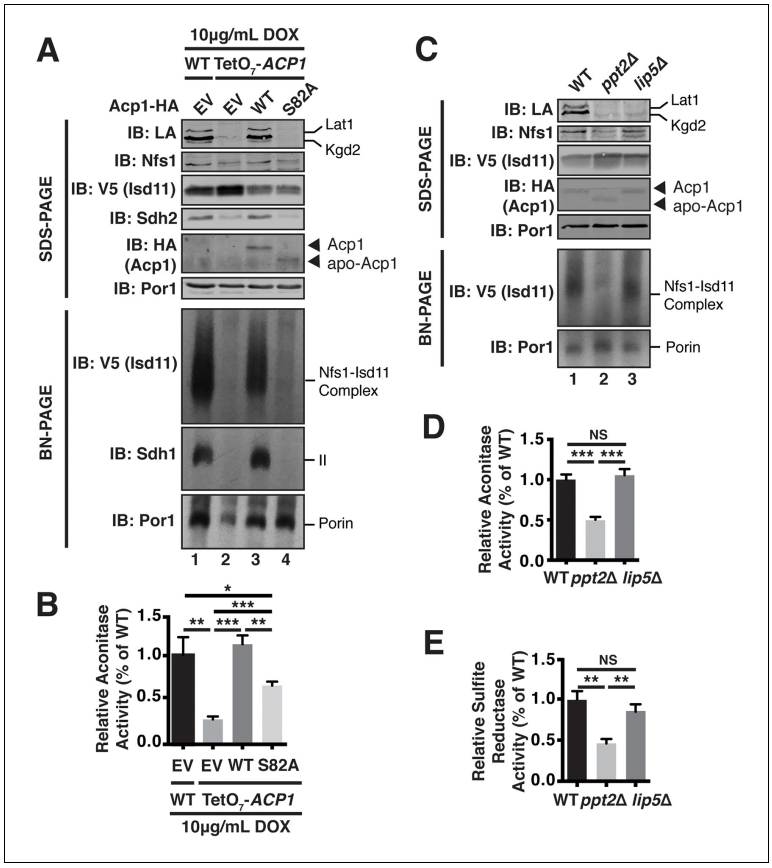

Figure 4. Acp1 requires a 4-PP-conjugated acyl chain to fully stabilize the ISU complex. (**A**) Isolated mitochondria from the indicated strains expressing the indicated genes by plasmid were either resolved by SDS-PAGE (upper panels) or solubilized in 1% digitonin and resolved by BN-PAGE (lower panels). The indicated proteins and protein complexes were assessed by immunoblot. Cells were grown for 18 hr in the presence of 10 µg/mL doxycycline. (**B**) Aconitase activity was measured in whole cell lysates from the indicated strains grown for 18 hr in the presence of 10 µg/mL doxycycline (± SEM; N = 3 biological replicates. *p<0.05, **p<0.005, ***p<0.0005). (**C**) Isolated mitochondria from the indicated strains were either resolved by SDS-PAGE (upper panels) or solubilized in 1% digitonin and resolved by BN-PAGE (lower panels). The indicated proteins and protein complexes were assessed by immunoblot. (**D**) Aconitase activity was measured in whole cell lysates from the indicated strains (± SEM; N = 3 biological replicates. ***p<0.0005). (**E**) Sulfite reductase activity was measured in whole cell lysates from the indicated strains (± SEM; N = 3 biological replicates. **p<0.005).
DOI: 10.7554/eLife.17828.014

The following source data and figure supplement are available for figure 4:

Source data 1. Source data for ***Figure 4***.
DOI: 10.7554/eLife.17828.015

Figure supplement 1. Acp1 requires a 4-PP-conjugated acyl chain to fully stabilize the ISU complex.
DOI: 10.7554/eLife.17828.016

These Aft1 target genes are also induced in cells lacking the two mitochondrial iron transporters Mrs3 and Mrs4 (***Figure 2C***). To further assess the perturbation of cytosolic FeS function, we quantified the activity of the cytosolic FeS-containing enzyme sulfite reductase and observed a diminution in $Acp1^{KD}$ cells (***Figure 2—figure supplement 2C***). Combined with the essential nature of *ACP1*, these data demonstrate that Acp1 is essential for FeS biogenesis.

We next sought to define the mechanism underlying the observed necessity of Acp1 for FeS biogenesis, focusing specifically on the ISU complex. $Acp1^{KD}$ cells exhibited a marked diminution of the assembled Nfs1-Isd11 complex, similar to depletion of the other ISU complex subunits (***Figure 3A***, ***Figure 3—figure supplement 1A,B***). Importantly, the Nfs1 and Isd11 protein that remain in these cells is found only in insoluble aggregates in contrast to WT cells where Nfs1 and Isd11 are soluble (***Figure 3B***). Thus, in the absence of Acp1, the Nfs1-Isd11 complex is destabilized, most likely causing a loss of cysteine desulfurase activity. To determine if mammalian ACP is also necessary for maintaining steady state levels of the FeS biogenesis complex in mammalian cells, C2C12 mouse myoblasts were transfected with a pool of siRNAs targeting *NDUFAB1* (the gene encoding mammalian ACP) or a control siRNA. While our methods were unable to detect the mammalian Nfs1-Isd11 complex by BN-PAGE, depletion of ACP in these cells was accompanied by a clear destabilization of the subunits of the mammalian FeS biogenesis machinery, NFS1, ISD11, and ISCU2, which is the mammalian version of Isu1 (***Figure 3C***). Thus, ACP plays an evolutionarily conserved role in stabilizing the ISU complex thereby enabling FeS biogenesis.

Interestingly, overexpression of the *MRS3* iron transporter resulted in robust stabilization of the Nfs1-Isd11 complex in $Acp1^{KD}$ cells, while not restoring lipoic acid biosynthesis (***Figure 3D***). Elevated Mrs3 expression also restored Sdh2 and Rip1 protein abundance and complex assembly as well as aconitase activity in $Acp1^{KD}$ cells (***Figure 3D*** and ***Figure 3—figure supplement 1C***). We tested whether overexpression of other components of the ISU complex stabilized the Nfs1-Isd11 complex in cells depleted of Acp1. Elevated levels of Isu1 yielded a modest stabilization and restored aconitase activity (***Figure 3D*** and ***Figure 3—figure supplement 1C***), while overexpression of Yfh1, the yeast frataxin homologue, had no effect (***Figure 3—figure supplement 1D***). We speculate that elevated Mrs3 may increase the Fe(II) occupancy of Isu1, which enables it to more effectively stabilize the ISU complex.

Acp1 requires a 4-PP prosthetic group to support mitochondrial fatty acid synthesis. The gene encoding 4-PP transferase, *PPT2,* is not essential, but the haploid deletion strain exhibits no growth in respiration-requiring medium and impaired growth on glucose, which does not require respiration (***Figure 1—figure supplement 2C*** and ***Figure 4—figure supplement 1A***). The growth impairment on glucose is not explained by any known function of ACP and therefore may relate to defects in FeS biogenesis.

To directly test the role of the 4-PP prosthetic group and the acyl chain that is conjugated to it, we investigated the ability of apo-Acp1 lacking 4-PP to support FeS biogenesis. Apo-Acp1 can be generated in vivo by mutating the invariant Ser (S82) to which 4-PP is conjugated (***Stuible et al., 1998***). While re-expression of WT Acp1 could fully restore the steady state abundance of the Nfs1-Isd11 complex in $Acp1^{KD}$ cells, expression of $Acp1^{S82A}$ had only modest effects (***Figure 4A***). These modest effects were sufficient to enable the $Acp1^{KD}$ cells expressing $Acp1^{S82A}$ to retain viability, albeit with impaired grow rate, and to exhibit a modest recovery of aconitase activity compared to $Acp1^{KD}$ cells (***Figure 4B***, ***Figure 4—figure supplement 1B***). Thus, the apparent absence of the Nfs1-Isd11 complex on BN gels is likely the result of a severely destabilized complex that is not capable of surviving the stringent detergent conditions of BN-PAGE and not the complete loss of the complex in vivo.

To further investigate the role of the 4-PP-conjugated acyl chain in FeS biogenesis we interrogated the effects of *PPT2* deletion on the function of Acp1 in FeS biogenesis. Like $Acp1^{KD}$ cells expressing $Acp1^{S82A}$, the Nfs1-Isd11 complex was severely depleted in *ppt2*Δ cells (***Figure 4C***). Furthermore, these cells exhibit a clear diminution in activity of FeS-containing enzymes in both the mitochondria and cytosol as represented by aconitase and sulfite reductase activity, respectively (***Figure 4D,E***). We also interrogated the ability of Acp1 to interact with Nfs1 in WT and *ppt2*Δ cells. While the steady state levels of Acp1 are not affected in *ppt2*Δ cells (***Figure 4C***), we observed a clear defect in the ability of Acp1 to interact with Nfs1 in this strain (***Figure 4—figure supplement 1C***). Therefore, the Acp1-conjugated 4-PP plays an important role in the interaction of Acp1 with the core Nfs1-Isd11 complex and in FeS biogenesis. Importantly, *lip5*Δ cells, which cannot synthesize

lipoic acid but remain competent for Acp1-dependent fatty acid synthesis (**Hiltunen et al., 2010**), maintain normal abundance of the Nfs1-Isd11 complex and aconitase and sulfide reductase activity (**Figure 4C–E**). Thus, the defects in FeS biogenesis observed in cells expressing apo-Acp1 are a result of the inability to generate an acyl-conjugated Acp1 species and not a defect in lipoic acid biosynthesis.

The data presented herein define a new and unexpected role of ACP in FeS biogenesis. ACP functions as a stable subunit of the ISU complex where it acts to stabilize the complex in part by exploiting a 4-PP-conjugated acyl chain. Unlike ACP, however, the acyl chain is not absolutely required for FeS biogenesis and viability, which raises the intriguing possibility that ACP is not simply an obligate subunit, but may exploit this unique interaction modality to provide additional structural or regulatory functions on FeS biogenesis. It is particularly intriguing to speculate that ACP may serve to coordinate mitochondrial fatty acid synthesis and FeS biogenesis, which represent two critical biosynthetic processes performed by mitochondria.

Materials and methods

Yeast strains and growth conditions

Saccharomyces cerevisiae BY4741 (*MATa, his3 leu2 met15 ura3), Saccharomyces cerevisiae* R1158 (BY4741 derivative; *MATa*, URA3::CMV-tTA, *his3 leu2 met15), Saccharomyces cerevisiae* W303a (*MATa, his3 leu2 met15 trp1 ura3*), and *Saccharomyces cerevisiae* DY150 (*MATa ade2-1 his3-11 leu2-3,112 trp1-1 ura3-52 can1-100(oc)*) were used as the wild-type strains where indicated. Each mutant was generated using a standard PCR-based homologous recombination method. The genotypes of all strains used in this study are listed in **Supplementary file 1**. Yeast transformation was performed by the standard TE/LiAc method and transformed cells were recovered and grown in synthetic complete glucose (SD) medium lacking the appropriate amino acid(s) for selection purposes. Medium used in this study includes YPA and synthetic minimal medium supplemented with 2% glucose, 2% raffinose, or 2% glycerol.

Growth assays were performed using synthetic minimal media supplemented with the appropriate amino acids and indicated carbon source. For plate-based growth assays, overnight cultures were back-diluted to equivalent ODs and spotted as 10-fold serial dilutions. For liquid culture growth assays, overnight cultures were back-diluted to equivalent ODs and grown at 30˚C. Growth was monitored by absorbance at 600 nm.

To shut down expression of *ACP1* in $TetO_7$-*ACP1*, over-night cultures were used to inoculate synthetic media containing either 2% glucose or 2% raffinose and 10 µg/mL DOX to an approximate OD_{600} of 0.05 and incubated for 16–24 hr as indicated. To shut down the expression in Gal-*ACP1*, Gal-*NFS1*, Gal-*ISD11*, Gal-*ISU1*, and Met3-*YFH1*, over-night cultured cells were used to inoculate in synthetic media containing 2% raffinose to an approximate OD_{600} of 0.05 and incubated from 24 to 32 hr as indicated. For *YFH1* shut down 2.5 mM methionine was added in the media.

Isolation of yeast mitochondria

Cell pellet was washed once with ddH_2O and incubated in TD buffer (100 mM Tris-SO_4, pH 9.4 and 100 mM DTT) for 15 min at 30˚C. Spheroplasts were obtained by incubating cells in SP buffer (1.2 M Sorbitol and 20 mM potassium phosphate, pH 7.4) supplemented with 0.3 mg/mL lyticase for 1 hr at 30˚C to remove the cell wall. Spheroplasts were gently washed once and homogenized in ice-cold SEH buffer (0.6 M sorbitol, 20 mM HEPES-KOH, pH 7.4, 2 mM $MgCl_2$, 1 mM EGTA) using a dounce homogenizer applied with 30–40 strokes. Crude mitochondria were then isolated by differential centrifugation.

Immunoprecipitation

Crude mitochondria were isolated and resuspended to a concentration of 5 mg/mL. Mitochondria was solubilized in 0.7% digitonin for 30 min. Followed by centrifugation at 20,000 ×g for 20 min. Cleared mitochondrial lysates were incubated with anti-HA antibody conjugated agarose (Sigma) for 2 hr. at 4°C. The agarose was washed 3–5 times and eluted in Laemmli buffer (65°C, 10 min). Elutions were resolved by SDS-PAGE and assessed by immunoblot.

Steady-state protein analysis

Yeast mitochondria were solubilized in Laemmli buffer. Samples were resolved by SDS-PAGE and assessed by immunoblot.

Blue native polyacrylamide gel electrophoresis (BN-PAGE)

BN-PAGE was performed as described previously (***Wittig et al., 2006***). Mitochondria were resuspended in lysis buffer (Invitrogen) and solubilized with 1% digitonin. Lysates were resolved on a 4%–16% gradient native gel (Invitrogen).

Protein aggregation assays

Mitochondria were solubilized in Triton-X100 lysis buffer (0.5% Triton-X100, 20 mM HEPES-KOH, pH 7.4, 150 mM KCl). The samples were incubated on ice for 30 min. and centrifuged at 30,000 ×g for 10 min.

Aconitase activity assays

Yeast cells were grown in SD medium to early log phase, resuspended in lysis buffer (50 mM Tris-HCl, 50 mM KCl, 2 mM sodium citrate dihydrate, 10% glycerol, 1 mM PMSF, and 7 mM β-mercaptoethanol), and stored at –80˚C overnight. After thawing on ice, cells were homogenized by vortexing with glass beads and cleared lysate was collected by centrifugation. Aconitase activity was measured by coupling with $NADP^+$- dependent isocitrate dehydrogenase activity. 30 µl of crude lysate was mixed with 150 µl of reaction mixture (1 M Tris-Cl pH 8.0, 10 mM $MgCl_2$, 10 mM $NADP^+$, 0.32 units of $NADP^+$- dependent Isocitrate Dehydrogenase), and 10 µl of 50 mM citrate. The reaction mixture was recorded at 340 nm for 2 min (15 s intervals). Aconitase activity was normalized to total protein concentration.

Sulfite reductase assays

To measure cytosolic iron, cells (50 ml cultures) were grown in SC –Met (To avoid repression of the enzyme expression by methionine) medium containing 2% glucose or raffinose as a carbon source till 1 of $OD_{600\ nm}$. Total cell lysate preparation and the enzyme assay was performed as described in (***Rutherford et al., 2005***) with modifications. Briefly, cell pellets were resuspended in buffer A (0.1 M Tris-Cl pH7.4, 10% glycerol, 1 mM EDTA pH 8.0, 1 mM phenylmethlysulfony fluoride (PMSF)) with lyticase and incubated 30˚C for 45 min. After disruption using glass beads, 50 µl of cell lysates were mixed with 400 µl of assay mix with or without sulfite. After incubation at 37˚C for 20 min, 100 µl of N,N-diethyl-p-phenylenediamine sulfate (DPD) and 100 µl of ferric chloride were added to the reaction mix to stop the reaction and incubated in the dark to develop the color for 20 min. The production of methylene blue was measured at 669 nm.

qPCR analysis

To quantify the expression of Fe regulon genes, total RNAs were extracted from yeast spheroplasts using RNeasy mini kit (QIAGEN). cDNA were synthesized from 1 µg of total RNA using High-Capacity cDNA Reverse Transcription Kit (Applied Biosystems). 2 µl of 10X diluted cDNA reaction mix were mixed with SYBR Green real-time PCR master mix (Thermo Fisher) with primers and the PCR reaction were performed using the Mastercycler ep *realplex* (Eppendorf). Expression of genes of interesting was normalized to actin and fold changes was analyzed using the $2^{-\Delta\Delta Ct}$ method.

Primers used (Primers were designed to have 60˚C of Tm using Primer3Plus online program)

ACT1_For ATTATATGTTTAGAGGTTGCTGCTTTGG
ACT1_Rev CAATTCGTTGTAGAAGGTATGATGCC
FIT2_For ACAAAGGTTGTCACCGAAGG
FIT2_Rev GATGATTCGACGGCTTGAGT
FIT3_For TCCGCTTTGGTTCTATCTGC
FIT3_Rev AGTGCTGCTGGCGTAAGAGT
ACP1_For ACTCTCCCAACATTGCCAAC
ACP1_Rev CAGCCACTTTGTCAGGGATT

Statistics

PRISM software was used to graph all quantitative data and perform statistical analyses. p values for pairwise comparisons were determined using a Student's t test.

Acknowledgements

This work was supported by RO1GM110755 (to DRW and JR). JR is an Investigator of the Howard Hughes Medical Institute. Plasmids and galactose-regulated gene strains were generously provided by Dr. Andrew Dancis, Dr. Roland Lill and Dr. Jerry Kaplan.

Additional information

Funding

Funder	Grant reference number	Author
Howard Hughes Medical Institute		Jared Rutter
National Institute of General Medical Sciences	RO1GM110755	Dennis R Winge Jared Rutter

The funders had no role in study design, data collection and interpretation, or the decision to submit the work for publication.

Author contributions

JGV, Conception and design, Acquisition of data, Analysis and interpretation of data, Drafting or revising the article; M-YJ, Acquisition of data, Analysis and interpretation of data, Drafting or revising the article; PW, Acquisition of data, Analysis and interpretation of data; Y-CC, Acquisition of data; SPG, Analysis and interpretation of data, Contributed unpublished essential data or reagents; DRW, JR, Conception and design, Analysis and interpretation of data, Drafting or revising the article

Author ORCIDs

Jonathan G Van Vranken, http://orcid.org/0000-0002-8931-852X
Dennis R Winge, http://orcid.org/0000-0003-1160-1189
Jared Rutter, http://orcid.org/0000-0002-2710-9765

Additional files

Supplementary files

• Supplementary file 1. Yeast strains used in this study. This table describes the name, genotype, and source of all yeast strains used in this investigation.
DOI: 10.7554/eLife.17828.017

References

Adam AC, Bornhövd C, Prokisch H, Neupert W, Hell K. 2006. The Nfs1 interacting protein Isd11 has an essential role in Fe/S cluster biogenesis in mitochondria. *The EMBO Journal* **25**:174–183. doi: 10.1038/sj.emboj.7600905, PMID: 16341090

Angerer H, Radermacher M, Mańkowska M, Steger M, Zwicker K, Heide H, Wittig I, Brandt U, Zickermann V. 2014. The LYR protein subunit NB4M/NDUFA6 of mitochondrial complex I anchors an acyl carrier protein and is essential for catalytic activity. *PNAS* **111**:5207–5212. doi: 10.1073/pnas.1322438111, PMID: 24706851

Atkinson A, Smith P, Fox JL, Cui TZ, Khalimonchuk O, Winge DR. 2011. The LYR protein Mzm1 functions in the insertion of the Rieske Fe/S protein in yeast mitochondria. *Molecular and Cellular Biology* **31**:3988–3996. doi: 10.1128/MCB.05673-11, PMID: 21807901

Brody S, Oh C, Hoja U, Schweizer E. 1997. Mitochondrial acyl carrier protein is involved in lipoic acid synthesis in Saccharomyces cerevisiae. *FEBS Letters* **408**:217–220. doi: 10.1016/S0014-5793(97)00428-6, PMID: 9187370

Carroll J, Fearnley IM, Shannon RJ, Hirst J, Walker JE. 2003. Analysis of the subunit composition of complex I from bovine heart mitochondria. *Molecular & Cellular Proteomics* **2**:117–126. doi: 10.1074/mcp.M300014-MCP200, PMID: 12644575

Chen OS, Crisp RJ, Valachovic M, Bard M, Winge DR, Kaplan J. 2004. Transcription of the yeast iron regulon does not respond directly to iron but rather to iron-sulfur cluster biosynthesis. *Journal of Biological Chemistry* **279**:29513–29518. doi: 10.1074/jbc.M403209200, PMID: 15123701

Cui TZ, Smith PM, Fox JL, Khalimonchuk O, Winge DR. 2012. Late-stage maturation of the Rieske Fe/S protein: Mzm1 stabilizes Rip1 but does not facilitate its translocation by the AAA ATPase Bcs1. *Molecular and Cellular Biology* **32**:4400–4409. doi: 10.1128/MCB.00441-12, PMID: 22927643

Dobrynin K, Abdrakhmanova A, Richers S, Hunte C, Kerscher S, Brandt U. 2010. Characterization of two different acyl carrier proteins in complex I from Yarrowia lipolytica. *Biochimica Et Biophysica Acta* **1797**:152–159. doi: 10.1016/j.bbabio.2009.09.007, PMID: 19766092

Feng D, Witkowski A, Smith S. 2009. Down-regulation of mitochondrial acyl carrier protein in mammalian cells compromises protein lipoylation and respiratory complex I and results in cell death. *Journal of Biological Chemistry* **284**:11436–11445. doi: 10.1074/jbc.M806991200, PMID: 19221180

Garland SA, Hoff K, Vickery LE, Culotta VC. 1999. Saccharomyces cerevisiae ISU1 and ISU2: members of a well-conserved gene family for iron-sulfur cluster assembly. *Journal of Molecular Biology* **294**:897–907. doi: 10.1006/jmbi.1999.3294, PMID: 10588895

Hiltunen JK, Autio KJ, Schonauer MS, Kursu VA, Dieckmann CL, Kastaniotis AJ. 2010. Mitochondrial fatty acid synthesis and respiration. *Biochimica Et Biophysica Acta* **1797**:1195–1202. doi: 10.1016/j.bbabio.2010.03.006, PMID: 20226757

Huttlin EL, Ting L, Bruckner RJ, Gebreab F, Gygi MP, Szpyt J, Tam S, Zarraga G, Colby G, Baltier K, Dong R, Guarani V, Vaites LP, Ordureau A, Rad R, Erickson BK, Wühr M, Chick J, Zhai B, Kolippakkam D, et al. 2015. The bioplex network: A systematic exploration of the human interactome. *Cell* **162**:425–440. doi: 10.1016/j.cell.2015.06.043, PMID: 26186194

Kispal G, Sipos K, Lange H, Fekete Z, Bedekovics T, Janáky T, Bassler J, Aguilar Netz DJ, Balk J, Rotte C, Lill R. 2005. Biogenesis of cytosolic ribosomes requires the essential iron-sulphur protein Rli1p and mitochondria. *The EMBO Journal* **24**:589–598. doi: 10.1038/sj.emboj.7600541, PMID: 15660134

Lill R, Diekert K, Kaut A, Lange H, Pelzer W, Prohl C, Kispal G. 1999. The essential role of mitochondria in the biogenesis of cellular iron-sulfur proteins. *Biological Chemistry* **380**:1157–1162. doi: 10.1515/BC.1999.147, PMID: 10595578

Majerus PW, Alberts AW, Vagelos PR. 1965. Acyl carrier protein, iv. the identification of 4'-phosphopantetheine as the prosthetic group of the acyl carrier protein. *PNAS* **53**:410–417. doi: 10.1073/pnas.53.2.410, PMID: 14294075

Mühlenhoff U, Balk J, Richhardt N, Kaiser JT, Sipos K, Kispal G, Lill R. 2004. Functional characterization of the eukaryotic cysteine desulfurase Nfs1p from Saccharomyces cerevisiae. *Journal of Biological Chemistry* **279**:36906–36915. doi: 10.1074/jbc.M406516200, PMID: 15220327

Rutherford JC, Ojeda L, Balk J, Mühlenhoff U, Lill R, Winge DR. 2005. Activation of the iron regulon by the yeast Aft1/Aft2 transcription factors depends on mitochondrial but not cytosolic iron-sulfur protein biogenesis. *Journal of Biological Chemistry* **280**:10135–10140. doi: 10.1074/jbc.M413731200, PMID: 15649888

Sackmann U, Zensen R, Röhlen D, Jahnke U, Weiss H. 1991. The acyl-carrier protein in Neurospora crassa mitochondria is a subunit of NADH:ubiquinone reductase (complex I). *European Journal of Biochemistry* **200**:463–469. doi: 10.1111/j.1432-1033.1991.tb16205.x, PMID: 1832379

Schonauer MS, Kastaniotis AJ, Hiltunen JK, Dieckmann CL. 2008. Intersection of RNA processing and the type II fatty acid synthesis pathway in yeast mitochondria. *Molecular and Cellular Biology* **28**:6646–6657. doi: 10.1128/MCB.01162-08, PMID: 18779316

Stuible HP, Meier S, Wagner C, Hannappel E, Schweizer E. 1998. A novel phosphopantetheine:protein transferase activating yeast mitochondrial acyl carrier protein. *Journal of Biological Chemistry* **273**:22334–22339. doi: 10.1074/jbc.273.35.22334, PMID: 9712852

Wiedemann N, Urzica E, Guiard B, Müller H, Lohaus C, Meyer HE, Ryan MT, Meisinger C, Mühlenhoff U, Lill R, Pfanner N. 2006. Essential role of Isd11 in mitochondrial iron-sulfur cluster synthesis on Isu scaffold proteins. *The EMBO Journal* **25**:184–195. doi: 10.1038/sj.emboj.7600906, PMID: 16341089

Wittig I, Braun HP, Schägger H. 2006. Blue native PAGE. *Nature Protocols* **1**:418–428. doi: 10.1038/nprot.2006.62, PMID: 17406264

Yi X, Maeda N. 2005. Endogenous production of lipoic acid is essential for mouse development. *Molecular and Cellular Biology* **25**:8387–8392. doi: 10.1128/MCB.25.18.8387-8392.2005, PMID: 16135825

Zhang L, Joshi AK, Hofmann J, Schweizer E, Smith S. 2005. Cloning, expression, and characterization of the human mitochondrial beta-ketoacyl synthase. Complementation of the yeast CEM1 knock-out strain. *Journal of Biological Chemistry* **280**:12422–12429. doi: 10.1074/jbc.M413686200, PMID: 15668256

eLIFE elifesciences.org

SHORT REPORT

Figures and figure supplements

The mitochondrial acyl carrier protein (ACP) coordinates mitochondrial fatty acid synthesis with iron sulfur cluster biogenesis

Jonathan G Van Vranken *et al*

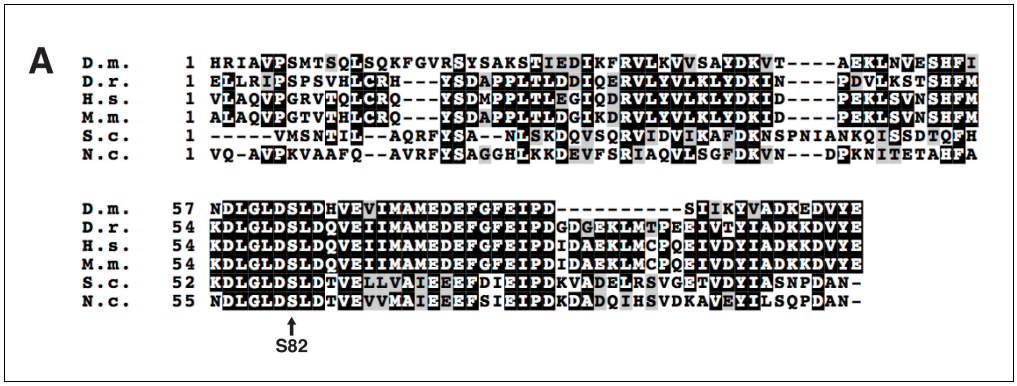

Figure 1—figure supplement 1. Protein sequence alignment of ACP from eukaryotes. (**A**) Protein sequence alignment of the ACP proteins from the indicated species (Clustal Omega). D.m. – *Drosophila melanogaster*, D.r. – *Danio rerio*, H.s. – *Homo sapiens*, M.m. – *Mus musculus*, S.c. – *Saccharomyces cerrevisiae*, N.c. – *Neuropsora crassa*. The invariant Ser residue to which 4-PP is conjugated is indicated.
DOI: 10.7554/eLife.17828.004

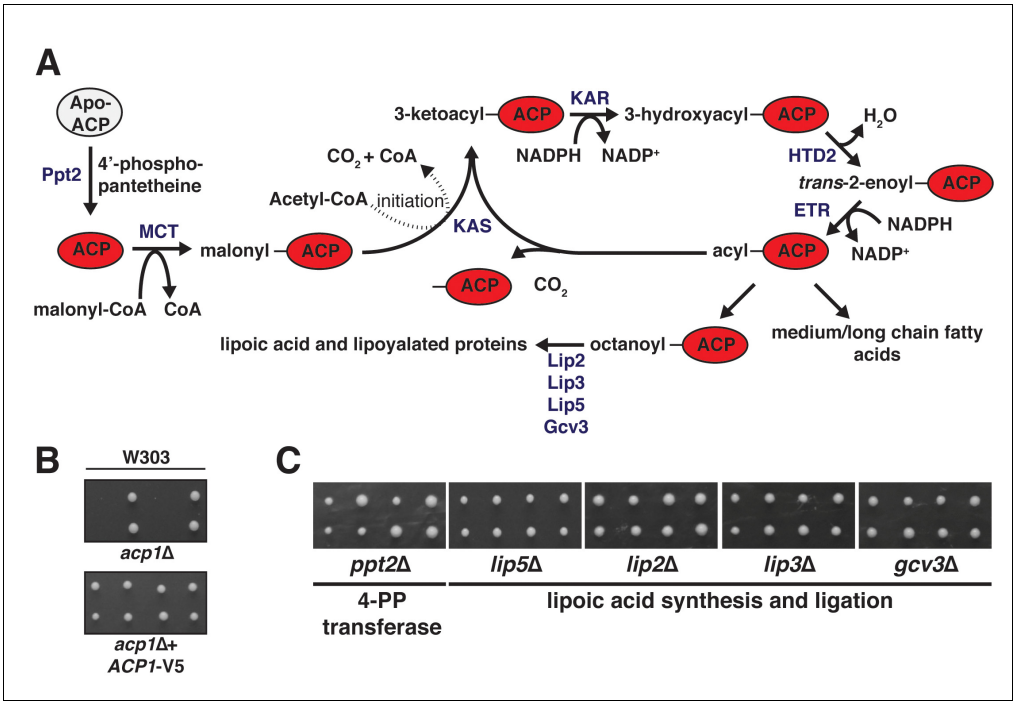

Figure 1—figure supplement 2. Eukarotic mitochondrial fatty acid biosynthesis (FASII) pathway. (**A**) Eukaryotic cells have maintained two distinct fatty acid synthesis pathways—the canonical cytoplasmic FASI and the mitochondrial FASII, which is homologous to the prokaryotic fatty acid synthesis pathway. FASII, which is dependent on ACP, is comprised of a set of monofunctional enzymes that catalyze the various steps in fatty acid synthesis. In order to facilitate mitochondrial fatty acid synthesis, apo-ACP must first be converted to holo-ACP by a 4'-phosphopantetheine transferase (Ppt2), which catalyzes the covalent attachment of the 4-phosphopantetheine prosthetic group (4-PP) to an absolutely conserved Ser residue on ACP. The 4-PP contains a terminal thiol that serves as the attachment site to enable Acp1 to scaffold *de novo* fatty acid synthesis. The enzymes of FASII use malonyl-coA to initiate the fatty acid chain and acetyl-coA for acyl chain elongation. The canonical product of FASII is octanoate, which is the precursor for lipoic acid, an important mitochondrial cofactor. Following ACP-dependent octanoate synthesis, Lip2, Lip3, Lip5, and Gcv3 support the synthesis of lipoic acid and ligation to its target proteins including the E3 component of pyruvate dehydrogenase and α-ketoglutarate dehydrogenase. Ppt2 – 4'phophopantetheine transferase; MCT – malonyl-coA transferase; KAS – ketoacyl synthetase; KAR – ketoacyl reductase; HTD2 – hydroxyacyl-thioester reductase type 2; ETR – enoyl-thioester reductase; Lip2, Lip3, Lip5, Gcv3 – lipoic acid biosynthesis and ligation. (**B**) *acp1*Δ heterozygous diploids in the W303 strain background were dissected with and without a plasmid expressing Acp1-V5 and spores were grown on YPAD medium for 2 days. (**C**) *ppt2*Δ, *lip5*Δ, *lip2*Δ, *lip3*Δ, and *gcv3*Δ heterozygous diploids were dissected and spores were grown on YPAD medium for 2 days.
DOI: 10.7554/eLife.17828.005

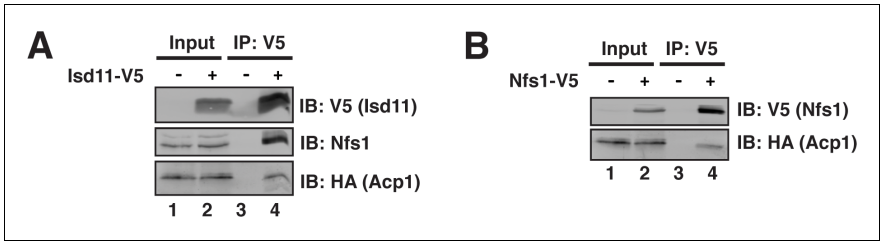

Figure 1—figure supplement 3. Acp1 is a stable subunit of the ISU complex. (**A**) Isd11-V5 and Acp1- HA were expressed from their endogenous loci and Isd11-V5 was immunoprecipitated from digitonin-solubilized mitochondria followed by the indicated immunoblots. (**B**) Nfs1-V5 and Acp1- HA were expressed from their endogenous loci and Nfs1-V5 was immunoprecipitated from digitonin-solubilized mitochondria followed by the indicated immunoblots.

DOI: 10.7554/eLife.17828.006

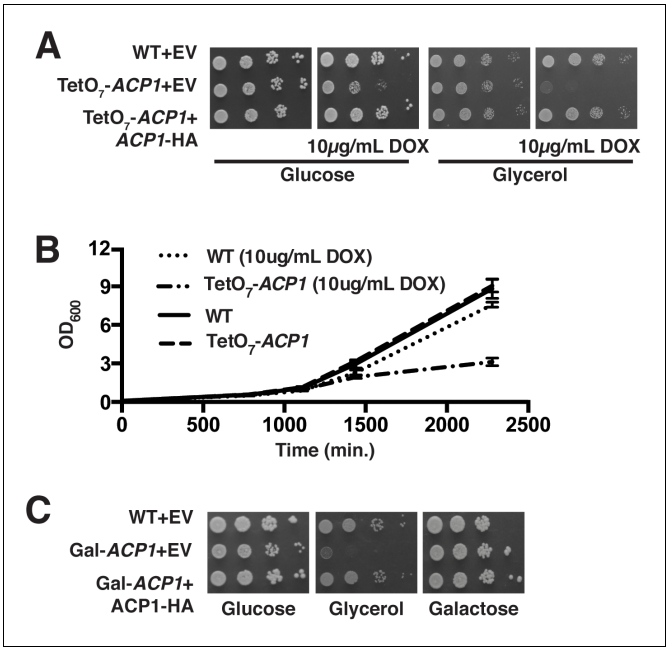

Figure 2—figure supplement 1. *ACP1* expression is required for cell proliferation. (**A**) Ten-fold serial dilutions of WT, TetO$_7$-*ACP1*, and TetO7-*ACP1* cells expressing Acp1-HA were plated on synthetic media containing the indicated carbon source with and without 10 μg/mL doxycycline (BY4741 background). (**B**) Liquid cultures (2% raffinose) with and without 10 μg/mL doxycycline were inoculated to an OD. 025 with either WT or TetO$_7$-*ACP1* cells. Growth was monitored by absorbance at 600 nm. (**C**) Ten-fold serial dilutions of WT, Gal-*ACP1*, and Gal-*ACP1* cells expressing Acp1-HA were serially diluted and plated on synthetic media containing the indicated carbon source. With pre-growth of the Gal-*ACP1* strain on glucose medium, subsequent plating of the cells on glucose shows moderate growth impairment. The depletion of Acp1 in TetO$_7$-*ACP1* cells is more efficient compared to Gal-*ACP1* cells.

DOI: 10.7554/eLife.17828.009

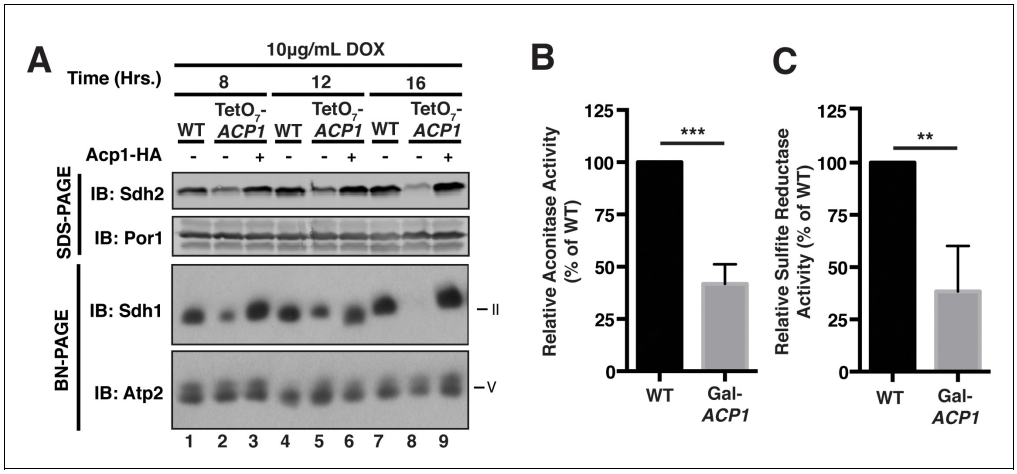

Figure 2—figure supplement 2. Acp1 is essential for FeS biogenesis. (**A**) Isolated mitochondria from WT, $TetO_7$-*ACP1*, or $TetO_7$-*ACP1* cells expressing Acp1-HA were harvested at the indicated times post addition of doxycycline were resolved by SDS-PAGE (upper panels) or solubilized in 1% digitonin and resolved by BN-PAGE (lower panels). (**B**) Aconitase activity was measured in mitochondrial lysates from WT and Gal-*ACP1* cells at 28 hr post-transfer to raffinose-containing medium (± SEM; N = 3 biological replicates. ***p<0.0005). (**C**) The cytosolic FeS-containing sulfite reductase activity was measured in whole cell lysates from WT and Gal-*ACP1* cells at 28 hr post-transfer to raffinose-containing medium (± SEM; N = 3 biological replicates. **p<0.005).

DOI: 10.7554/eLife.17828.010

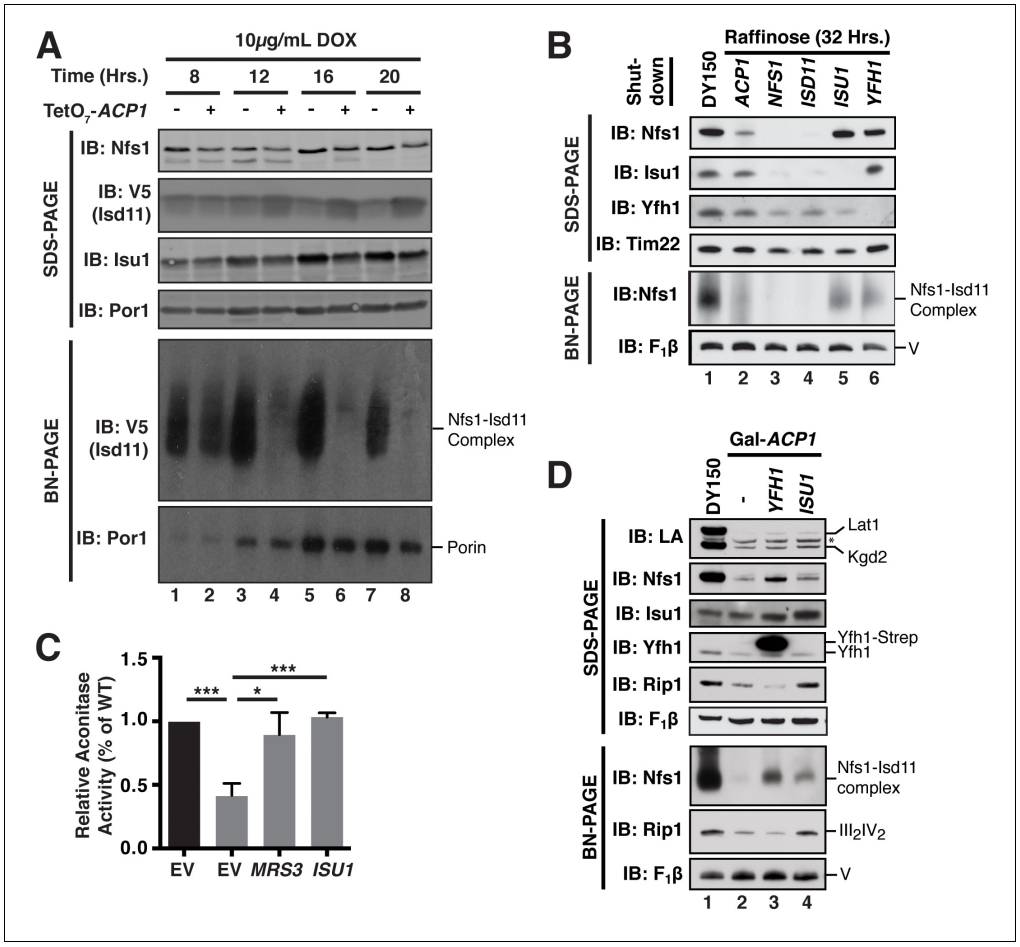

Figure 3—figure supplement 1. ACP promotes FeS biogenesis by maintaining the stability of the ISU (Nfs1-Isd11) complex. (**A**) Isolated mitochondria from WT and $TetO_7$-*ACP1* cells harvested at the indicated time points post-addition of doxycycline were resolved by SDS-PAGE (upper panel) or solubilized in 1% digitonin and resolved by BN-PAGE (lower panel). (**B**) Indicated strains were grown in raffinose for 32 hr to repress expression of the indicated genes. *YFH1* was depleted in a *Met3-YFH1* strain cultured in the presence of 2.5 mM methionine. Isolated mitochondria from each strain was either resolved by SDS-PAGE (upper panel) or solubilized in 1% digitonin and resolved by BN-PAGE (lower panel). Depletion of *ISD11*, but not *ISU1* subunit destabilizes Nfs1-Isu11 complex on BN-PAGE as *ACP1* depletion does, suggesting Acp1 acts through Isd11 to destabilize Nfs1. (**C**) Aconitase activity was measured in mitochondrial lysates from WT and Gal-*ACP1* cells overexpressing *MRS3* or *ISU1* harvested at 28 hr post-transfer to raffinose-containing medium (± SEM; N = 3 biological replicates. *p<0.05, ***p<0.0005). (**D**) Isolated mitochondria from the WT and Gal-*ACP1* strains expressing the indicated gene via a 2 μ plasmid at 28 hr post-transfer to raffinose-containing medium were either resolved by SDS-PAGE (lower panels) or solubilized in 1% digitonin and resolved by BN-PAGE (upper panels). The indicated proteins and protein complexes were assessed by immunoblot. * indicates non-specific band.

DOI: 10.7554/eLife.17828.013

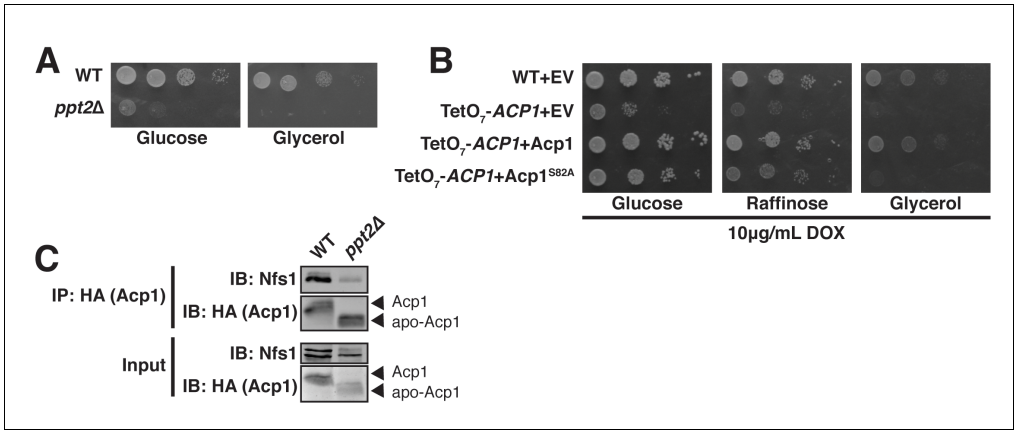

Figure 4—figure supplement 1. Acp1 requires a 4-PP-conjugated acyl chain to fully stabilize the ISU complex. (**A**) Ten-fold serial dilutions of the indicated strains plated on synthetic medium with either glucose or glycerol. (**B**) Ten-fold serial dilutions of the indicated strains expressing the indicated plasmids were plated on synthetic media containing 10 µg/mL doxycycline and either glucose, raffinose, or glycerol. (**C**) Purified mitochondria from WT and *ppt2*Δ cells expressing Acp1-HA were solubilized by digitonin (input) and then subjected to anti-HA immunoprecipitation. The resulting eluates and input samples were subjected to SDS-PAGE.

DOI: 10.7554/eLife.17828.016

Table 4-S1. Yeast strains used in this study.

Strain	Genotype	Source
WT (BY4741)	*MAT*a, *his3 leu2 met15 ura3*	Open Biosystems
*acp1*Δ + Acp1-HA	*MAT*a, *his3 leu2 met15 ura3 acp1::hygMX ACP1-HA (plasmid)*	This study
*ppt2*Δ	*MAT*a, *his3 leu2 met15 ura3 ppt2::natMX*	This study
WT (W303)	*MAT*a, *his3 leu2 met15 trp1 ura3*	This Study
*acp1*Δ + Acp1-V5	*MAT*a, *his3 leu2 met15 trp1 ura3 acp1::hygMX ACP1-V5 (plasmid)*	This Study
WT (R1158; BY4741 derivative)	*MAT*a, URA3::CMV-tTA, *his3 leu2 met15*	GE Dharmacon
$TetO_7$-*ACP1*	*MAT*a, URA3::CMV-tTA, *his3 leu2 met15 acp1::Kan$_R$TetO$_7$-CYC1TATA-ACP1*	This study
$TetO_7$-*NFS1*	*MAT*a, URA3::CMV-tTA, *his3 leu2 met15 nfs1::Kan$_R$TetO$_7$-CYC1TATA-NFS1*	GE Dharmacon
$TetO_7$-*ISD11*	*MAT*a, URA3::CMV-tTA, *his3 leu2 met15 isd11::Kan$_R$TetO$_7$-CYC1TATA-ISD11*	This study
WT *NFS1*-V5	*MAT*a, URA3::CMV-tTA, *his3 leu2 met15 nfs1::NFS1-V5-natMX*	This study
$TetO_7$-*ACP1 NFS1-V5*	*MAT*a, URA3::CMV-tTA, *his3 leu2 met15 acp1::Kan$_R$TetO$_7$-CYC1TATA-ACP1 nfs1::NFS1-V5-natMX*	This study
WT ISD11-V5	*MAT*a, URA3::CMV-tTA, *his3 leu2 met15 isd11::ISD11-V5-natMX*	This study
$TetO_7$-*ACP1 ISD11-V5*	*MAT*a, URA3::CMV-tTA, *his3 leu2 met15 acp1::Kan$_R$TetO$_7$-CYC1TATA-ACP1 isd11::ISD11-V5-natMX*	This study
WT (DY150)	*MAT*a *ade6 his3-11 leu2-3,112 trp1-1 ura3-52 can1-100(oc)*	This study
Gal-*ACP1*	*MATa ade6 his3-11 leu2-3,112 trp1-1 ura3-52 can1-100(oc) KanMX*::pGal-*ACP1*	This study
Gal-*NFS1*	*MAT*a *ura3-52 lys2-801_amber ade2-101_ochre trp1-Δ63 his3-Δ200 leu2-Δ1* cyh2 *nfs1::HIS3 URA3*::pGal-*NFS1*	Andrew Dancis
Gal-*ISD11*	*MAT*a *ura3-52 lys2-801_amber ade2-101_ochre trp1-Δ63 his3-Δ200 leu2-Δ1* cyh2 *HIS3MX6*::pGal-*ISD11*	Andrew Dancis
Gal-*ISU1*	*MAT*a *ura3-52 lys2-801_amber ade2-101_ochre trp1-Δ63 his3-Δ200 leu2-Δ1* pRS406-gamma *isu2* (*URA3*) *HIS3MX6*::pGal-*ISU1*	Andrew Dancis
Met-*YFH1*	*MAT*a *ade2-1 his3-11 leu2-3,112 trp1-1 ura3-52 can1-100(oc) yfh1::HIS3* pTF63-Met3-*YFH1* (*URA3*)	Jerry Kaplan

CHAPTER 5

MITOCHONDRIAL FATTY ACID SYNTHESIS COUPLES ACETYL-COA SENSING WITH ELECTRON TRASPORT CHAIN BIOGENESIS

Jonathan G. Van Vranken, Sara M. Nowinski, Katie J. Clowers, Mi-Young Jeong, Yeyun Ouyang, Jordan A. Berg, Steven P. Gygi, Dennis R. Winge, and Jared Rutter

Abstract

The electron transport chain (ETC) is an important player in cellular energy conversion, but can also generate potentially damaging derivatives when not carrying a steady flux of reducing equivalents. Therefore, the cell must balance the metabolic capacity of mitochondria with the availability of substrate. In addition to being the major fuel of the TCA cycle and ETC, acetyl-CoA is also the carbon donor for mitochondrial fatty acid synthesis (FASII). We demonstrate that, in the presence of mitochondrial acetyl-CoA, FASII-synthesized acyl chains accumulate on the acyl carrier protein and signal ETC biogenesis through direct physical interactions with the LYR protein family of ETC assembly factors. By coupling acetyl-CoA levels with ETC assembly, this system provides an elegant mechanism for coordinating the assembly of each ETC complex with one another and with substrate availability. Thus, ETC biogenesis is suppressed and mitochondrial metabolic homeostasis is maintained even in the absence of substrate.

Introduction

Mitochondrial acetyl-CoA is the primary substrate that fuels oxidative phosphorylation. It is oxidized by the TCA cycle to provide the reducing equivalents (NADH and $FADH_2$) that feed the electron transport chain (ETC). These complexes, comprised of subunits encoded by both the nuclear and mitochondrial genomes, couple the passing of electrons through numerous redox-active cofactors to the establishment of an electrochemical gradient across the inner mitochondrial membrane, which ATP synthase (complex V; CV) exploits to generate adenosine triphosphate. While this system provides an efficient source of cellular energy, it can also generate potentially deleterious

reactive oxygen species, particularly when electron availability and ETC capacity are not maintained in balance (*1*). Therefore, the cell must coordinate the assembly and activity of ETC complexes with substrate availability. Herein, we demonstrate that acetyl-CoA coordinates the biogenesis of the ETC through acylation of the mitochondrial acyl carrier protein (ACP).

Eukaryotic mitochondria have maintained a prokaryote-like fatty acid synthesis pathway (FASII) that is structurally and functionally distinct from the FASN-dependent cytosolic pathway (*2*). This pathway employs a number of mono-functional enzymes that transiently interact with ACP—the soluble scaffold for fatty acid synthesis—to catalyze the step-wise elongation of nascent acyl chains (Figure 5-1A,B). In order to support this pathway, ACP utilizes a 4'-phosphopantetheine prosthetic group (4'-PP), which is covalently attached to an invariant Ser residue and provides the terminal thiol upon which fatty acid synthesis is initiated and elongated (Figure 5-1A,B) (*3, 4*). It has been thought that the primary function of FASII was the synthesis of octanoate, the eight-carbon precursor of lipoic acid, which is a required cofactor for mitochondrial enzymes (*5*). Curiously, FASII can synthesize ACP-bound acyl chains significantly longer than eight carbons however no functional importance has yet to be attributed to these extended acyl chains (*6*).

Results

To begin to understand the role of mitochondrial FASII in the maintenance of mitochondrial physiology, we sought to interrogate the consequences of *MCT1* deletion on the cellular proteome using quantitative tandem mass spectrometry after isobaric

labeling (Figure 5-1C,D). Mct1 is the malonyl-CoA transferase that is required to initiate FASII and thus cells lacking this enzyme are devoid of ACP acylation (*7*). We compared the steady state abundance of over 4700 proteins and found notable changes not only within mitochondria but also in other cellular compartments (Figure 5-1E and Figure 5-2A). The most obvious change was a profound and specific depletion of proteins involved in cellular respiration and oxidative phosphorylation (Figure 5-2A-C). In fact, almost all ETC complex subunits were lost in FASIIΔ cells, while other membrane-associated mitochondrial complexes were unaffected (Figure 5-2C). Consistent with these results, ETC complexes were also undetectable by immunoblot after blue-native- or SDS-PAGE in FASIIΔ strains (*mct1*Δ and *oar1*Δ; Figure 5-2D).

Having recently discovered that ACP supports iron-sulfur cluster (FeS) biogenesis through a direct physical interaction with the FeS biogenesis complex (*8*), we hypothesized that ACP may promote ETC assembly using a related mechanism. To test this hypothesis, fully functional $Acp1^{HA/FLAG}$, expressed at endogenous levels, was immunoprecipitated from digitonin-solubilized mitochondrial extracts. The resulting eluates were analyzed by mass spectrometry to identify interacting proteins, which revealed a number of candidates connecting ACP to ETC biogenesis. Of these candidates, we first confirmed a physical interaction between Acp1 and Rpm2, the protein subunit of mitochondrial RNase P (Figure 5-3A). It has been previously reported that FASII is required to support mitochondrial translation by promoting maturation of RNase P (*9*). Thus, in the absence of ACP acylation, RNase P activity is lost and translation of the mitochondrial genome is prevented. Consistent with these reports, the mitochondria-encoded proteins of the ETC that were detectable by mass spectrometry (Cox1, Cox2,

Cox3, and Atp6) were among the most severely depleted proteins in *mct1*Δ cells (Figure 5-4A). Furthermore, the steady state abundance of Rpm2 itself was severely decreased (Figure 5-3G). Combined with previous findings, these data suggest that acylated ACP supports mitochondrial translation and ETC biogenesis, likely through a physical interaction with RNase P.

In addition to Rpm2, Acp1 also co-purified with each member of the evolutionarily conserved LYR protein family—Sdh6, Sdh7, Mzm1, Fmc1, and Isd11 (Figure 5-4B,C). In general, these proteins, which are named for a highly conserved tripartite Leu-Tyr-Arg (LYR) motif, function as complex-specific late stage ETC assembly factors (*10-15*). Sdh6 and Sdh7, Mzm1, and Fmc1, support the assembly of complex II, complex III, and complex V, respectively, whereas Isd11 is an essential component of the FeS biogenesis machinery (*10-15*). In higher eukaryotes, this family has expanded considerably to include, in addition to direct orthologues of Sdh6, Sdh7, Mzm1, and Isd11, two stable accessory subunits of complex I and several others with unclear functions (*16*). Fmc1 is not conserved in mammals and seems to be atypical in its function (see below). ACP-LYR interactions were confirmed by immunoprecipitation of $Acp1^{HA/FLAG}$ from mitochondria expressing $Sdh6^{V5}$, $Sdh7^{V5}$, $Mzm1^{V5}$, $Fmc1^{V5}$, and $Isd11^{V5}$ fusion proteins (Figure 5-3B-F). This family-wide interaction with ACP is corroborated by large scale mass spectrometry interaction studies (*17-19*) and recent high-resolution structures of ACP-LYR complexes, which demonstrate that the LYR motif is critical for mediating the interaction (*20, 21*). We also found that the 4'-PP prosthetic group of ACP is critical for the majority of ACP-LYR interactions, as an $Acp1^{S82A}$ mutant protein, which cannot bind 4'-PP, was incapable of interacting with

Sdh6, Sdh7, Mzm1, and Isd11 (Figure 5-4D-G). Interestingly, Fmc1 was still able to interact with Acp1^{S82A}, however the implications of this discrepancy remain unclear (Figure 5-4H). Finally, deletion of *MCT1* depleted most, but not all, of the LYR proteins, suggesting that ACP not only interacts with these proteins but that its acylation is important for supporting their stability and function (Figure 5-3G). Taken together, these results demonstrate that acylated ACP interacts with a network of ETC assembly factors with the potential to coordinate complex biogenesis.

Because FASIIΔ cells have such profound defects in mitochondrial translation, it is difficult to use this system to study the impact of ACP acylation on LYR-dependent assembly of the ETC. Instead, we sought to investigate the role of ACP in supporting the function of each LYR independently. Deletion of each member of this family results in the specific destabilization of certain complexes, which can be rescued by reexpression of the deleted gene (Figure 5-3H). In order to independently prevent the interaction of each LYR family member with ACP, mutant proteins were generated in which the LYR motif was substituted with three Ala residues. Even when over-expressed, Sdh6$^{\Delta LYR}$, Sdh7$^{\Delta LYR}$, and Mzm1$^{\Delta LYR}$ were unable to complement their respective mutant strains (Figure 5-3H and Figure 5-4I-K,M). Fmc1$^{\Delta LYR}$, on the other hand, rescued growth and ETC assembly, further contributing to the notion that Fmc1 is unique among the yeast LYR protein family (Figure 5-3H and Figure 5-4L,M). Taken together these data demonstrate that the LYR proteins require the LYR motif, which mediates the ACP interaction, to function as complex-specific assembly factors.

ETC biogenesis is dependent on FASII-catalyzed acylation of ACP (Figure 5-2). ACP also interacts with an entire family of ETC assembly factors (Figure 5-3).

Therefore, we hypothesized that ACP acylation may serve as a signal to activate ETC assembly and sought to identify the relevant acyl-ACP species. In WT cells, $Acp1^{HA/FLAG}$ can be resolved by SDS-PAGE into three clearly defined bands (identified as 1, 2, and 3), each of which represents a different Acp1 species (Figure 5-5A and Figure 5-6B). Band 1, which accumulates in FASIIΔ cells, likely represents deacyl/holo-ACP, which is bound to 4'-PP but devoid of acylation (Figure 5-5A). Band 2 co-migrates with $Acp1^{S82A}$ and is likely to be apo-ACP lacking 4'-PP (Figure 5-5A and Figure 5-6A). Finally, because the accumulation of band no. 3 is dependent on FASII and holo-ACP, it is likely an acylated form of ACP, which we will define as acyl-ACP (Figure 5-5A and Figure 5-6A,B) (*22*). A number of other ACP-containing species that migrate higher than deacyl/holo-ACP accumulate reproducibly in FASIIΔ cells (Figure 5-5A). These bands are sensitive to reducing agents like β-mercaptoethanol (Figure 5-6B) and thus, likely represent spurious ACP disulfide-linked species. Because the mature form of ACP contains no Cys residues, the only free thiol capable of participating in disulfide bonds is the terminal thiol of the 4'-PP prosthetic group. Since these higher molecular weight species can only form when this thiol is unmodified, these disulfide species are markers of ACP deacylation.

It has been reported that ectopic mitochondria-targeted expression of a peroxisomal medium-chain fatty acyl-CoA ligase (mito-*FAA2*) can restore respiratory growth in FASIIΔ cells (*23, 24*). We confirmed this (Figure 5-6C) and demonstrated that mito-Faa2 almost completely rescued the defects in ETC complex assembly and subunit accumulation (Figure 5-5B). Importantly, mutants competent for FASII but deficient in lipoic acid synthesis and ligation (*lip5*Δ) also have severe defects in ETC complex

assembly (Figure 5-5B) and ACP acylation (Figure 5-5A), which likely results from a loss of pyruvate dehydrogenase (PDH) activity (see below). Expression of mito-*FAA2* augmented ETC complex assembly in these cells, however, because these mutants still cannot synthesize lipoic acid, they remain respiratory deficient (Figure 5-6C). Thus, the severe phenotype observed in FASIIΔ strains cannot be explained by a defect in lipoic acid synthesis but likely result from a failure to generate acyl-ACP.

Having demonstrated that mito-Faa2 can restore respiratory growth and ETC biogenesis in FASIIΔ cells, we next wanted to understand the mechanism underlying this rescue. Expression of mito-*FAA2* failed to restore respiratory growth in *ppt2*Δ cells, demonstrating that holo-ACP is required for this construct to rescue FASIIΔ defects (Figure 5-6D). This suggests that mito-Faa2 may restore ETC biogenesis in FASIIΔ cells through FASII-independent re-acylation of ACP. Indeed, expression of mito-*FAA2* partially restored acyl-ACP in *mct1*Δ cells and also decreased the abundance of the high molecular weight disulfide linkages, which serve as marks of ACP deacylation (Figure 5-5C). These data suggest that acylation of ACP is sufficient to promote ETC biogenesis independent of FASII.

Upon identifying acyl-ACP as the ACP species required for supporting ETC biogenesis, we wanted to determine if it was sufficient to activate the LYR network to initiate ETC assembly. To that end, $Sdh6^{V5}$ and $Mzm1^{V5}$ were immunoprecipitated from cells and the bound ACP species were assessed by immunoblot. Consistent with the ability of acyl-ACP to facilitate ETC biogenesis, Sdh6 and Mzm1 both exhibited a clear preference for binding to acyl-ACP over deacyl/holo-ACP (Figure 5-5D and Figure 5-6E). Despite this preference, however, ACP acylation and FASII are not necessarily

required for all ACP-LYR interactions as LYR proteins that remain stable in FASIIΔ cells can still bind ACP (Figure 5-6F-J). Taken together, these data suggest that ACP acylation is not simply required for the ACP-LYR physical interactions but instead serves as a signal to activate the assembly network driven by the LYR proteins. This conclusion is further supported by high-resolution structural studies of three distinct ACP-LYR complexes (*20, 21*). In all cases, an acylated form of ACP (likely acyl-ACP/band 3) binds the LYR protein and embeds its acyl chain deep within the hydrophobic core of the LYR. As such, the position of the ACP-bound acyl chain is ideal for allosterically signaling to activate the assembly function of the LYR proteins.

In addition to the profound depletion of the ETC subunits, *mct1*Δ cells displayed an increased abundance of proteins involved in mitochondrial acetyl-CoA generation (Figure 5-7A). This could suggest that the cell perceives loss of FASII and the resulting ACP deacylation as indicators of mitochondrial acetyl-CoA depletion. Therefore, we hypothesized that ACP acylation might regulate ETC assembly in coordination with mitochondrial acetyl-CoA levels. To test this hypothesis, an *mpc1*Δ strain was employed as a genetic model of mitochondrial acetyl-CoA depletion. Mpc1 is an essential subunit of the mitochondrial pyruvate carrier and deletion of this gene prevents the import of pyruvate into mitochondria, thereby preventing PDH-dependent generation of mitochondrial acetyl-CoA (*25*). Indeed, depletion of mitochondrial acetyl-CoA through *MPC1* deletion results in a significant diminution of ETC complexes and respiratory growth (Figure 5-7B and Figure 5-8A), which is coincident with a depletion of acyl-ACP and corresponding accumulation of deacyl/holo-ACP (Figure 5-7B). This phenotype is reminiscent of *lip5*Δ cells, which have reduced levels of ACP acylation (Figure 5-5A)

and ETC complex assembly (Figure 5-5B). This is consistent with acetyl-CoA depletion, as defects in lipoic acid synthesis will inhibit PDH, thereby preventing pyruvate-derived acetyl-CoA synthesis.

In order to better understand the mechanisms underlying this phenotype, the whole cell proteomic profile of *mpc1*Δ cells was quantified and compared to WT and *mct1*Δ cells. Like *mct1*Δ, *mpc1*Δ cells also exhibited increased abundance of proteins involved in generating mitochondrial acetyl-CoA (Figure 5-7A), however, the steady state abundance of ETC complex subunits was considerably different in these two strains. In fact, the majority of the ETC subunits were unaffected in the *mpc1*Δ mutant (Figure 5-7C). Importantly, acetyl-CoA-depleted mitochondria displayed no defects in mitochondrial translation as evidenced by normal abundance of mitochondria-encoded proteins, Cox1, Cox2, Cox3 and Atp6 as well as Rpm2 (Figure 5-7D and Figure 5-8B). Thus, the mitochondrial translation defect observed in *mct1*Δ cells is likely an extreme effect of complete FASII deletion and not a typical response to normal variations in mitochondrial acetyl-CoA.

On the other hand, the LYR proteins, which were depleted in the *mct1*Δ strain, were also lost in the *mpc1*Δ mutant (Figure 5-7D). Consistent with this observation, the ETC complex subunits that are the most depleted in the *mpc1*Δ strain are Rip1 and Sdh2, the direct binding partners of LYR proteins (LYR targets), Mzm1 and Sdh6/Sdh7, respectively (Figure 5-7C & Figure 5-8C). Focusing on complex III assembly, it is possible to gain further insights into the ACP-LYR network. Deletion of the complex III-specific LYR protein, Mzm1, causes a phenotype in which a sub-assembly of complex III lacking Rip1 and Qcr10 accumulates (*11, 12*). Because all other complex III subunits

remain stable in *mpc1*Δ cells (Figure 5-8C), it is likely that this subcomplex assembles but deacyl/holo-ACP fails to activate Mzm1 to incorporate Rip1 and Qcr10. This suggests that in mitochondrial acetyl-CoA-depleted conditions, ACP deacylation prevents the activation of complex III, and presumably other complexes. By restricting the incorporation of LYR target proteins, this network provides the cell a mechanism by which assembly of these complexes can be tuned to acute substrate depletion.

Finally, we hypothesized that augmenting ACP acylation in *mpc1*Δ cells could stimulate ETC biogenesis independent of mitochondrial acetyl-CoA abundance. Therefore, we expressed mito-*FAA2* in *mpc1*Δ cells and assayed ETC biogenesis. Mito-*FAA2* increased respiratory growth and restored complex II and complex III assembly to WT levels by supporting the incorporation of LYR target proteins, Sdh2 and Rip1, into their respective complexes (Figure 5-7E,D). Taken together, these data demonstrate that mitochondrial acetyl-CoA depletion causes ACP deacylation, which prevents ETC assembly and activation.

Conclusion

The data presented herein define a novel and unexpected role of mitochondrial fatty acid synthesis in regulating ETC assembly. It carries out this function through the acetyl-CoA-dependent synthesis of ACP-bound fatty acyl chains. Acyl-ACP then directly interacts with each member of the LYR protein family and, in an acyl chain-dependent manner, stimulates their ETC complex assembly function. In addition to ETC biogenesis, acetyl-CoA, FASII and ACP are also required for the activity of the TCA cycle enzymes PDH and α-ketoglutarate dehydrogenase through the synthesis of lipoic acid. As such,

this pathway provides an elegant mechanism whereby the primary substrate of mitochondrial metabolism signals the assembly and activation of the two main systems of mitochondrial catabolism. It is clear that one of the most damaging mediators of mitochondrial dysfunction is an imbalance of metabolic activities, which leads to inappropriate accumulation of reduced or oxidized electron carriers and other intermediary metabolites. We propose that by coordinating assembly of the ETC complexes with one another and with the availability of substrate, this newly uncovered regulatory role for FASII maintains a balanced and healthy mitochondrial metabolism.

Materials and Methods

Yeast strains and growth conditions

Saccharomyces cerevisiae BY4741 (*MATa, his3 leu2 met15 ura3*) was used as the wild-type strains where indicated. Each mutant was generated in diploid cells using a standard PCR-based homologous recombination method. The genotypes of all strains used in this study are listed in Table 5-1. Yeast transformation was performed by the standard TE/LiAc method and transformed cells were recovered and grown in synthetic complete glucose (SD) medium lacking the appropriate amino acid(s) for selection purposes. Medium used in this study includes YPA and synthetic minimal medium supplemented with 2% glucose or 2% raffinose. Growth assays were performed using synthetic minimal media supplemented with the appropriate amino acids and indicated carbon source. For plate-based growth assays, overnight cultures were back-diluted to equivalent ODs and spotted as 10-fold serial dilutions. Cells were allowed to grow for 2-3 days at 30°C.

Isolation of yeast mitochondria

Cell pellet was washed once with ddH_2O and incubated in TD buffer (100 mM Tris-SO_4, pH 9.4 and 100 mM DTT) for 15 min at 30°C. Spheroplasts were obtained by incubating cells in SP buffer (1.2 M Sorbitol and 20 mM potassium phosphate, pH 7.4) supplemented with 0.3 mg/mL lyticase for 1 hour at 30°C to remove the cell wall. Spheroplasts were gently washed once and homogenized in ice-cold SEH buffer (0.6 M sorbitol, 20 mM HEPES-KOH, pH 7.4, 2 mM $MgCl_2$, 1mM EGTA) using a dounce homogenizer applied with 30-40 strokes. Crude mitochondria were then isolated by differential centrifugation. In order to reliably maintain ACP acylation during the mitochondrial isolation 10mM N-ethylmaleimide was added to the SEH buffer.

Steady-state protein analysis

Yeast mitochondria were solubilized in Laemmli buffer. Samples were resolved by SDS-PAGE and assessed by immunoblot. In order to maintain ACP acylation during electrophoresis, 10 mM NEM was added to the Laemmli buffer.

Immunoprecipitation

Crude mitochondria were isolated and resuspended to a concentration of 5 mg/mL in XWA buffer. Mitochondria was solubilized in 0.7% digitonin for 30 mins. Followed by centrifugation at 20,000 x g for 20 mins. Cleared mitochondrial lysates were incubated with anti-HA antibody conjugated agarose (Sigma) for 2 hrs. at 4°C. The agarose was washed 3-5 times and eluted in Laemmli buffer (65°C, 10 mins). Elutions were resolved by SDS-PAGE and assessed by immunoblot. In order to reliably maintain

ACP acylation during the mitochondrial isolation, 10mM N-ethylmaleimide was added to IP buffers.

Blue native polyacrylamide gel electrophoresis (BN-PAGE)

BN-PAGE was performed as described previously (*26*). Mitochondria were resuspended in lysis buffer (Invitrogen) and solubilized with 1% digitonin. Cleared mitochondrial lysates were prepared by centrifugation at 20,000xg for 15-20 mins. Lysates were resolved on a 3%-12% or 4%-16% gradient native gel (Invitrogen).

Proteomics

In order to fully use the sample multiplexing ability, an 11-plex experiment was designed containing the following proteome-wide comparisons: wt (n=3), *mct1*Δ (n=3), *mpc1*Δ (n=30), and wt_extra (samples for an unrelated experiment) (n=2). Cell pellets from each condition were resuspended at 4°C in buffer containing 8M urea, 50mM EPPS pH 8.5, 50mM NaCl, and protease inhibitors. Chilled zirconium oxide beads were added to cell slurries. Cells were lysed using a MiniBeadbeater (Biospec products, Bartlesville, OK) at 4°C in 2mL screw cap tubes for 5 cycles of 30 seconds each, with 1 min pauses between cycles to avoid overheating. After centrifugation, clarified lysates were transferred to new tubes. Bicinchoninic acid (BCA) protein assay (Thermo Fischer Scientific) was performed to determine protein concentration. Proteins were then subjected to disulfide reduction with 5mM tris (2 carboxyethyl) phosphine (TCEP), (room temperature, 30 min) and alkylation with 10 mM iodoacetamide (room temperature, 30 min in the dark). 15 mM dithiotreitol was used to quench excess

iodoacetamide (room temperature, 15 min in the dark). Proteins (200ug) were then chloroform/methanol precipitated and washed with methanol prior to air drying. Samples were resuspended in 8 M urea, 50 mM EPPS, pH 8.5, and then diluted to <1M urea with 50mM EPPS, pH 8.5. Proteins were digested for 16 hours with LysC (1:100 enzyme:protein ratio) at room temperature, followed by trypsin (1:100 enzyme:protein ratio) for 6 hours at 37°C. Peptides were quantified using Pierce Quantitative Colorimetric Peptide Assay. TMT-11 reagents (0.8mg) were dissolved in 40uL anhydrous acetonitrile, and 7uL was used to label 70ug peptides in 30% (v/v) acetonitrile. Labeling proceeded for 1 hour at room temperature, until reaction was quenched using 7uL 5% hydroxylamine. TMT-labeled peptides were then pooled, vacuum centrifuged to dryness, and cleaned using 50mg Sep-Pak (Waters). The pooled TMT-labeled peptide sample was fractionated using BPRP HPLC. We used an Agilent 1260 Infinity pump equipped with a degasser and a single wavelength detector (set at 220 nm). Peptides were subjected to a 50 min linear gradient from 8% to 40% acetonitrile in 10 mM ammonium bicarbonate pH 8 at a flow rate of 0.6 mL/min over an Agilent 300Extend C18 column (3.5 μm particles, 4.6 mm ID and 250 mm in length). We collected a total of 96 fractions, then consolidated those into 24 and vacuum centrifuged to dryness. Twelve of the 24 fractions were resuspended in a 5% acetonitrile, 1% formic acid solution. Fractions were desalted via StageTip, dried via vacuum centrifugation, and reconstituted in 5% acetonitrile, 5% formic acid for LC-MS/MS processing. Mass spectrometry data were collected using an Orbitrap Fusion Lumos mass spectrometer (Thermo Fischer Scientific) equipped with a Proxeon EASY-nLC 1000 liquid chromatography (LC) system (Thermo Fisher Scientific). Peptides were separated on a 100 μm inner diameter microcapillary

column packed with ~35 cm of Accucore C18 resin (2.6 μm, 150 Å, Thermo Fisher Scientific). Approximately 2ug peptides were separated using a 2.5 h gradient of acidic acetonitrile. We used the multinotch MS3-based TMT method (*27*). The scan sequence began with a MS1 spectrum (Orbitrap analysis; resolution 120,000; mass range 400−1400 Th). MS2 analysis followed collision-induced dissociation (CID, CE = 35) with a maximum ion injection time of 150 ms and an isolation window of 0.5 Da. The 10 most abundant MS1 ions of charge states 2-6 were selected for MS2/MS3 analysis. To obtain quantitative information, MS3 precursors were fragmented by high-energy collision-induced dissociation (HCD, CE = 55) and analyzed in the Orbitrap (resolution was 50,000 at 200 Th) with a maximum ion injection time of 150 ms and a charge state-dependent variable isolation window of 0.7 to 1.2 Da (*28*). MS2 mass spectra were processed using a SEQUEST-based software pipeline (*27, 29, 30*). Spectra were converted to mzXML using a modified version of ReAdW.exe. Database searching used the yeast proteome downloaded from Uniprot (Magrane and Consortium, 2014) in both forward and reverse directions, along with common contaminating protein sequences. Searches were performed using a peptide mass tolerance of 20 ppm, and a fragment ion tolerance of 0.9 Da. These wide-mass-tolerance windows were chosen to maximize sensitivity in conjunction with SEQUEST searches and linear discriminant analysis (*29, 31*). TMT tags on lysine residues and peptide N termini (+229.163 Da) and carbamidomethylation of cysteine residues (+57.021 Da) were set as static modifications, while oxidation of methionine residues (+15.995 Da) was set as a variable modification. Peptide-spectrum matches (PSMs) were adjusted to a 1% false discovery rate (FDR) (*32*). Linear discriminant analysis was used to filter PSMs, as described previously (*29*), while

considering the following parameters: XCorr, ΔCn, missed cleavages, adjusted PPM, peptide length, fraction of ions matched, charge state, and precursor mass accuracy. PSMs were identified, quantified, and collapsed to a 1% peptide false discovery rate (FDR) and then collapsed further to a final protein-level FDR of 1%. PSMs were quantified from MS3 scans; those with poor quality, MS3 spectra with total TMT reporter signal-to-noise ratio that is <200, or no MS3 spectra were excluded from quantitation. Protein quantitation was performed by summing the signal-to-noise values for all peptides for a given protein. Each TMT channel was summed across all quantified proteins and normalized to enforce equal protein loading. Each protein's quantitative measurement was then scaled to 100. In Figure 5-2, the first 6 channels were used (wt vs *mct1*Δ). For Figure 5-7, 9 channels were used (wt vs *mct1*Δ vs *mpc1*Δ).

Statistics

The signal-to-noise ratios for each of the six channels were scaled to represent the percent of total signal in the six channels. Student's t tests were performed in Excel (2-tailed). P values were adjusted using the Benjamini-Hochberg approach for the 4,716 proteins that were tested. Significance was determined based on an adjusted P-value of <0.01. Heat maps and dendrograms in Figure 5-1, D to E were generated using JMP. Heat maps in Figures 5-2C, 5-7A, and 5-7C were generated using R. The Volcano plot was generated in Excel. PRISM software was used to graph all quantitative data and perform statistical analyses. P values for pairwise comparisons were determined using a Student's t test. Error bars represent the standard deviation.

References

1. K. E. Wellen, C. B. Thompson, Cellular metabolic stress: Considering how cells respond to nutrient excess. *Molecular Cell* **40**, 323-332 (2010).

2. J. K. Hiltunen, K. J. Autio, M. S. Schonauer, V. A. S. Kursu, C. L. Dieckmann, A. J. Kastaniotis, Mitochondrial fatty acid synthesis and respiration. *Biochimica et Biophysica Acta (BBA) - Bioenergetics* **1797**, 1195-1202 (2010).

3. P. W. Majerus, A. W. Alberts, P. R. Vagelos, Acyl carrier protein, IV. The identification of 4′ -phosphopantetheine as the prosthetic group of the acyl carrier protein. *Proceedings of the National Academy of Sciences* **53**, 410-417 (1965).

4. H.-P. Stuible, S. Meier, C. Wagner, E. Hannappel, E. Schweizer, A novel phosphopantetheine-protein transferase activating yeast mitochondrial acyl carrier protein. *Journal of Biological Chemistry* **273**, 22334-22339 (1998).

5. S. Brody, C. Oh, U. Hoja, Mitochondrial acyl carrier protein is involved in lipoic acid synthesis in Saccharomyces cerevisiae. *FEBS Letters* **408**, 217-220 (1997).

6. L. Zhang, A. K. Joshi, J. Hofmann, E. Schweizer, S. Smith, Cloning, expression, and characterization of the human mitochondrial β-Ketoacyl synthase. *Journal of Biological Chemistry* **280**, 12422-12429 (2005).

7. R. Schneider, B. Brors, F. Bürger, S. Camrath, H. Weiss, Two genes of the putative mitochondrial fatty acid synthase in the genome of Saccharomyces cerevisiae. *Current Genetics* **32**, 384-388 (1997).

8. J. G. Van Vranken, M.-Y. Jeong, P. Wei, Y.-C. Chen, S. P. Gygi, D. R. Winge, J. Rutter, The mitochondrial acyl carrier protein (ACP) coordinates mitochondrial fatty acid synthesis with iron sulfur cluster biogenesis. *eLife* **5**, e17828 (2016).

9. M. S. Schonauer, A. J. Kastaniotis, J. K. Hiltunen, C. L. Dieckmann, Intersection of RNA processing and the type II fatty acid synthesis pathway in yeast mitochondria. *Molecular and Cellular Biology* **28**, 6646-6657 (2008).

10. U. Na, W. Yu, J. E. Cox, D. K. Bricker, K. Brockmann, J. Rutter, C. S. Thummel, D. R. Winge, The LYR factors SDHAF1 and SDHAF3 mediate maturation of the iron-sulfur subunit of succinate dehydrogenase. *Cell Metabolism* **20**, 253-266 (2014).

11. A. Atkinson, P. Smith, J. L. Fox, T.-Z. Cui, O. Khalimonchuk, D. R. Winge, The LYR Protein Mzm1 functions in the insertion of the rieske Fe/S protein in yeast mitochondria. *Molecular and Cellular Biology* **31**, 3988-3996 (2011).

12. T.-Z. Cui, P. M. Smith, J. L. Fox, O. Khalimonchuk, D. R. Winge, Late-stage maturation of the rieske Fe/S protein: Mzm1 stabilizes Rip1 but does not facilitate its translocation by the AAA ATPase Bcs1. *Molecular and Cellular Biology* **32**, 4400-4409 (2012).

13. L. Lefebvre-Legendre, J. Vaillier, H. Benabdelhak, J. Velours, P. P. Slonimski, J.-P. di Rago, Identification of a nuclear gene (FMC1) required for the assembly/stability of yeast mitochondrial F1-ATPase in heat stress conditions. *Journal of Biological Chemistry* **276**, 6789-6796 (2001).

14. N. Wiedemann, E. Urzica, B. Guiard, H. Müller, C. Lohaus, H. E. Meyer, M. T. Ryan, C. Meisinger, U. Mühlenhoff, R. Lill, N. Pfanner, Essential role of Isd11 in mitochondrial iron–sulfur cluster synthesis on Isu scaffold proteins. *The EMBO Journal* **25**, 184-195 (2006).

15. A. C. Adam, C. Bornhövd, H. Prokisch, W. Neupert, K. Hell, The Nfs1 interacting protein Isd11 has an essential role in Fe/S cluster biogenesis in mitochondria. *The EMBO Journal* **25**, 174-183 (2006).

16. H. Angerer, The superfamily of mitochondrial Complex1_LYR motif-containing (LYRM) proteins. *Biochemical Society Transactions* **41**, 1335-1341 (2013).

17. B.J. Floyd, E.M. Wilkerson, M.T. Veling, C.E. Minogue, C. Xia, E.T. Beebe, R.L. Wrobel, H. Cho, L.S. Kremer, C.L. Alston, K.A. Gromek, B.K. Dolan, A. Ulbrich, J.A. Stefely, S.L. Bohl, K.M. Werner, A. Jochem, M.S. Westphall, J.W. Rensvold, R.W. Taylor, H. Prokisch, J.-Ja P. Kim, J.J. Coon, D.J. Pagliarini, Mitochondrial protein interaction mapping identifies regulators of respiratory chain function. *Molecular Cell* **63**, 621-632 (2016).

18. E.L. Huttlin, L. Ting, R.J. Bruckner, F. Gebreab, M.P. Gygi, J. Szpyt, S. Tam, G. Zarraga, G. Colby, K. Baltier, R. Dong, V. Guarani, L.P. Vaites, A. Ordureau, R. Rad, B.K. Erickson, M. Wühr, J. Chick, B. Zhai, D. Kolippakkam, J. Mintseris, R.A. Obar, T. Harris, S. Artavanis-Tsakonas, M.E. Sowa, P. De Camilli, J.A. Paulo, J. W. Harper, S.P. Gygi, The BioPlex network: A systematic exploration of the human interactome. *Cell* **162**, 425-440 (2015).

19. H. Angerer, Eukaryotic LYR proteins interact with mitochondrial protein complexes. *Biology* **4**, 133-150 (2015).

20. S. A. Cory, J. G. Van Vranken, E. J. Brignole, S. Patra, D. R. Winge, C. L. Drennan, J. Rutter, D. P. Barondeau, Structure of human Fe–S assembly subcomplex reveals unexpected cysteine desulfurase architecture and acyl-ACP–ISD11 interactions. *Proceedings of the National Academy of Sciences* **114**, E5325-E5334 (2017).

21. K. Fiedorczuk, J. A. Letts, G. Degliesposti, K. Kaszuba, M. Skehel, L. A. Sazanov, Atomic structure of the entire mammalian mitochondrial complex I. *Nature* **538**, 406-410 (2016).

22. D. K. Shintani, J. B. Ohlrogge, The characterization of a mitochondrial acyl carrier protein isoform isolated from Arabidopsis thaliana. *Plant Physiology* **104**, 1221-1229 (1994).

23. A. Harington, E. Schwarz, P. P. Slonimski, C. J. Herbert, Subcellular relocalization of a long-chain fatty acid CoA ligase by a suppressor mutation alleviates a respiration deficiency in Saccharomyces cerevisiae. *The EMBO Journal* **13**, 5531-5538 (1994).

24. A. J. Kastaniotis, K. J. Autio, R. T. Sormunen, J. K. Hiltunen, Htd2p/Yhr067p is a yeast 3-hydroxyacyl-ACP dehydratase essential for mitochondrial function and morphology. *Molecular Microbiology* **53**, 1407-1421 (2004).

25. D. K. Bricker, E. B. Taylor, J. C. Schell, T. Orsak, A. Boutron, Y.-C. Chen, J. E. Cox, C. M. Cardon, J. G. Van Vranken, N. Dephoure, C. Redin, S. Boudina, S. P. Gygi, M. Brivet, C. S. Thummel, J. Rutter, A mitochondrial pyruvate carrier required for pyruvate uptake in yeast, Drosophila, and humans. *Science* **337**, 96 (2012).

26. I. Wittig, H.-P. Braun, H. Schagger, Blue native PAGE. *Nat. Protocols* **1**, 418-428 (2006).

27. G. C. McAlister, D. P. Nusinow, M. P. Jedrychowski, M. Wühr, E. L. Huttlin, B. K. Erickson, R. Rad, W. Haas, S. P. Gygi, MultiNotch MS3 enables accurate, sensitive, and multiplexed detection of differential expression across cancer cell line proteomes. *Analytical Chemistry* **86**, 7150-7158 (2014).

28. J. A. Paulo, J. D. O'Connell, R. A. Everley, J. O'Brien, M. A. Gygi, S. P. Gygi, Quantitative mass spectrometry-based multiplexing compares the abundance of 5000 S. cerevisiae proteins across 10 carbon sources. *Journal of Proteomics* **148**, 85-93 (2016).

29. E. L. Huttlin, M. P. Jedrychowski, J. E. Elias, T. Goswami, R. Rad, S. A. Beausoleil, J. Villén, W. Haas, M. E. Sowa, S. P. Gygi, A tissue-specific atlas of mouse protein phosphorylation and expression. *Cell* **143**, 1174-1189 (2010).

30. G. C. McAlister, E. L. Huttlin, W. Haas, L. Ting, M. P. Jedrychowski, J. C. Rogers, K. Kuhn, I. Pike, R. A. Grothe, J. D. Blethrow, S. P. Gygi, Increasing the multiplexing capacity of TMTs using reporter ion isotopologues with isobaric masses. *Analytical Chemistry* **84**, 7469-7478 (2012).

31. S. A. Beausoleil, J. Villen, S. A. Gerber, J. Rush, S. P. Gygi, A probability-based approach for high-throughput protein phosphorylation analysis and site localization. *Nature Biotechnology* **24**, 1285-1292 (2006).

32. J. E. Elias, S. P. Gygi, Target-decoy search strategy for increased confidence in large-scale protein identifications by mass spectrometry. *Nature Methods* **4**, 207-214 (2007).

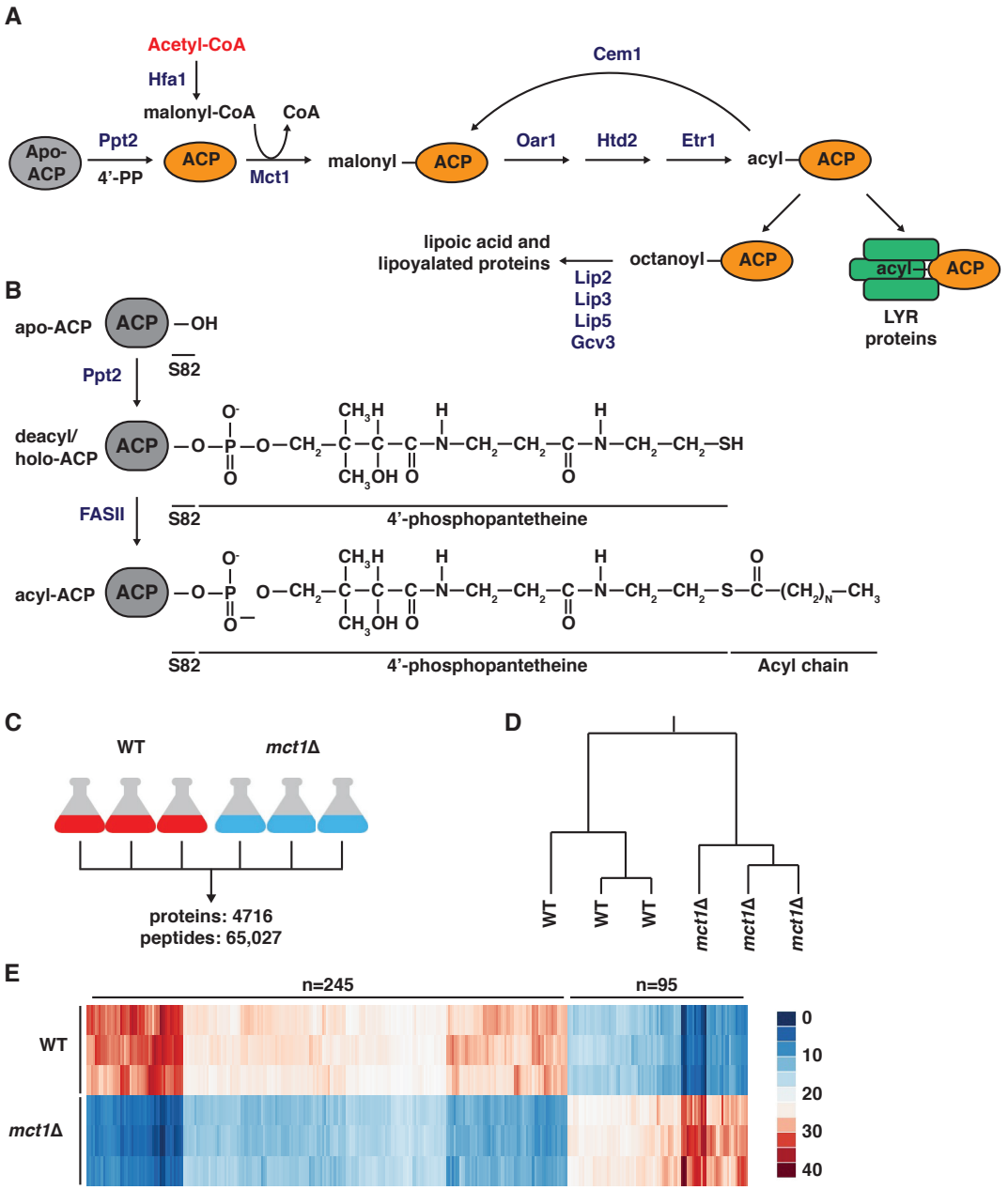

Figure 5-1. FASII is required for oxidative metabolism and ETC assembly. A. Model of mitochondrial fatty acid synthesis (FASII). B. Model of various ACP species. Apo-ACP is converted to deacyl/holo-ACP by Ppt2-dependent addition of 4'-PP to Ser82 of ACP. Deacyl/holo-ACP is acylated by FASII. C. Proteomic workflow for WT vs. *MCT1* deletion. D. Dendrogram plot demonstrating that replicates cluster as expected. E. Heat map for significantly changing proteins (corrected p value < 0.01 and fold-change >1.5). Intensities represent % of TMT reporter ion signal for each of the six channels.

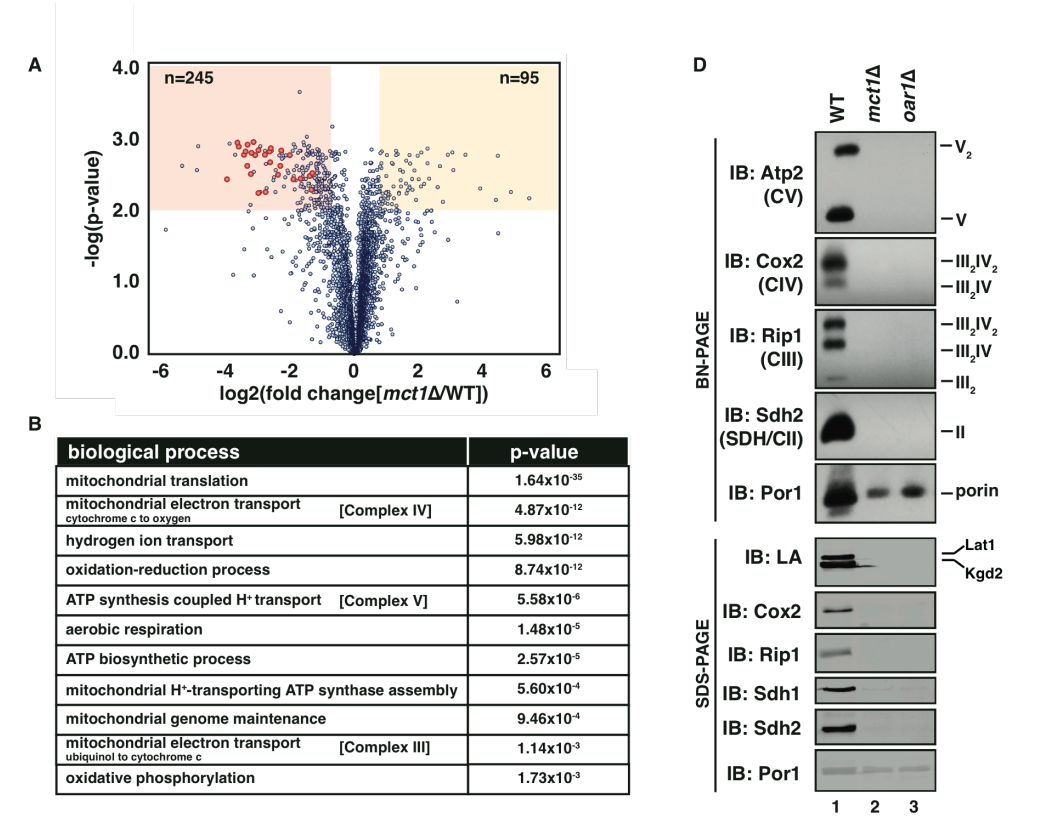

Figure 5-2. FASII is required for cellular respiration and ETC biogenesis. A. Volcano plot highlighting proteins that are significantly altered in expression in *mct1*Δ cells. Significantly depleted proteins involved in oxidative phosphorylation are emphasized in red. B. Gene set enrichment analysis of the 245 proteins depleted in in *mct1*Δ cells compared to WT. Indicated are gene ontologies and associated p-values. C. Heat map showing the fold change of the indicated proteins in *mct1*Δ cells compared to WT. Proteins indicated in red are encoded by the mitochondrial genome. D. Mitochondrial lysates were separated by BN-PAGE (upper panel) or SDS-PAGE (lower panel). Indicated antibodies were used to assess abundance of complexes and subunits.

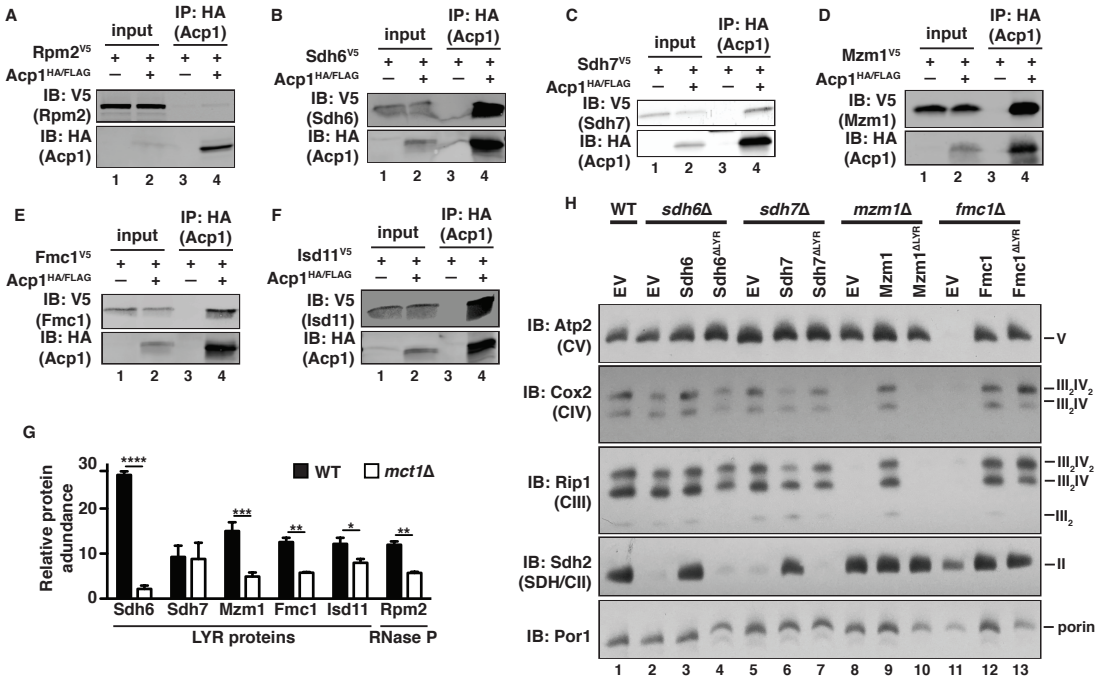

Figure 5-3. ACP coordinates a mitochondrial network that is required for ETC assembly. A-F. Acp1$^{HA/FLAG}$ was immunoprecipitated from mitochondrial lysates expressing the indicated proteins. Inputs and eluates were resolved by SDS-PAGE and immunoblotted for HA (Acp1$^{HA/FLAG}$) and V5 (Rpm2^{V5} and LYR^{V5} fusions). G. Relative abundance of the indicated proteins in WT and *mct1*Δ cells (N=3). H. Mitochondrial lysates expressing the indicated plasmids were separated by BN-PAGE and immunoblotted with the indicated antibodies. I. Error bars represent the standard deviation. *p<0.05, **p<0.005, ***p<0.0005, ****p<0.00005.

Figure 5-4. ACP coordinates the LYR assembly network. A. Relative abundance of the indicated proteins in WT and *mct1*Δ cells (N=3). B. Sequence alignment of the LYR protein family is *Saccharomyces cerevisiae*. The LYR motif in each protein is indicated. C. Table describing the function and target of each LYR protein family member. Indicated is the complex associated with each LYR protein and the specific LYR target. LYR target proteins are the complex subunits to which an LYR protein directly binds. D-H. WT and S82A $Acp1^{HA/FLAG}$ were immunoprecipitated from mitochondrial lysates expressing the indicated proteins. Inputs and eluates were resolved by SDS-PAGE and immunoblotted for HA ($Acp1^{HA/FLAG}$) and V5 (LYR^{V5} fusions). I-L. Ten-fold serial dilutions of the indicated strains harboring the indicated plasmids were plated on synthetic medium with either glucose or glycerol and grown for 2-3 days. L. Mitochondrial lysates expressing the indicated plasmids were separated by SDS-PAGE and immunoblotted with the indicated antibodies. Error bars represent the standard deviation. ***$p<0.0005$, ****<0.00005.

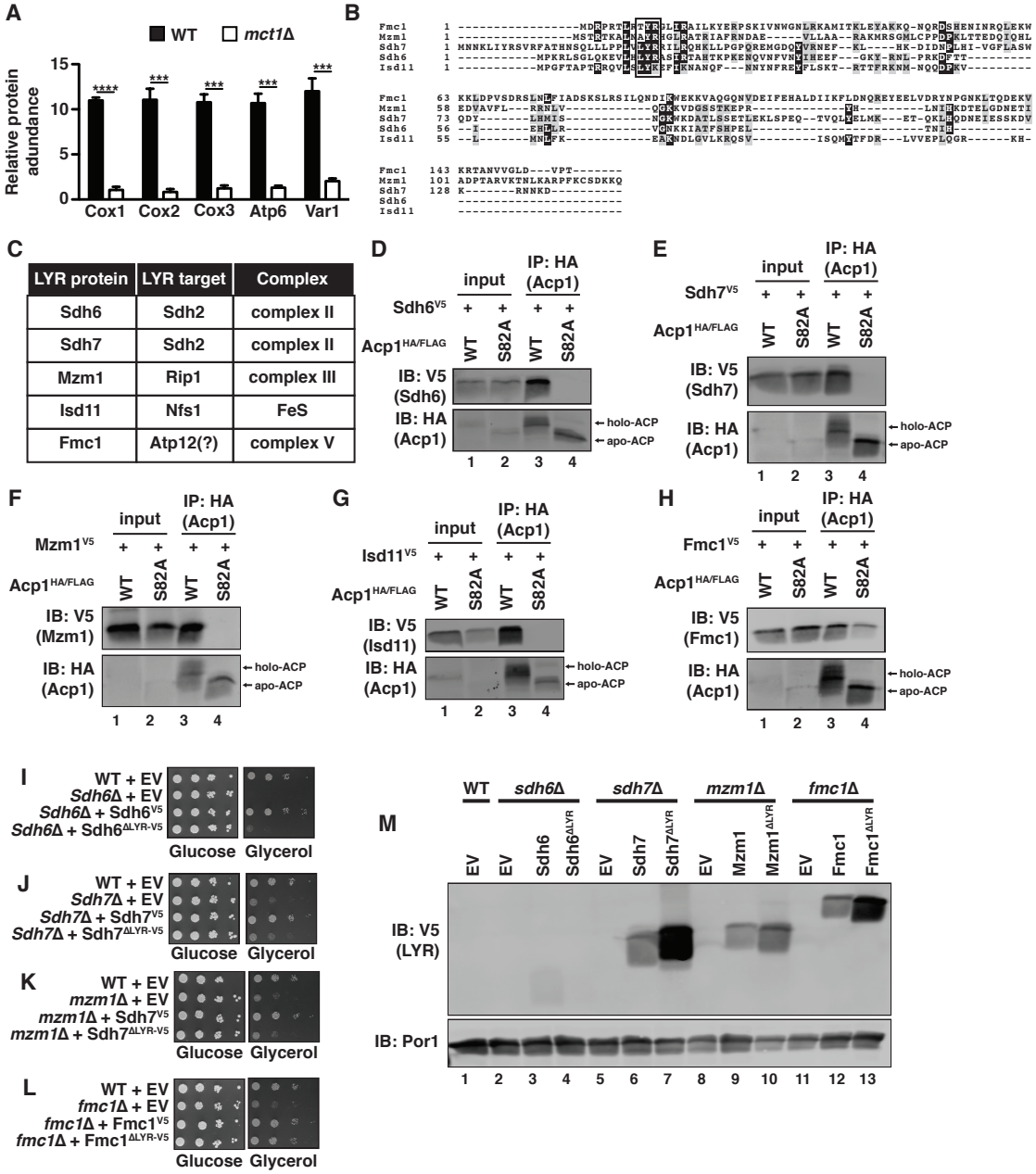
A
WT
mct1Δ
Relative protein adundance
Cox1
Cox2
Cox3
Atp6
Var1
B
C
LYR protein
LYR target
Complex
Sdh6
Sdh2
complex II
Sdh7
Sdh2
complex II
Mzm1
Rip1
complex III
Isd11
Nfs1
FeS
Fmc1
Atp12(?)
complex V
D
input
IP: HA (Acp1)
Sdh6V5
Acp1HA/FLAG
WT
S82A
IB: V5 (Sdh6)
IB: HA (Acp1)
holo-ACP
apo-ACP
E
Sdh7V5
IB: V5 (Sdh7)
F
Mzm1V5
IB: V5 (Mzm1)
G
Isd11V5
IB: V5 (Isd11)
H
Fmc1V5
IB: V5 (Fmc1)
I
WT + EV
Sdh6Δ + EV
Sdh6Δ + Sdh6V5
Sdh6Δ + Sdh6ΔLYR-V5
Glucose
Glycerol
J
Sdh7Δ + EV
Sdh7Δ + Sdh7V5
Sdh7Δ + Sdh7ΔLYR-V5
K
mzm1Δ + EV
mzm1Δ + Sdh7V5
mzm1Δ + Sdh7ΔLYR-V5
L
fmc1Δ + EV
fmc1Δ + Fmc1V5
fmc1Δ + Fmc1ΔLYR-V5
M
WT
sdh6Δ
sdh7Δ
mzm1Δ
fmc1Δ
EV
Sdh6
Sdh6ΔLYR
Sdh7
Sdh7ΔLYR
Mzm1
Mzm1ΔLYR
Fmc1
Fmc1ΔLYR
IB: V5 (LYR)
IB: Por1

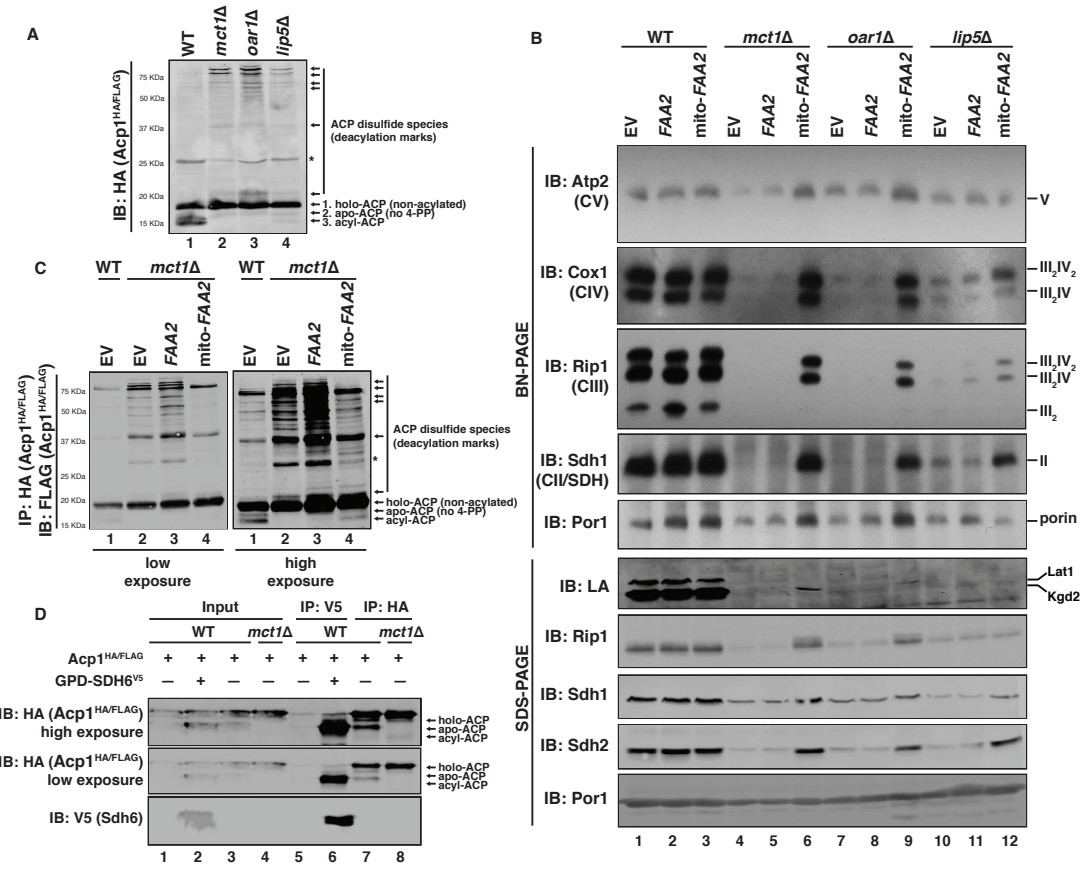

Figure 5-5. ACP acylation is sufficient to stimulate ETC assembly. A. Mitochondrial lysates expressing Acp1$^{HA/FLAG}$ were separated by SDS-PAGE in the presence of 10mM NEM and immunoblotted for HA to identify Acp1-containing bands. B. Mitochondrial lysates expressing the indicated plasmids were separated by BN-PAGE (upper panel) or SDS-PAGE (lower panel) and immunoblotted with the indicated antibodies. While mito-Faa2 only weakly restores protein lipoylation in FASII mutant cells, this appears to be sufficient to support respiratory growth C. Acp1$^{HA/FLAG}$ was immunoprecipitated from mitochondrial lysates, separated by SDS-PAGE in the presence of 10mM NEM, and immunoblotted for FLAG to identify Acp1-containing bands D. Acp1$^{HA/FLAG}$ or GPD-Sdh6^{V5} were immunoprecipitated from mitochondrial lysates expressing the indicated proteins, separated by SDS-PAGE in the presence of 10 mM NEM, and immunoblotted for HA (Acp1$^{HA/FLAG}$) and V5 (Sdh6^{V5}). * indicates nonspecific bands in A and C.

Figure 5-6. ACP acylation is required for ETC assembly. A. WT of S82A Acp1$^{HA/FLAG}$ were immunoprecipitated from mitochondrial lysates, separated by SDS-PAGE in the presence of 10mM NEM, and immunoblotted for FLAG. B. Mitochondrial lysates expressing Acp1$^{HA/FLAG}$ were separated by SDS-PAGE in the presence of 10mM NEM or 1% β-mercapoethanol and immunoblotted for HA. C. Ten-fold serial dilutions of the indicated strains harboring the indicated plasmids were plated on synthetic medium with either glucose or glycerol and grown for 2-3 days. D,E. *acp1*Δ (D) and ppt2Δ (E) heterozygous diploids harboring the indicated plasmids were dissected and spores were grown on YPAD medium for 2 days. F. Ten-fold serial dilutions of the indicated strains harboring the indicated plasmids were plated on synthetic medium with either glucose or glycerol and drown for 2-3 days. G. Acp1$^{HA/FLAG}$ or GPD-Mzm1^{V5} were immunoprecipitated from mitochondrial lysates expressing the indicated proteins, separated by SDS-PAGE in the presence of 10 mM NEM, and immunoblotted for HA (Acp1$^{HA/FLAG}$) and V5 (Mzm1^{V5}). H-L. Acp1$^{HA/FLAG}$ was immunoprecipitated from mitochondrial lysates expressing the indicated proteins, separated by SDS-PAGE, and immunoblotted for HA (Acp1$^{HA/FLAG}$) and V5 (LYR^{V5} fusions). * indicates nonspecific bands in A and B.

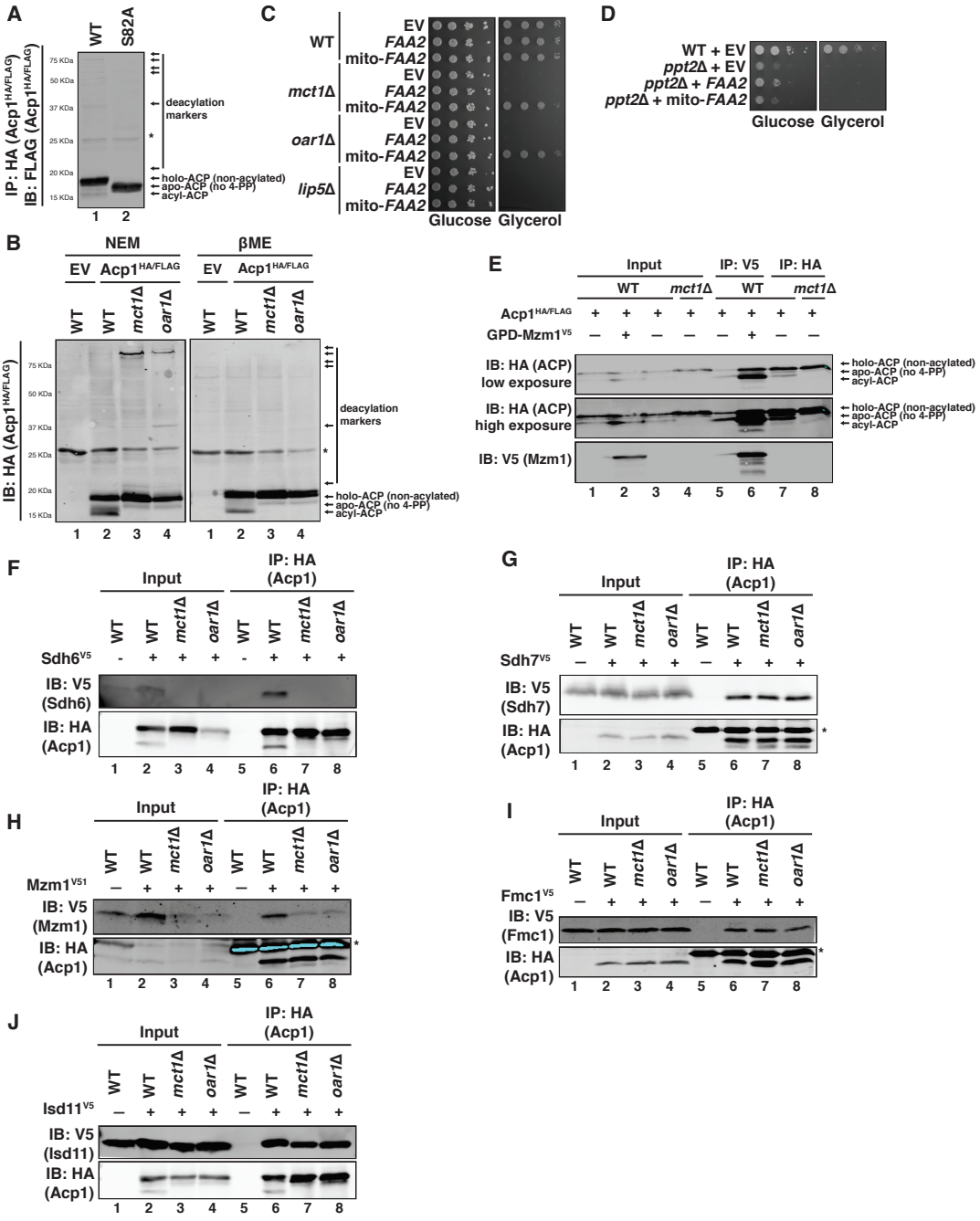
A
WT
S82A
IP: HA (Acp1HA/FLAG)
IB: FLAG (Acp1HA/FLAG)
75 KDa
50 KDa
37 KDa
25 KDa
20 KDa
15 KDa
deacylation markers
holo-ACP (non-acylated)
apo-ACP (no 4-PP)
acyl-ACP
1 2
C
WT
mct1Δ
oar1Δ
lip5Δ
EV
FAA2
mito-FAA2
Glucose Glycerol
D
WT + EV
ppt2Δ + EV
ppt2Δ + FAA2
ppt2Δ + mito-FAA2
Glucose Glycerol
B
NEM
βME
EV
Acp1HA/FLAG
WT
mct1Δ
oar1Δ
IB: HA (Acp1HA/FLAG)
deacylation markers
holo-ACP (non-acylated)
apo-ACP (no 4-PP)
acyl-ACP
1 2 3 4 1 2 3 4
E
Input
IP: V5
IP: HA
WT
mct1Δ
Acp1HA/FLAG
GPD-Mzm1V5
IB: HA (ACP) low exposure
IB: HA (ACP) high exposure
IB: V5 (Mzm1)
holo-ACP (non-acylated)
apo-ACP (no 4-PP)
acyl-ACP
1 2 3 4 5 6 7 8
F
Input
IP: HA (Acp1)
WT
mct1Δ
oar1Δ
Sdh6V5
IB: V5 (Sdh6)
IB: HA (Acp1)
1 2 3 4 5 6 7 8
G
Input
IP: HA (Acp1)
Sdh7V5
IB: V5 (Sdh7)
IB: HA (Acp1)
*
1 2 3 4 5 6 7 8
H
Input
IP: HA (Acp1)
Mzm1V51
IB: V5 (Mzm1)
IB: HA (Acp1)
*
1 2 3 4 5 6 7 8
I
Input
IP: HA (Acp1)
Fmc1V5
IB: V5 (Fmc1)
IB: HA (Acp1)
*
1 2 3 4 5 6 7 8
J
Input
IP: HA (Acp1)
Isd11V5
IB: V5 (Isd11)
IB: HA (Acp1)
1 2 3 4 5 6 7 8

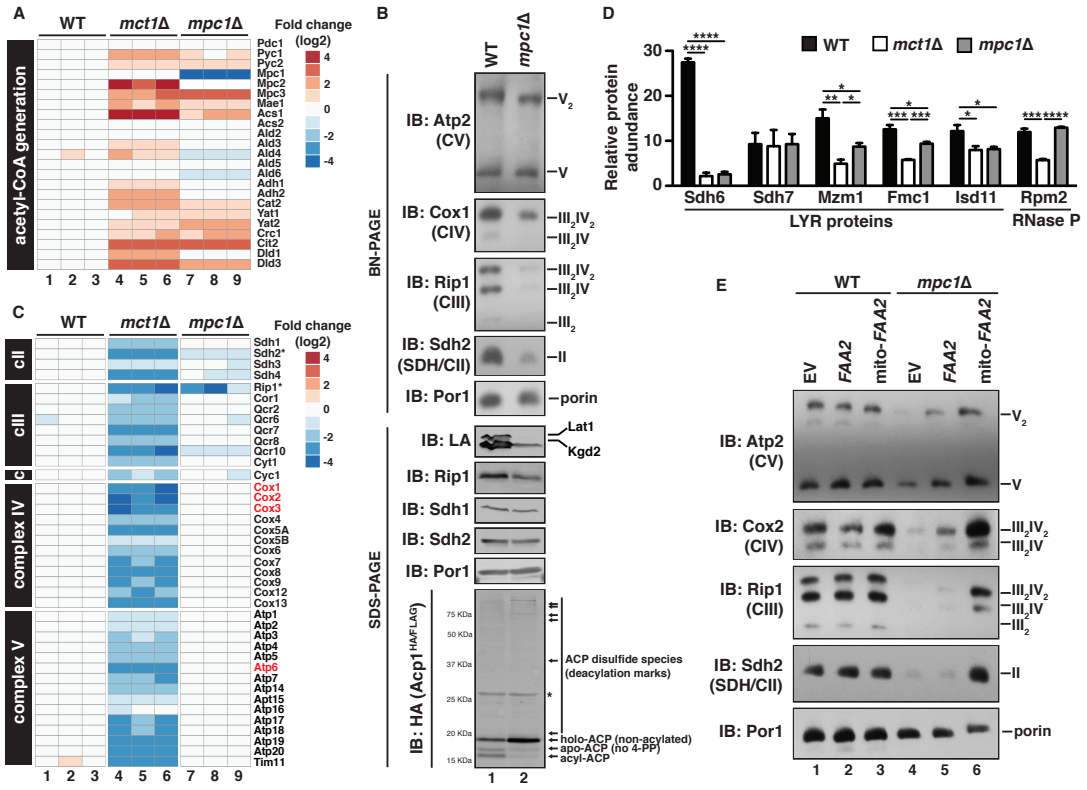

Figure 5-7. Mitochondrial acetyl-CoA is required for ETC assembly. A. Heat map showing the fold change of the indicated proteins in *mct1*Δ and *mpc1*Δ cells compared to WT. B. Mitochondrial lysates were separated by BN-PAGE (upper panel) or SDS-PAGE (lower panel) in the presence of 10mM NEM and immunoblotted with the indicated antibodies. C. Heat map showing the fold change of the indicated proteins in *mct1*Δ and *mpc1*Δ cells compared to WT. Proteins in red are encoded by the mitochondrial genome. Proteins with * are direct LYR target proteins. D. Relative abundance of the indicated proteins in WT, *mct1*Δ, and *mpc1*Δ cells (N=3). E. Mitochondrial lysates expressing the indicated plasmids were solubilized in 1% digitonin, separated by BN-PAGE, and immunoblotted with the indicated antibodies. Error bars represent the standard deviation. *p<0.05, **p<0.005, ***p<0.0005, ****p<0.00005.

Figure 5-8. Mitochondrial acetyl-CoA is required for ETC biogenesis. A. Ten-fold serial dilutions of the indicated strains harboring the indicated plasmids were plated on synthetic medium with either glucose or glycerol and grown for 2-3 days. B,C. Relative abundance of the indicated proteins in WT, *mct1*Δ, and *mpc1*Δ cells (N=3). D. Mitochondrial lysates expressing the indicated plasmids were separated by SDS-PAGE and immunoblotted with the indicated antibodies. Error bars represent the standard deviation. *p<0.05, **p<0.005, ***p<0.0005, ****p<0.00005.

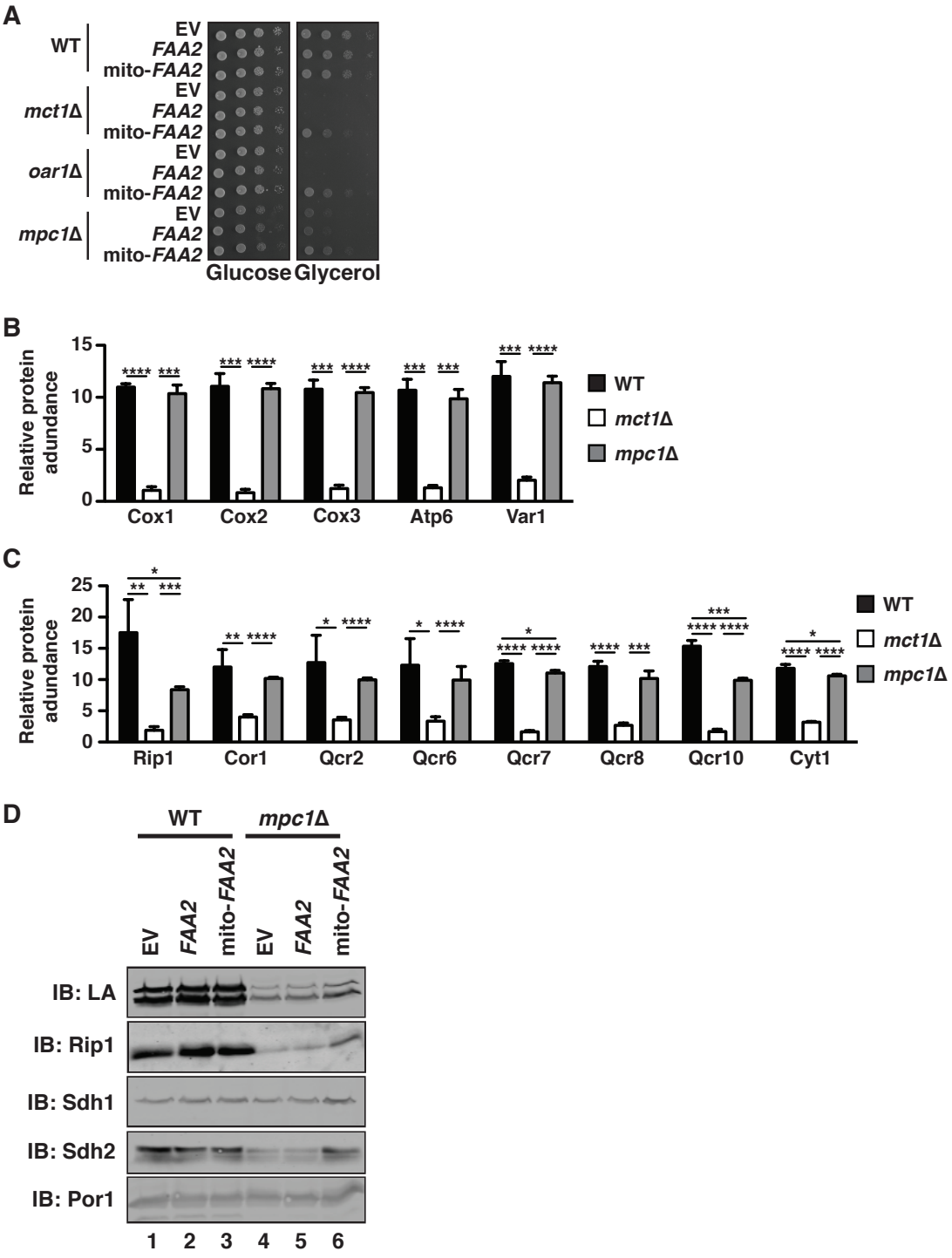
A
WT
EV
FAA2
mito-FAA2
mct1Δ
EV
FAA2
mito-FAA2
oar1Δ
EV
FAA2
mito-FAA2
mpc1Δ
EV
FAA2
mito-FAA2
Glucose
Glycerol
B
Relative protein adundance
15
10
5
0
Cox1
Cox2
Cox3
Atp6
Var1
WT
mct1Δ
mpc1Δ
C
Relative protein adundance
25
20
15
10
5
0
Rip1
Cor1
Qcr2
Qcr6
Qcr7
Qcr8
Qcr10
Cyt1
WT
mct1Δ
mpc1Δ
D
WT
mpc1Δ
EV
FAA2
mito-FAA2
EV
FAA2
mito-FAA2
IB: LA
IB: Rip1
IB: Sdh1
IB: Sdh2
IB: Por1
1 2 3 4 5 6

Table 5-1. Yeast strains used in this study.

Strain	Genotype	Source
WT (BY4741)	*MAT*a, *his3 leu2 met15 ura3*	Open Biosystems
*mct1*Δ	*MAT*a, *his3 leu2 met15 ura3 mct1::natMX*	This study
*oar1*Δ	*MAT*a, *his3 leu2 met15 trp1 ura3 oar1::natMX*	This Study
*lip5*Δ	*MAT*a, *his3 leu2 met15 trp1 ura3 sdh6::natMX*	This Study
*sdh6*Δ	*MAT*a, *his3 leu2 met15 trp1 ura3 sdh6::natMX*	This Study
*sdh7*Δ	*MAT*a, *his3 leu2 met15 trp1 ura3 sdh7::natMX*	This study
*mzm1*Δ	*MAT*a, *his3 leu2 met15 trp1 ura3 mzm1::natMX*	This Study
*fmc1*Δ	*MAT*a, *his3 leu2 met15 trp1 ura3 fmc1::natMX*	This study
*mpc1*Δ	*MAT*a, *his3 leu2 met15 trp1 ura3 mpc1::hygMX*	This study
*ppt2*Δ	*MAT*a, *his3 leu2 met15 trp1 ura3 mpc1::natMX*	This study

CHAPTER 6

CONCLUDING REMARKS

Mitochondria play important roles in numerous aspects of cell biology. As a result, dysfunction in this organelle is associated with many forms of human disease. In order to better understand the etiology of these pathologies, we initiated a project to interrogate previously uncharacterized mitochondrial proteins. In particular, we focused on proteins and protein families with a high degree of conservation throughout eukaryotic evolution. These studies have significantly enhanced our understanding of numerous aspects of mitochondrial biology, including the biogenesis of the electron transport chain (ETC). This dissertation describes the identification and characterization of a novel succinate dehydrogenase (SDH) assembly factor, as well as a novel nutrient-responsive ETC biogenesis network. Together, these studies shine new light on the fundamental process of ETC assembly and, furthermore, raise important questions regarding the role of ETC biogenesis in the maintenance of cellular physiology.

Using three eukaryotic model systems—yeast, *Drosophila*, and mammalian cell lines—we characterized the function of the SDHAF4/Sdh8 protein family. Yeast *SDH8* and *Drosophila Sdhaf4* mutants both present with classical metabolomics phenotypes of SDH deficiency, which is characterized by an accumulation of succinate and corresponding depletion of fumarate and malate. This defect in SDH activity resulted

from a decrease in the steady state abundance of individual subunits, as well as the fully assembled holocomplex.

Yeast was used as the primary model to interrogate the molecular function of Sdh8. Consistent with the observed defects in SDH activity and assembly, Sdh8 interacts directly with Sdh1, the catalytic subunit of SDH. Importantly, Sdh8 does not interact with the SDH holocomplex or any other SDH subunits. Disruption of the SDH complex, by deleting genes encoding the other structural subunits, results in the emergence and accumulation of a subassembly that contains both Sdh1 and Sdh8. Thus, Sdh8 likely acts as a chaperone for Sdh1 prior to its association with Sdh2 and integration into the SDH complex. Free Sdh1 is capable of oxidizing succinate outside of the SDH complex, which results in the spurious generation of reactive oxygen species. By interacting with free Sdh1, Sdh8 prevents the production of these deleterious byproducts and helps maintain mitochondrial homeostasis.

To garner a better understanding of the role of this protein family in the maintenance of mitochondrial health, we used *Drosophila* to interrogate the physiological consequences of *Sdhaf4* deletion. Consistent with human SDH deficiency, flies lacking Sdhaf4 present with severe progressive neurodegeneration and reduced lifespan.

Importantly, there remain numerous reports of SDH-deficient pathologies with no mutations in any of the SDH core subunits or known assembly factors. The molecular and phenotypic insights gained from the characterization of the SDHAF4 gene family raise the intriguing possibility that mutations in this gene may explain this discrepancy. In the end, these studies have not only revealed important insights into the SDH assembly pathway, but have also further established SDH deficiency in disease.

The ETC chain complexes are not simple enzymes but, rather, highly intricate membrane-bound complexes. As such, assembly of these complexes requires the coordinated synthesis of the individual subunits and redox-active cofactors. Furthermore, the assembly process must also be capapble of responding to nutrient availability. The data presented herein firmly establish mitochondrial fatty acid synthesis (FASII) and the acyl carrier protein (ACP) in the regulation and coordination of ETC biogenesis.

ACP1, the gene encoding yeast ACP, is essential for cell viability, while the genes encoding the FASII enzymes are not. Thus, we hypothesized that ACP must perform a function independent of FASII and sought to define this novel function. ACP interacts with the core subunits of the iron sulfur cluster (Fes) biogenesis machinery, each of which is also required for cell viability. Furthermore, ACP is absolutely required for the synthesis of FeS.

Next we wanted to further interrogate the role of FASII in the maintenance of mitochondrial physiology. Indeed, FASII is known to catalyze the synthesis of acyl chains as long as 12-14 carbons; however, no functional importance has ever been attributed to these extended acyl chains. Our data demonstrate that synthesis of these ACP-bound fatty acids serve as a signal to activate ETC biogenesis. As such, ACP acylation is necessary and sufficient to support ETC assembly through direct physical interaction with a network of ETC assembly factors, known as the LYR protein family. This protein family interacts preferentially with acyl-ACP and this interaction is required to activate the LYR network.

Because this system uses posttranslational acylation of ACP to activate ETC biogenesis, we hypothesized that FASII may coordinate ETC assembly with the levels of

mitochondrial acetyl-CoA. Indeed, depletion of mitochondrial acetyl-CoA results in a stark diminution in the steady state abundance of the ETC complexes. Furthermore, these cells exhibit a significant decrease in the abundance of acyl-ACP, suggesting that ACP acylation is sensitive to fluctuations in nutrient availability. Thus, upon depletion of mitochondrial acetyl-CoA, ACP becomes deacylated thereby inhibiting the LYR network of ETC assembly factors. In the end, we propose that by coordinating assembly of the ETC complexes with one another and with the availability of substrate, this newly uncovered regulatory role for FASII maintains a balanced and healthy mitochondrial metabolism.

Finally, in addition to ETC biogenesis, ACP, FASII, and acetyl-CoA are all required to activate the TCA cycle. As such, this pathway provides an elegant mechanism whereby the primary substrate of mitochondrial metabolism signals the assembly and activation of the two main systems of mitochondrial catabolism.

Biology is infinitely complex and despite the best efforts of generations of scientists, there remain enormous gaps in our understanding of the most basic aspects of cell biology. Motivated by this, we sought to focus our attention on identifying and characterizing novel aspects of mitochondrial biology. This strategy has resulted has significantly enriched our understanding of fundamental biological processes from mitochondrial quality control to metabolite transport. This dissertation has focused on the process of ETC biogenesis, an essential process in cellular energy generation. The discovery of multiple new pathways that both support and regulate the assembly of these complexes highlight the importance searching for new and unexpected aspects of biology.